AD 297 026

UNCLASSIFIED

11-63-2-5

Spectrolab

12484 GLADSTONE AVE.
SYLMAR, CALIF.

COPY NO. 060

INVESTIGATION OF OPTICAL COATINGS

FOR SOLAR CELLS

Technical Summary Report No. 2

1 July 1961 through 31 December 1961
Contract No. DA 36-039 SC-87449
Order No. 40647-PM-61-93-93
ARPA Order No. 80-61

U.S.Army Signal Research and Development Laboratory, Fort Monmouth, New Jersey

Prepared by
Dr. F. E. Fuller, Senior Physicist

The work performed under this contract was made possible by the support of the Advanced Research Projects Agency under Order No. 80-61, through the United States Army Signal Research and Development Laboratory.

OBJECT: Study of thermal equilibrium coatings for use with concentrator type solar photovoltaic converters with particular emphasis on spectrally selective reflective coatings of the multilayer interference type.

S P E C T R O L A B
11921 Sherman Way
North Hollywood, California

TABLE OF CONTENTS

LIST OF ILLUSTRATIONS AND TABLES

Table No.

Section 1
PURPOSE

Photovoltaic conversion of solar energy for auxiliary power in space vehicles is, at present, the most practical source of auxiliary power of this type and is, essentially, the only proven method. Current space programs rely almost exclusively on photovoltaic conversion by silicon solar cells for all but the shortest of space flights. Similarly, silicon cells can also be employed for the conversion of solar energy to electrical energy in earth-bound applications.

In general, our purpose is to improve the design of silicon cell power systems by improving the dependability and performance and by reducing the cost. The following three factors contribute to the efficiency of conversion of solar radiant energy to electrical energy by silicon solar cells:

1. the performance characteristics of the silicon solar cell,
2. the radiation incident on the solar cell, and
3. the heat transfer environment of the silicon solar cell.

The photovoltaic cell performance "characteristics" refer to curves showing electrical power , current, and voltage output data as functions of:

1. the total intensity of the incident radiation,
2. the spectral distribution of the incident radiation, and
3. the cell temperature.

The incident radiation can be described in terms of the total intensity, the spectral distribution, and the angle of incidence upon the photovoltaic cell assembly. The heat transfer environment of the photovoltaic cell is important since there is considerable reduction of solar cell conversion efficiency with increasing cell temperature.

More specifically, this particular program is concerned with the use of concentrated and filtered solar radiation on silicon photovoltaic cells in solar power systems. The purpose of this study of concentration of such radiation is to increase the power obtained per unit cell area, thus reducing the weight and the cost. It is anticipated that filtering will afford important increases of power output per cell by rejecting radiations which mostly heat the cells and by accepting only the radiations which most advantageously yield power output.

Since the first use of silicon cells on Vanguard I, considerable progress has been made in improving the efficiency of the basic solar cell and in improving the efficiency gain effected by cell coating to increase the radiation of heat and, to some extent, to reduce the absorption of radiation which merely heats the cells.

In addition, the use of filters on the radiation concentrating surfaces is also considered in this study as a further means of increasing the power obtained per cell. The proper application of filters and concentrators to solar energy conversion results in a reduction in the weight and cost of the system.

In order to design the solar cells, filters and concentrators in a photovoltaic cell solar power system and to evaluate the cost and performance of the system, it is necessary to consider the entire power system.

The studies of the first six months of the contract work period will lead to the delivery of sample spectrally selective optical coatings on glass substrates, in accordance with the contract statement of work.

Section 2

ABSTRACT

Performance analyses of silicon cell solar power systems using radiation concentration and filtering have been obtained. The performance characteristics of silicon photovoltaic cells and filters have been studied with respect to the relation of their characteristics to the power system design and performance. The elementary conditions of system design for optimum performance have been established. The elements of a plan have been outlined for the development of adequate methods for the design and performance analysis of photovoltaic cell solar power systems using radiation concentration and filtering. Also, a basic plan for the construction of a prototype solar power system with concentration and filtering has been outlined.

Section 3

PUBLICATIONS, LECTURES, REPORTS AND CONFERENCES

The following publications, lectures, reports and conferences have resulted directly from research and development by Spectrolab under Contract No. DA 36-039 SC-87449 during the report period 1 July 1961 through 31 December 1961.

Reports

Monthly Letter of Progress reports for the report period have been submitted as follows:

No. 1, July 1961; No. 2, August 1961; No. 3, September 1961; No. 4, October 1961; No. 5, November 1961; No. 6, December 1961. Also, the first semi-annual report was submitted, i.e. Technical Summary Report No.1, 1 June 1961 through 30 June 1961.

Section 4

FACTUAL DATA

Task A. Performance Studies of Solar Power System Using Silicon Cells

Phase 1. An Elementary Study of Solar Cell Performance with Radiation Concentration and Filtering.

The analysis of this section is based upon cells which are typical of those in production during 1960. The particular cell which is the subject of this study will be designated "1960 non-gridded red cell". The spectral sensitivity of this cell is shown in Fig. 1. The cell was covered with a Solakote "A" filter for the improvement of its emissivity and absorptivity. The spectral emissivity of the "1960 non-gridded red cell" with Solakote "A" filter is shown in Figure 2. The performance of the "1960 non-gridded red cell" for conditions of deep space under air-mass-zero insolation (see Fig.1) was determined using the following simple approximations of the radiative heat transfer properties of the cell and panel surfaces:

Cell surface-area utilization	0.90
Coated-cell emissivity	0.87
Coated-cell solar absorptivity	0.91
Effective emissivity of non-active front panel surface	0.65
Effective absorptivity of non-active front panel surface	0.20
Rear panel surface emissivity	0.90
Thermal conductance from front panel surface to rear panel surface	∞

The relative performance of this cell as a function of temperature is shown in Figure 3.

Under the above-described conditions, the equilibrium temperature would be 317°K at unity concentration ratio for cells having an efficiency of ten percent. Fig. 4 compares the curve of equilibrium temperature as a function of incident energy for ten-percent efficient bare cells with the same data for Solakote "A" coated cells of ten-percent efficiency. Also, using the aforementioned approximations, curves of the equilibrium temperature, the thermal degradation (i.e., the relative efficiency) and the relative output of 1960 non-gridded red cells having Solakote "A" filters were obtained as functions of the incident energy and are shown in Figure 5. The saturation effect of high irradiation on the performance of silicon cells was neglected in computing these curves. The relative output curve indicates that the cell output rises rather slowly with incident energy and reaches a broad peak at approximately 310 mw/cm^2 incident energy, at which point the equilibrium temperature of the cell is 387°K. At incident energies exceeding 310 mw/cm^2, the output decreases with increasing irradiation.

The performance curves shown in Fig. 6 as functions of incident energy, but at constant cell temperature, indicate that output efficiency will be further degraded at high illumination levels. As will be indicated later, this is due to cell series-resistance.

In Fig. 5 it is shown that for an achromatic concentrator, a maximum output gain of only about 28 percent is achieved at an energy concentration ratio of 310/140 = 2.2, and an area concentration ratio of 2.2/rs, where "r" is the concentrator reflectance and "s" is the area utilization factor. Since the solar cell has varying spectral sensitivity and an approximately constant absorptivity over the spectral range of the incident radiation, an additional gain can be achieved by concentrating only the part of the spectrum which is most active in producing electrical power and by eliminating the regions for which the thermal degradation predominates.

It is clear from basic considerations that under the conditions described, the maximum output for such a cell array (using 1960 non-gridded "red" cells) would result from monochromatic irradiation at a wavelength of about 820 mμ and an intensity of about 310 mw/cm^2 (ignoring saturation effects). For truly monochromatic light, this would require an infinite concentration ratio. Fortunately, suitably reducing the concentration ratio does not great affect the output.

An analysis of cell output as a function of area concentration ratio, assuming 310 mw/cm^2 incident energy on the cell, was made by varying the bandwidth transmitted to the solar cell. The results of this analysis presented in Fig. 7 show that by spectral selection and concentration it is possible, in an ideal sense, to increase the cell output from 1.28 to 3.04 times that of a coated, oriented, non-concentrated and, substantially, non-filtering system. Thus, the relative output is reduced by only 4 percent for a reduction in concentration ratio from infinity to 10. Therefore, the physical factors with respect to size, weight, tracking accuracy, and mechanical and optical design (to provide uniformity) which are associated with large concentration ratios, and which contribute to some of the major advantages of photovoltaic solar conversion as compared to other solar energy power sources, are still valid for a photovoltaic system with filtering and concentration which is associated with a low concentration ratio.

There are negligible gains, and in fact, disadvantages for area concentration ratios greater than 10. However, the relative output falls off rapidly as the area concentration ratio is reduced below 10. For an area concentration ratio of 7, the relative output is down to 2.64, 13 percent below the maximum. The desirable concentration ratio for a given problem would be the result of a compromise obtained by evaluating numerous factors, e.g., complexity, reliability, orientation requirements. For the particular cells and heat transfer environment used in the analysis, the optimum concentration ratio will lie between 2.2 and 10. The results of this preliminary and elementary analysis are summarized in Table 4-I. An important conclusion from these results is that the maximum silicon solar cell output obtained with radiation filtering and concentration, in the deep thermal environment, is about three times the output obtained without filtering and concentration. This maximum of power output under these conditions is due to the opposite effects of the increase of power due to illumination and the degradation of power by cell heating. Of course, if by some means this cell heating is limited as the cell illumination is increased, the maximum silicon solar cell output is much higher and will be limited most probably by cell series-resistance.

It should be emphasized that the foregoing conclusions apply to the "1960 non-gridded red cell", for which the cell series-resistance has been neglected. In addition, these conclusions are based on the heat transfer environment of deep space. In ground applications of solar power systems it is necessary to also consider radiative heat transfer from the sky and terrain as well as heat transfer by convection to the atmosphere, in determining photovoltaic cell temperatures.

Phase 2. Further Studies of Solar Cell Performance with Radiation Concentration and Filtering.

(a) System Configuration.

For these studies, the solar power system is a Cassegrainian configuration of primary and secondary mirrors with an array of silicon solar cells as shown in Figure 8A. The system is assumed to be operating in deep space. The performance of this system has been investigated for various silicon cells and reflection filter designs. (The heat transfer environment is the same in all cases and such that the cell temperatures are determined by the data in Figures 9 through 13).

(b) Solar Cell Array Equilibrium Temperature Analysis.

The following analysis relates steady-state cell temperature to: (a) the incident energy to the cell, (b) the cell conversion efficiency, and (c) the reflector-array geometry for a Cassegrainian reflector system.

The following assumptions were made:

(1) All radiant flux incident on the cell is either absorbed as thermal energy or converted into electrical energy. (Present day cells have high absorptivity characteristics. This characteristic is particularly valid for reflector-filtering concentrator systems since reflection of filtered energy by the cell degrades system overall efficiency.)

(2) All solar energy reflected by the primary reflector is uniformly distributed upon the secondary reflector of the Cassegrainian system.

(3) Emissivity of non-reflective surface (back surface) of primary reflector is 0.95, attainable with coatings.

(4) Emissivity of reflective surfaces is 1.0. (Present reflective coatings have emissivities of approximately 0.95.)

(5) Emissivity of shaded surface of Cassegrainian array is 0.95, attainable with coatings.

(6) The surface properties of the directly sun-lighted surface of the Cassegrainian secondary reflector are:

$\alpha = 0.09$, $\epsilon = 0.90$ (coating properties anticipated in the near future).

(7) Uniform distribution of reflected flux upon the array. (Departure from this assumption is small for the D/d values considered.)

(8) Absorptivity of the reflective surface of the secondary reflector is 0.05 for the Cassegrainian system. (This is presently attainable for selective wavelengths.)

(9) The paraboloidal reflector rim subtends an angle of 100° at its focal point.

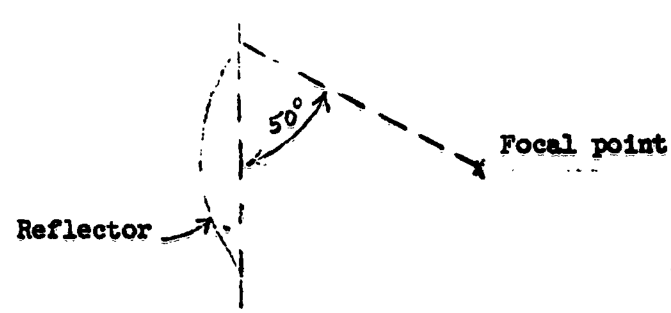

(10) Thermal gradients within the array as well as within the primary and secondary reflectors were neglected. (These gradients are minimal due to weight and thermal distortion considerations.)

(11) Planetary effects such as albedo and surface radiation were neglected.

The following nomenclature was used to define the heat transfer environment of the Cassegrainian solar power system:

A_{proj}	Projected area
A	Surface area
α	Surface solar absorptivity
S	Solar flux
d	Array and secondary reflector diameter
D	Primary reflector diameter
F_e	Emissivity factor
F_A	Configuration factor
σ	Stefan-Boltzmann constant
T	Temperature (°K)
S_c	Flux incident to cell
β	Percent cell conversion of incident energy into electrical energy

Subscripts:

p1	Reflective surface of primary reflector
p2	Non-reflective surface of primary reflector
s1	Surface of secondary reflector
s2	Other reflector surface (relative to s1)
c1	Photovoltaic cell side of array
c2	Other surface of array (relative to c1)
sp	Space

(c) **Analysis:**

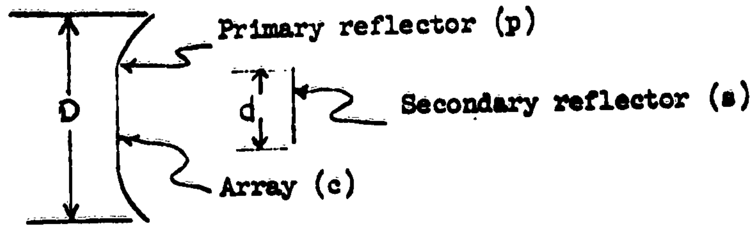

CASSEGRAINIAN FLUX CONCENTRATION REFLECTOR SYSTEM

A heat balance for a Cassegrainian flux concentration reflector system can be expressed, in terms of flux incident to the cell, by the following three equations:

$$\frac{A_{p_{proj}}}{A_p}\left[\alpha_{p_1} S-\left(\frac{S_c}{1-\alpha_{s_1}}\right)\left(\frac{d^2}{D^2-d^2}\right)\right]=\left[F_{e_{p_2-sp}}F_{A_{p_2-sp}}+F_{e_{p_1-sp}}F_{A_{p_1-sp}}+F_{e_{p_1-s_1}}F_{A_{p_1-s_1}}+F_{e_{p_1-c_1}}F_{A_{p_1-c_1}}\right]\sigma T_p^4 - F_{e_{p_1-s_1}}F_{A_{p_1-s_1}}\sigma T_s^4 - F_{e_{p_1-c_1}}F_{A_{p_1-c_1}}\sigma T_c^4, \tag{I}$$

$$\frac{A_{s_{proj}}}{A_s}\left[S\alpha_{s_2}+\frac{S_c\,\alpha_{s_1}}{1-\alpha_{s_1}}\right]=\left[F_{e_{s_2-sp}}F_{A_{s_2-sp}}+F_{e_{s_1-sp}}F_{A_{s_1-sp}}+F_{e_{s_1-c_1}}F_{A_{s_1-c_1}}+F_{e_{s_1-p_1}}F_{A_{s_1-p_1}}\right]\sigma T_s^4 - F_{e_{s_1-c_1}}F_{A_{s_1-c_1}}\sigma T_c^4 - F_{e_{s_1-p_1}}F_{A_{s_1-p_1}}\sigma T_p^4. \tag{II}$$

$$(1-\beta)S_c=\left[F_{e_{c_2-sp}}F_{A_{c_2-sp}}+F_{e_{c_1-sp}}F_{A_{c_1-sp}}+F_{e_{c_1-s_1}}F_{A_{c_1-s_1}}+F_{e_{c_1-p_1}}F_{A_{c_1-p_1}}\right]\sigma T_c^4 - F_{e_{c_1-s_1}}F_{A_{c_1-s_1}}\sigma T_s^4 - F_{e_{c_1-p_1}}F_{A_{c_1-p_1}}\sigma T_p^4. \tag{III}$$

The resulting cell temperatures (to the fourth power) are shown as Figures 9 to 13 for various concentration ratios, C_R, as functions of flux incident to cell and percent cell conversion of incident energy. The results in these figures are based on complete absorptivity of flux incident to the cells. Thus, for systems incorporating flux filtering by the cell, or for systems incorporating low-absorptivity cells, the results will have to be modified.

(d) Performance Analyses.

The power output of a solar cell may be increased by increasing the intensity of the light impinging on it with a solar concentrating-mirror system. However, as previously demonstrated, a point is reached at which an increase in light intensity produces more thermal degradation of the cell than increase in power output. Figure 14 contains a curve of a typical temperature characteristic of an experimental gridded "red" silicon solar cell. A similar curve for a "blue" cell is shown in Figure 15. Also, the response of the cell varies with wavelength and does not best match the solar spectrum in space. If spectrally selective filters are used on the surface of the mirror, the wavelengths of the solar spectrum that contribute more to the heating of the cells than to the power output may not be reflected by the mirror but may instead be transmitted by it, and thus be removed from the working beam finally reaching the solar cells. With this control over the spectrum and temperature of the cells, we may choose our operating conditions to maximate the power output for each physical concentration ratio, that is, $C_R = (D)^2 - 1$.

In the study of this design and performance problem the following cases are considered:

(1) Experimental 1960 gridded "red" cell with its maximum power-temperature characteristic used with ideal concentrator filters.

(2) Heliotek gridded "blue" cell with the "red" cell maximum power-temperature characteristic used with ideal concentrator filters.

(3) Experimental gridded "red" cell with its maximum power-temperature characteristic used with realizable*concentrator filters.

(4) Heliotek gridded "blue" cell with the "red" cell maximum power-temperature characteristic used with realizable*concentrator filters.

(5) Heliotek gridded "blue" cell with its maximum power-temperature characteristic used with ideal filters.

(6) Heliotek gridded "blue" cell with its maximum power-temperature characteristic used with realizable*filters.

The assumptions of the performance analyses are:

(1) The ideal filters used have 100-percent reflectivity in the band-pass region and zero-percent reflectivity in the band-stop region.

---

* "Realizable" is used in the sense that, given sufficient time and effort, it should be possible according to previous experience to produce such a filter, although such filters are not within the present production capability.

(2) The spectral reflection and transmission characteristics of the realizable concentrator filters are shown in Figures 16, 17 and 18.

(3) The response of the solar cell to each wavelength of solar energy is degraded by temperature in the same ratio so that the shape of the response curve remains constant and only its amplitude changes.

(4) The power output of the cell at constant temperature is a linear function of illumination. (For relatively low concentrations, this statement is true.)

(5) The load impedance matches that of the array for any operating condition.

Nomenclature with respect to the spectral characteristics of the solar radiation, relative cell response, and concentration filter reflectance:

β — Percent conversion of energy incident on the solar cell to electrical power.

β_m — The number by which the average response between λ_A and λ_B is multiplied to give the average response between a narrower band-pass region chosen between limits at an equal height on the R_λ curve,

$$\beta_m = \frac{\int_{\lambda_1}^{\lambda_2} R_\lambda S_\lambda \, d\lambda \Big/ \int_{\lambda_1}^{\lambda_2} S_\lambda \, d\lambda}{\int_{\lambda_A}^{\lambda_B} R_\lambda S_\lambda \, d\lambda \Big/ \int_{\lambda_A}^{\lambda_B} S_\lambda \, d\lambda}$$

R_λ The relative response of the solar cell to a wavelength of light, λ.

S_λ The intensity of the solar energy at a wavelength, λ.

λ Wavelength.

λ_A, λ_B The lower and upper cut-off wavelengths of the solar cell, respectively.

λ_1, λ_2 The lower and upper cut-off wavelengths of the filter, respectively.

N_T Coefficient of temperature degradation of the solar cell.

The following calculations have been performed for two types of silicon solar cells: one, called the "experimental 'red' cell", has a spectral response curve which peaks at 0.82 micron; the other, commonly called the "Heliotek 'blue' cell", has a spectral response curve which peaks at 0.85 micron. Graphs of both are presented in Figures 23 and 24. In addition, Figures 23 and 24 include, for the red and blue cells, respectively, the cumulative solar energy and power output as a fraction of the total between λ_A and λ_B. The data for "S" is just the Johnson Curve, the air-mass-zero solar spectrum in space near the earth, where the total flux is 140 mw/cm^2. Of this, the red cell, having cut-off wavelengths of 0.405 micron and 1.165 microns, responds to 95.8 mw/cm^2, while the blue cell, having cut-off wavelengths of 0.36 micron and 1.20 microns responds to 103.5 mw/cm^2.

In order to choose a systematic method of considering the cut-off wavelengths of the filters, we have chosen those wavelengths which fall at equal relative response heights. This "R_λ" designates the bandwidth used by specifying the region located between equal response heights on the response curve of the cell. The fraction of the solar energy and cell power output occurring in the region found by choosing filter band-pass limits at equal height on the response curve of the cell, is shown in Figures 21 and 22 for red and blue cells, respectively. In addition, $(\beta_m - 1)$ is also plotted, where β_m is the multiplier of the average absolute efficiency, at the reference temperature, between λ_A and λ_B, necessary to obtain the average efficiency within the R_λ limits, as defined in the nomenclature. The power output of the array for varying concentration ratios and ideal filter band-pass widths is shown in Figures 19, 20a and 20b for the red and the blue cells, respectively.

For both the red and the blue cells, it was assumed in the calculations that the average absolute value of the response between λ_A and λ_B at 303°K is 13.3 percent. This assumes an absolute peak response of the red cell at 25 percent and of the blue cell at only 21.4 percent. The following analysis and specific example will indicate how the curves in Figures 19, 20a and 20b were constructed.

(e) Optimization Procedure for Ideal Filters.

The first step in the optimization procedure is to determine the method for selecting the bandwidth and the center-line of the filter passband. A preliminary check shows that even for the relatively low concentration ratio of 4, it is not desirable to use the total broad-band energy since narrowing the band-pass limits a small amount, in any arbitrary manner, has the effect of increasing the power output.

Since all of the broad-band energy will not be used, the portion that is used should be chosen in a manner such that with any given amount of solar energy input, the average efficiency of converting solar energy to electrical energy will be the highest. This is done by choosing the filter band-pass limits at equal heights on the response curve of the cell. This choice has a twofold effect on increasing the power output for any energy input. First, with the highest conversion efficiency at a constant temperature, the output is highest. Second, with more of the input energy being converted to electrical energy, there is less that is being converted only into heating, and therefore less thermal degradation.

Now, it remains to use the curves herein presented to find the actual operating point of the cell. This is done in the following example for the experimental "red" cell:

(1) Choose a concentration ratio and R_λ value. In this case, select $C_R = 4$ and $R_\lambda = 0.5$.

(2) The broad-band energy which, without filtering, would be concentrated on the solar-cell array is:

$$S_{conc.} = (C_R) \int_{\lambda_A}^{\lambda_B} S_\lambda \, d\lambda = (4)(95.8) = 383.5 \ mw/cm^2$$

(3) The energy in the R_λ limit of 0.5 is found with the help of Figure 21. From the abscissa of $R_\lambda = 0.5$, we find the corresponding ordinate of the fraction of:

$$\int_{\lambda_A}^{\lambda_B} S_\lambda \, d\lambda$$

that is in that limit, or (0.534). Thus, $S_{conc. \text{ and filter}} = 383.5 \times 0.534 = 204.5 \text{ mw/cm}^2$.

(4) $\beta_{303°K}$ can now be found. From Figure 21, $\beta_m - 1 = 0.46$, or $\beta_m = 1.46$. Hence, if the average absolute value of the response of the cell between λ_A and λ_B is 13.3 percent, then

$$\beta_{303°K} = 1.46 \times 13.3 = 19.42 \text{ percent,}$$

the average absolute response in the wavelength limits dictated by $R_\lambda = 0.5$, and at the temperature 303° K.

(5) The β chosen above will be thermally degraded. Therefore, the actual β of the cell will be less. For the first approximation, choose: $\beta = 14$ percent. Then, from Figure 10 above the 204.5 mw/cm^2 abscissa, we find the $(\text{temperature})^4$ for $\beta = 14$ by interpolating between the $\beta = 10$ and $\beta = 15$ lines:

$$T^4_{(\beta = 14)} = 166 \times 10^8 \text{ °K}^4, \text{ or } T = 358.5° \text{ K.}$$

From Figure 14 we find the thermal degradation coefficient to be:

$$N_T = 0.666$$

$$\beta_T = 19.42\ (0.666) = 12.9 \text{ percent}$$

Hence, we see that our estimate of β was too high, so we make a new lower estimate:

$$\beta = 12.6; \quad T^4 = 169 \times 10^8; \quad T = 360.6;$$

$$\beta = 19.42\ (0.653) = 12.65 \text{ percent.}$$

The two β's now agree as closely as can be expected with the graphical accuracies involved. The power output is then:

$$P = 0.1265\ (204.5) = 24.8 \text{ mw/cm}^2.$$

This procedure is repeated for a number of R_λ values for each concentration ratio until the curves in Figures 19, 20a and 20b are generated. We see that for each concentration ratio, the power output peaks at higher R values for higher concentration ratios. Obviously, neglecting size and weight considerations, the greatest power output will be for $R_\lambda = 1.00$, $C_R = \infty$

(f) Results of Performance Analyses.

Using the methods and the thermal environment data previously discussed, the performance of three "ideal" and three "realizable" filters for use with the "red" and "blue" silicon cells was estimated. Curves for realizable filters are shown in Figures 16, 17 and 18, in the "dotted-line" curves. The "solid-line" curves are convenient approximations used in the computation. The realizable filter characteristics were determined for use with a "red" cell with peak spectral response at wavelength $\lambda = 0.82$ micron. These filters will require from nine to sixteen layers. As the bandwidth narrows, the number of layers required increases. Each ideal filter has the same cut-off wavelength as the corresponding realizable filter and also has zero transmittance in the passband and perfect transmittance outside the passband, as previously defined. For both the red and blue cells, the solar insolation was assumed to be 140 mw/cm^2 and the broad-band efficiency (between λ_A and λ_B) of both cells was assumed to be 13.3 percent at 303°K. This gives the red cell a peak efficiency of 25 percent, and the blue cell a peak of 21.4 percent. Thus, it is seen immediately that for equal broad-band efficiencies, and at high concentration ratio, C_R, the red cell performs better than the blue. However, for equal peak efficiencies, the opposite is true.

The computations and results for the ideal filters are shown in Table 4 - IV. From Figures 23 and 24, the R_λ values corresponding to the filter cutoffs were found and tabulated. In those few cases where the "left" and "right" values of R_λ differ by a small amount, the average is given. The concentration ratios may be checked against Figures 19 and 20 by noting which curves peak at the specified values of R_λ. Finally, the output power was read from the peak values of these curves, and tabulated in Table 4 - IV.

Table 4 - V shows computations made for the performance of the realizable filters.

It is especially important to note here that the "experimental silicon gridded 'red' cell" (with temperature coefficient of 0.0060/°C) and the "Heliotek silicon gridded 'blue' cell" are actual existing cell types. The hypothetical silicon gridded blue cell, on the other hand, is a purely hypothetical cell with the same characteristics as the existing Heliotek "blue" cell, except for the temperature power coefficient which is the same as that for the "red" cell. This hypothetical cell is included in order to demonstrate the critical importance of the temperature-power coefficient. For comparison with the results in Table 4-II, the cell power outputs at a concentration ratio of one and with no filters, except as used on the cell in all cases, are as shown in Table 4-III.

For the higher concentration ratios the cell power outputs are much greater with the ideal filters than with the realizable filters; however, for the lowest concentration ratios the power outputs per cell are only slightly higher for the ideal filter. The reduction of power output with the realizable filters is due almost entirely to the excessive heating effect of the radiation transmitted to the solar cells by the realizable filters outside their passbands. This effect is relatively less at the lowest concentration ratio since in this case the heat transmitted to the cell outside the passband is small in comparison to that transmitted in the wide passband. With the ideal filter the maximum power output per cell occurs at the highest concentration ratio; however, with the realizable filters the maximum power output per cell occurs at an optimum concentration ratio between 9 and 4. The curves on Figure 25 are presented for better understanding of the results in Table 4-II. In Figure 25 curves for the silicon-cell relative spectral response, $R(\lambda)$, and the normalized relative solar spectral response are shown for the "red" and the "blue" cells. The total areas under the solar spectral reaponse curves are equal since they are normalized. The power output of a solar cell due to a spectral band of solar radiation as estimated in this report is:

$$H_o f \eta \Delta A$$

where H_o = total solar incidence, mw/cm^2.

f = transmittance of filter system in the spectral band, $\Delta\lambda$.

η = cell efficiency.

ΔA = area under the solar spectral response curve in the spectral band, $\Delta\lambda$.

The spectral response curves are critically significant inasmuch as, for a given radiation concentration ratio, the maximum power output per cell under the conditions of this study occurs for both the ideal and realizable filters, when the filter cut-off wavelengths are at equal values of $R(\lambda)$ on each side of the $R(\lambda)$ curve. This data, with the spectral reflectance characteristics of the filters, the temperature of the cells, and the cell temperature-power characteristics, determinesthe cell power output. Thus, for example, let us compare the outputs of both the "red" and the "blue" cells with the temperature-power coefficient 0.0060/°C. These cases, for the same concentration ratios and filters, differ only as the "red" and "blue" cells characteristic curves on Figure 25 differ. For these corresponding cases, the power output of the "red" cells exceeds the power output for the "blue" cells only as the area under the solar spectral response curves within the filter passband in Figure 25 for the "red" exceeds that for the "blue" cell. The increase of power of the blue cell with its proper temperature-power coefficient, 0.0041/°C, is due to both its lower temperature-power coefficient and to the filters which are optimum for the "blue" cells.

(g) A Summary Statement of the Elementary Design Conditions for Optimum Performance of a Silicon-Cell Solar Power System Using Radiation Filtering and Concentration.

The elementary design conditions for optimum performance of a silicon-cell solar power system which employs both filtering and concentration have been previously discussed and analyzed in this report.

Consider first the case where the greatest maximum power per cell is sought. For ideal filters, the filter pass-bandwidth should be small and at the wavelength of cell maximum spectral response and with the small bandwidth, the illumination concentration ratio should be so high that the combined conditions of illumination intensity and cell temperature yield the maximum power output. For realizable filters, the illumination concentration ratio will be in the range 6 to 12, depending on the filter performance, and the corresponding filter passband limits will intersect the solar-cell relative response curve at equal values on the high and low wavelength sides of the curve. As the filter performance improves, the illumination concentration ratio will become higher and the filter pass-bandwidth will be narrower for the greatest maximum power performance. For the case of the maximum power per unit area of system solar beam aperture, the radiation concentration ratio is only slightly greater than unity, even with ideal filters. With realizable filters, the greatest power per unit solar beam aperture occurs at radiation concentration ratio of unity and a concentrator filter yields little, if any, advantage. Thus, it is not to be expected that radiation concentration and filtering will yield more power per unit area of solar beam.

(h) Major Conclusions of the System Performance Analyses.

For silicon cell solar power systems operating in deep space heat transfer environment:

(1) The greatest possible power output per cell with radiation concentration and filtering is three to four times as great as the power output without concentration and filtering, depending on the cell performance characteristics.

(2) The feasible power output per cell, with presently available silicon cells and presently feasible filters, is three times greater with radiation concentration and filtering than without concentration and filtering. This power output per cell will occur at a concentration ratio in the range 6 to 12.

(3) The maximum power output per cell is critically dependent on the silicon cell and filter performance characteristics.

TABLE 4 - I

Elementary Study of Solar-Cell Output with Radiation Filtering and Concentration

Concentration Ratio, C_R	Temperature °K	Filters	Power Output (percent)
1	317°	None	100
2.2	-	Solakote "A"	128
10	-	Perfect narrow band	282
∞	387°	Perfect narrow band	304

TABLE 4 - II

SUMMARY OF RESULTS FOR SOLAR CELL OUTPUTS WITH RADIATION FILTERING AND CONCENTRATION

Solar Cell	Experimental Silicon Gridded "red"			Heliotek Silicon Gridded "blue"			Heliotek Silicon Gridded "blue"		
Temperature Power Coefficient	"red" cell .0060/° C Figure 5-14			"red" cell .0060/° C Figure 5-14			"blue" cell .0041/°C Figure 5-15		
Concentration ratio, C_R	16	9	4	16	9	4	16	9	4
Filters Cutoff Wave-length (microns)	.77 .89	.72 .92	.625 .975	.77 .89	.72 .92	.625 .975	.695 .925	.630 .950	.500 1.020
Ideal Filter: Power Output (mw/cm^2)	35.25	32.25	26.90	29.60	28.50	25.30	41.40	38.40	30.70
Realizable Filters:	SL120/83	SL200/82	SL350/80	SL120/83	SL200/82	SL350/80	SL230/81	SL320/79	SL520/76
Power Output (mw/cm^2)	15.10	24.80	24.80	14.0	22.6	23.7	31.2	35.3	29.5

TABLE 4-III

CELL POWER OUTPUTS WITHOUT CONCENTRATION OR FILTERS

CELL	EXPERIMENTAL SILICON GRIDDED "RED"	HELIOTEK SILICON GRIDDED "BLUE"	HELIOTEK SILICON GRIDDED "BLUE"
Temperature-Power Characteristic	"Red" cell .0060/°C Figure 5-14	"Red" cell .0060/°C Figure 5-14	"Blue" cell .0041/°C Figure 5-15
Output Power (mw/cm^2)	10.5	11.4	12.2

TABLE 4 - IV

COMPUTATION OF SOLAR CELL OUTPUT WITH IDEAL FILTERS
ON ONE CONCENTRATOR MIRROR

Solar Cell	Experimental Silicon Gridded "red"			Hypothetical Silicon Gridded "blue"			Heliotek Silicon Gridded "blue"		
Temperature-Power Characteristic	"Red" Cell .0060/° C Figure 5-14			"Red" Cell .0060/°C Figure 5-14			"Blue" Cell .0041/° C Figure 5-15		
Concentrator ratio, C_R	16	9	4	16	9	4	16	9	4
Ideal Filters									
Bandwidth Microns	.120	.200	.350	.120	.200	.350	.230	.320	.520
Cutoff Wavelength (microns)	.77 .89	.72 .92	.625 .975	.77 .89	.72 .92	.625 .975	.695 .925	.630 .950	.500 1.020
R_λ	.91	.82	.60	.97	.91	.74	.89	.79	.51
Output Power mw/cm^2	35.25	32.55	26.90	29.60	28.50	25.30	41.40	38.50	30.70

TABLE 4 - V

COMPUTATION OF SOLAR CELL OUTPUT WITH REALIZABLE FILTER ON ONE CONCENTRATOR MIRROR

1. Solar Cell	Experimental Silicon Gridded "red"			Heliotek Silicon Gridded "blue"			Heliotek Silicon Gridded "blue"		
2. Temperature Power Characteristic	"red" cell .0060/° C Figure 5-14			"red" cell .0060/°C Figure 5-14			"blue" cell .0041/°C Figure 5-15		
3. Concentration Ratio, C_R	16	9	4	16	9	4	16	9	4
Filters:									
4. Bandwidth Microns	.120	.200	.350	.120	.200	.350	.230	.320	.520
5. Cutoff Wavelengths, Microns	.77	.72	.625	.77	.72	.625	.695	.630	.500
	.89	.92	.975	.89	.92	.975	.925	.950	1.020
6. Filter Number	SL120/83	SL200/82	SL350/80	SL120/83	SL200/82	SL350/80	SL230/81	SL320/79	SL520/76
7. R_λ	.91	.82	.61	.98	.92	.75	.89	.79	.51
Fraction of Solar Energy between λ_1 and λ_2									
8. $\dfrac{\int_{\lambda_1}^{\lambda_2} S(\lambda)\,d\lambda}{\int_{\lambda_A}^{\lambda_B} S(\lambda)\,d\lambda}$	.19	.23	.44	.17	.21	.40	.25	.37	.65

9. Reflectance x fraction of solar energy in two bands: λ_A to λ_1 and λ_2 to λ_B	.08	.08	.06	.08	.08	.06	.07	.06	.03
10. Reflectance x fraction of solar energy outside range of λ_A to λ_B	.02	.02	.02	.02	.02	.02	.02	.02	.02
11. Sum: (8) + (9) + (10)*	.29	.33	.52	.27	.31	.48	.34	.45	.70
12. Incident flux, ideal filter, $(C_R) \cdot (8) \cdot \int_{\lambda_A}^{\lambda_B} S_\lambda \, d\lambda$ (mw/cm^2)	291	198	169	291	198	169	414	344	269
13. Flux incident to cells with realizable filters $(C_R) \cdot (11) \cdot \int_{\lambda_A}^{\lambda_B} S_\lambda \, d\lambda$ (mw/cm^2)	445	284	199	445	284	199	564	420	290
14. Cell temperature, ideal filter °K	390	355	342	391	356	343	424	406	386
15. Cell temperature realizable filter °K	443	394	358	444	396	359	472	430	395

*Numbers in parentheses refer to corresponding item numbers on this page.

TABLE 4 - V (Cont'd)

16. Temperature degradation factor, ideal filter	.47	.68	.76	.46	.67	.74	.51	.58	.66
17. Temperature degradation factor, realizable filter	.16	.45	.67	.15	.44	.66	.31	.48	.62
18. Fraction of cell response between λ_1 and λ_2 $\frac{\int_{\lambda_1}^{\lambda_2} S(\lambda) R_\lambda d\lambda}{\int_{\lambda_A}^{\lambda_B} S(\lambda) R_\lambda d\lambda}$	.26	.40	.68	.20	.35	.62	.29	.45	.77
19. Reflectance x fraction of solar radiation outside range λ_1 to λ_2 $R \times [(8)-(18)]$*	.07	.06	.03	.08	.06	.04	.07	.05	.02
20. Sum: (18) + (19)*	.33	.46	.71	.28	.41	.66	.36	.50	.79
Output of cells with ideal filters mw/cm²	35.25	32.55	26.90	29.60	28.50	25.30	41.40	38.50	30.70
21. Ratio: $\frac{(17) \times (20)}{(16) \times (18)}$*	.43	.71	.92	.46	.79	.95	.75	.92	.96
Output of cells with realizable filters mw/cm²	15.1	24.8	24.8	14.0	22.6	23.7	31.2	35.3	29.5

*See footnote on preceding page.

TASK B. Silicon Solar Cell Performance Characteristics

The development of filters and concentrators to be used in systems for the conversion of solar radiation to electrical power by means of silicon photovoltaic cells requires wide and accurate knowledge of the silicon cell performance characteristics.

Phase 1. The principal characteristic curves for silicon solar cells are:

(1) Curves of cell current vs. cell voltage for various illumination intensities and temperatures.

This data is for a constant, usually a standard, temperature and for the same spectral distribution of energy in the incident radiation. Typical silicon cell I-V curves are shown in Figures 26, A-2 and A-8b.*

(2) Cell maximum-power output.

At a particular point of each I-V curve the cell output power determined by the product, $P = VI$, is a maximum. The maximum power points are located in Figures 26 and A-2. The maximum power outputs for a cell are to be identified with the same conditions as the I-V curves from which they were determined, i.e., the angle of incidence, the temperature, and the intensity and spectral energy distribution of radiation. At maximum power,

$$P = P_{max}, \ V = V_{mp}, \ I = I_{mp}.$$

(3) Temperature effects on P_{max}, V_{max} and I_{max}.

Figure 26 shows a typical set of I-V curves for various temperatures. In Figures 27 and 28 maximum power, P_{max}; voltage at maximum power, V_{mp}; and current at

---

*Figure designations preceded by letter "A" refer to figures appearing in the Appendix to this report.

$I = I_{mp}$ (all for the I-V curves of Figure 26) are plotted as functions of temperature. The effect of temperature on cell maximum power is usually presented as relative efficiency at maximum power, as, for example, in Figures 14 and 15 which consist of the curves for an experimental gridded "red" cell and for a typical Heliotek gridded "blue" cell.

(4) Effect of illumination intensity on cell maximum power output, maximum-power-point voltage, and efficiency.

This data is plotted in Figure A-4 for experimental cells A-N-12 and A-N-16. The I-V curves for these cells are shown in Figure A - 2. Also shown in Figure A - 4 is the effect of increased insolation for three hypothetical cells of similar characteristics to the aforementioned experimental cells, except that the three hypothetical cells have series resistances of 0, 0.5 and 1.0 ohms, respectively.

(5) Relative spectral response.

The relative spectral response curves of an experimental gridded "red" cell and of a typical Heliotek gridded "blue" cell are shown in Figures 23 and 24. The relative spectral response is denoted by $R(\lambda)$ and is defined as the following ratio:

$$R(\lambda) = \frac{\text{Short circuit current per unit incident ratiation intensity per unit of spectral bandwidth, at the wavelength, } \lambda.}{\text{Peak value of the short-circuit current per unit incident radiation intensity per unit of spectral bandwidth.}}$$

It is assumed in the performance analyses in this report that silicon-cell maximum power response to a broad spectral band of high intensity radiation is

$$P_{max} = p_{\lambda max} \int R(\lambda)S(\lambda)d\lambda \qquad (1)$$

where $p_{\lambda max}$ = solar cell maximum power per unit of spectral bandwidth and per unit of illumination intensity at $\lambda = \lambda_{max}$, and

λ_{max} = λ at which $R(\lambda) = 1$.

The exact extent to which Equation (1) is valid remains to be investigated and determined. In support of the supposition represented by Equation (1), it is well known that the maximum power output to broad-band illumination is, except for small effects due to cell series resistance, proportional to the total illumination, as indicated in Figure A - 3 (revised). As indicated in Figure A - 4, the maximum power voltage changes very little with illumination but, as is well known, the cell short circuit current, I_{sc}, and the cell maximum power current, I_{mp}, are both for cells with acceptably small series resistance proportional to illumination intensity.

The effect of cell series resistance on I_{max} and I_{sc}, as functions of cell illumination, is presented in Figure A - 3 (revised). (The series resistances of Heliotek gridded "blue" cells are in the range 0.38 to 0.48 ohm.)

(6) Silicon cell assembly spectral normal absorptive characteristics.

The spectral normal absorptance is the ratio of the energy absorbed by the surface to the energy incident upon it for normally incident radiation at any particular wavelength. The spectral absorptance of the cell assembly is important with respect to: (a) radiations for which the cells yield power, (b) radiations which merely heat the cells, and (c) ultraviolet radiations which may damage the cell cover adhesive. Since the silicon cells are opaque in the spectral range of interest, normal absorptance may be determined from measurements of reflectance. The absorptance and reflectance, as well as the relative spectral response, are important for angles of incidence less than 90° in some applications. The spectral absorptance of the solar cells is closely related, physically, to their spectral emittance.

(7) Silicon-cell assembly hemispherical total emittance.

Hemispherical total emittance is defined as the ratio of: (a) the total energy radiated at all wavelengths from a surface to the hemisphere of space surrounding the surface, to (b) the total energy radiated at all wavelengths by a black body at the same temperature. This emittance is critically important with respect to the operating temperature of the silicon cells. For solar cells with spectrally selective absorptance, the spectral emittance is also selective, and thus, the hemispherical total emittance may vary somewhat with temperature. The hemispherical total emittance of silicon cell assemblies is measured by existing techniques. An example of emittance measurements for a Heliotek gridded silicon cell covered with a Solakote "B" filter is presented in Figure 29.

In addition to the discussion of the serious effects of cell series resistance on maximum power output, the report by M. Wolf and Hans Rauschenbach, "Series

Resistance Effects on Solar Cell Measurements,"* also includes a careful discussion of the relation of illumination intensity to the I-V curve and hence to maximum power output. This relationship is such that at constant cell temperature the I-V curves for various intensities of illumination all fit upon each other (to a good approximation) when shifted, both (a) vertically, by an increment of current due to the increment of illumination, and (b) horizontally, by a voltage drop due to the increment of current flowing in the series resistance of the cell. An example of I-V curve shifting is shown in Figure 30; the I-V curves for the solar irradiances 100, 200, and 300 mw/cm^2, which all fit the curve for 400 mw/cm^2 quite well. This method of I-V curve shifting can be used to determine the "light current" and to estimate cell series resistance.

Phase 2. Summary of Silicon Solar Cell Characteristics Relative to the Performance of Solar Power Systems with Radiation Filtering and Concentration.

The following characteristics of silicon photovoltaic cells are critically important to the attainment of high performance of solar power systems using concentrated and filtered radiation on such cells:

(1) Short circuit current spectral response.
(2) Temperature degradation of maximum power and voltage.
(3) Spectral normal absorptance.
(4) Hemispherical total emittance.

Of course, high maximum spectral response occurring in the spectral region of high solar irradiance and small temperature degradation of maximum power will each contribute

*Paper No. CP 61-1006 presented at the American Institute of Electrical Engineers meeting, 23-25 August, 1961 at Salt Lake City Utah. (Included in revised form as appendix of Spectrolab Technical Summary Report No. 2, June 1961, this contract.)

to high system performance. Also, it is highly important that the series resistance of the cells be suitably small so that at high illumination intensities the response remains proportional to illumination intensity. As the power system analyses in this report show, the temperature degradation effect is a major one, especially at the high temperatures which occur at high radiation intensities. The spectral normal absorptance is of importance since it is desirable that the radiation which is converted to power be absorbed and the radiation which would merely heat the cell be reflected. Also, the hemispherical total emittance of the solar cells should be high in order that heat may be rejected by the cell at favorably low temperatures.

As a result of the foregoing solar power system analyses, more specific criteria have evolved with respect to solar-cell performance characteristics.

Task C. Filter Performance Characteristics.

The system performance analyses of this report consider the "idealized" filter as well as filters which are physically attainable. Ideally, the filters should permit all radiation within a particular spectral band to reach the cell faces and should prevent all radiation outside this passband from reaching the cells. Under actual physical conditions, less than this ideal will be attained. It should be possible to produce filters having characteristic curves corresponding to those in Figures 16, 17 and 18. As indicated in the performance analyses, the performance of the solar power system is critically dependent on filter performance.

Elementary considerations indicate that the best system performance will be attained in systems using both filtering and concentration by accomplishing a major part of the radiation filtering at the concentrator surfaces. Additional improvement can then be attained by means of covers on the solar cells. These covers should be designed for optimum performance specifically with respect to:

(1) The protection of the solar cells from damage by contact with other materials and the atmosphere.

(2) The protection of the solar cells from damage by electron bombardment in space.

(3) Hemispherical total emittance.

All of the aforementioned must be attained without serious impairment of the transmission of the radiation effective in yielding power output. The production of a filter on the silicon cells which emits strongly in the spectral range 1 to 4 microns and which also reflects strongly in this range is difficult, if not impossible. However, by designing the cell and its filter for emission and providing a filter on the concentrator for the required reflectance, both may be accomplished. Since excellent cell filters already exist which take into account the aforementioned requirements, the studies discussed in this report were primarily concerned with the use of filters on the concentrator surfaces. Moreover, reflection filters were considered, exclusively, since this type of filter has better performance characteristics and is more suitable, physically, to the optical arrangement of the system.

Section 5

CONCLUSIONS

The employment of concentration and filtering of the radiation incident on the photovoltaic cells of solar power systems will afford valuable improvements in cost and weight of solar power systems. These improvements will result from increased power per cell, but not from increased power per unit solar beam area. The available increase of power per cell will significantly reduce system cost and weight, however.

The next steps toward the development of prototypes are:

1. To develop reflecting filters on concentrator surfaces.
2. To develop and apply adequate design and performance methods to prototype designs.

Section 6

OUTLINE OF A PLAN FOR FUTURE WORK

1. Fabricate reflection filters on concentrator surfaces.

2. Develop adequate methods of performance analysis:

   (a) Use test results to define and determine a valid relative spectral response of solar cells including temperature effects.

   (b) Develop methods and obtain data for computing cell temperatures in solar power systems in deep space, in earth orbit, and, in particular, on the surface of the earth.

   (c) Establish complete, detailed mathematical methods for designing photovoltaic solar power systems which are optimum for specified performance, cost, size and weight.

3. Design and evaluate prototype solar power systems for particular applications.

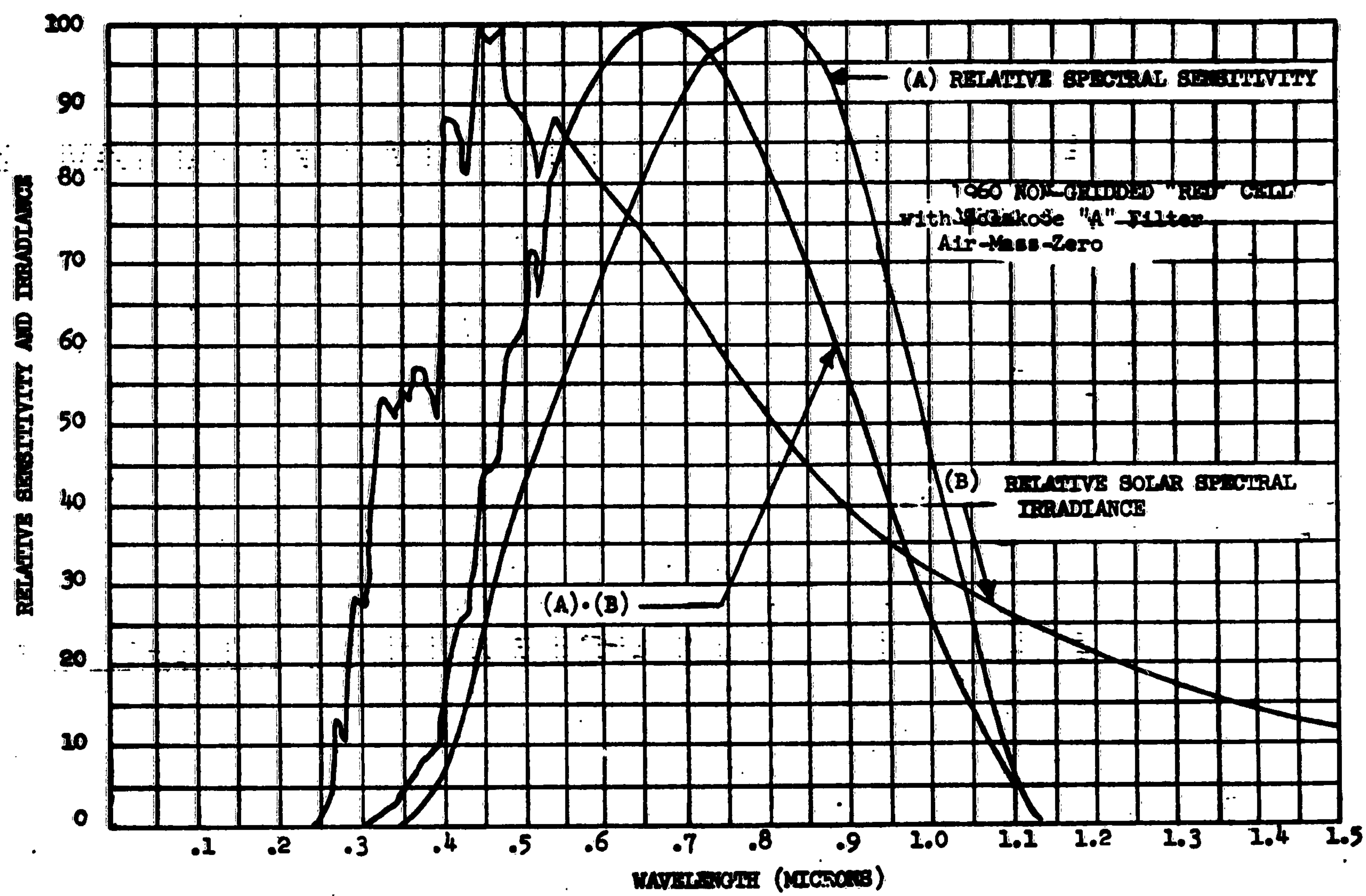

FIGURE 1. TYPICAL SILICON CELL RELATIVE SPECTRAL RESPONSE RELATIVE SOLAR SPECTRAL IRRADIANCE, AND THEIR PRODUCT.

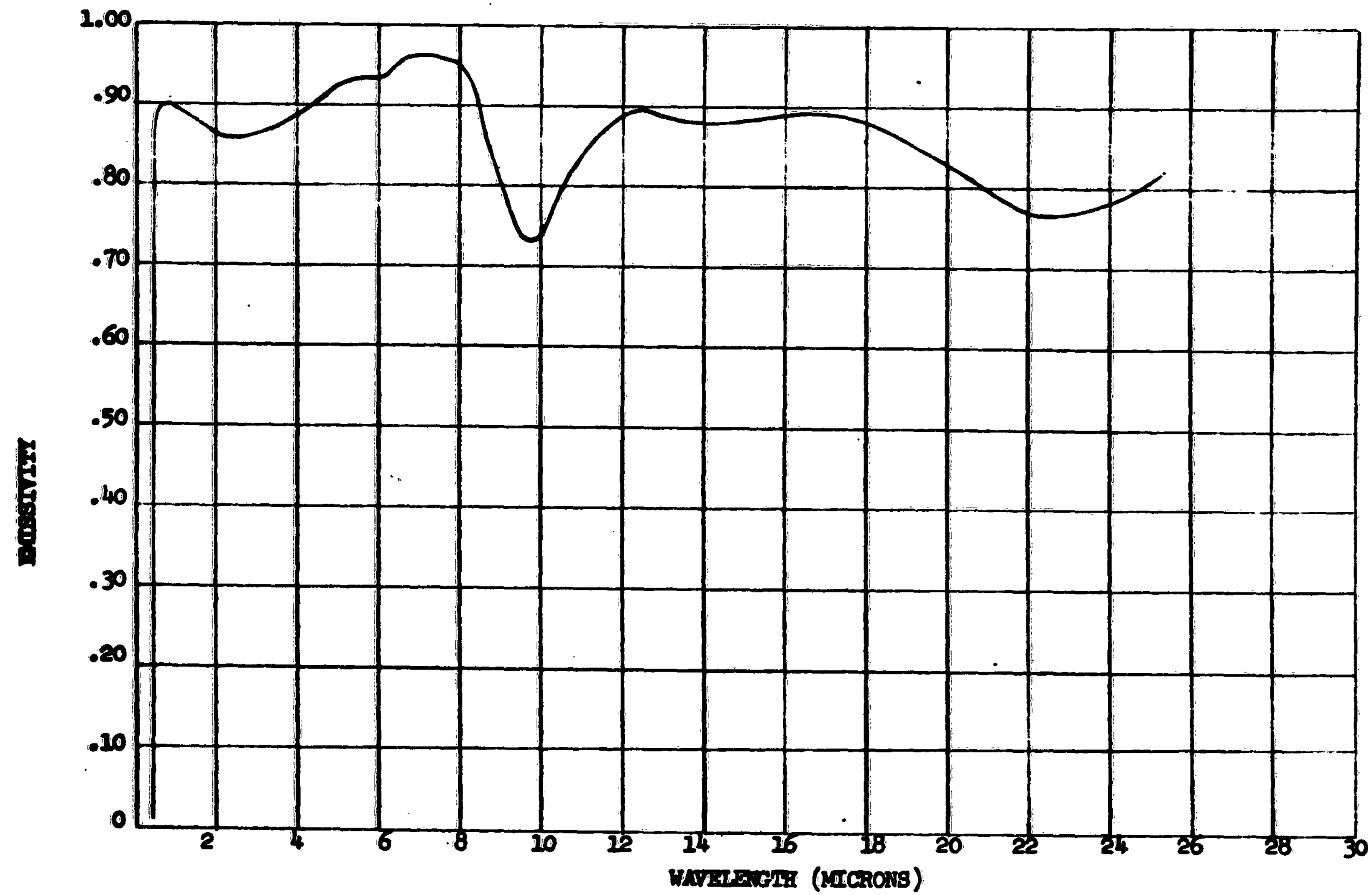

FIGURE 2. SPECTRAL EMISSIVITY OF TYPICAL 1960 NON-GRIDDED "RED" CELL WITH SOLAKOTE "A" FILTER.

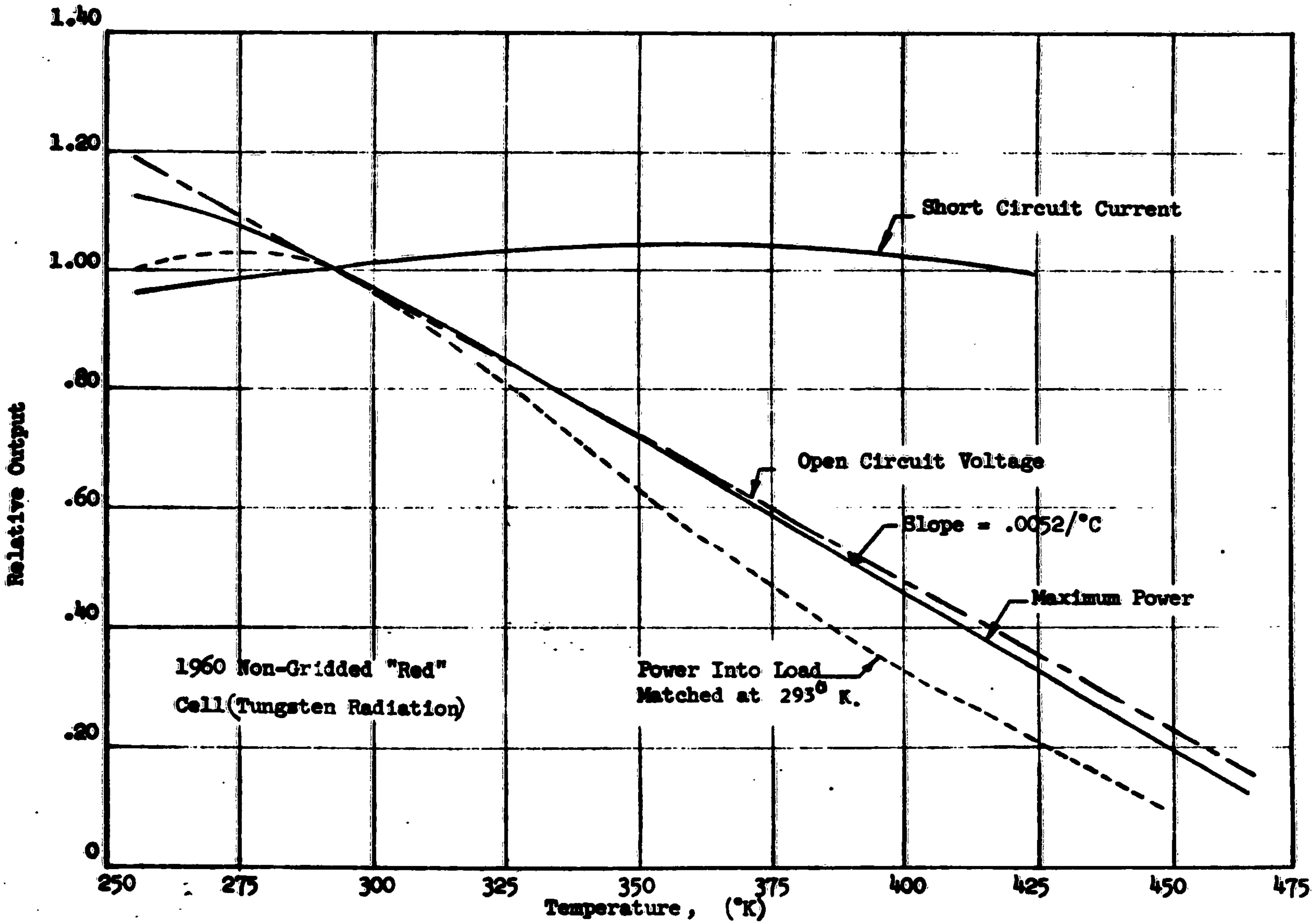

Figure 3. Relative Thermal Effects on Open Circuit Voltage, Short Circuit Current, Maximum Power, and Power Into a Matched Load* for Typical Silicon Solar Cell.

* Room Temperature

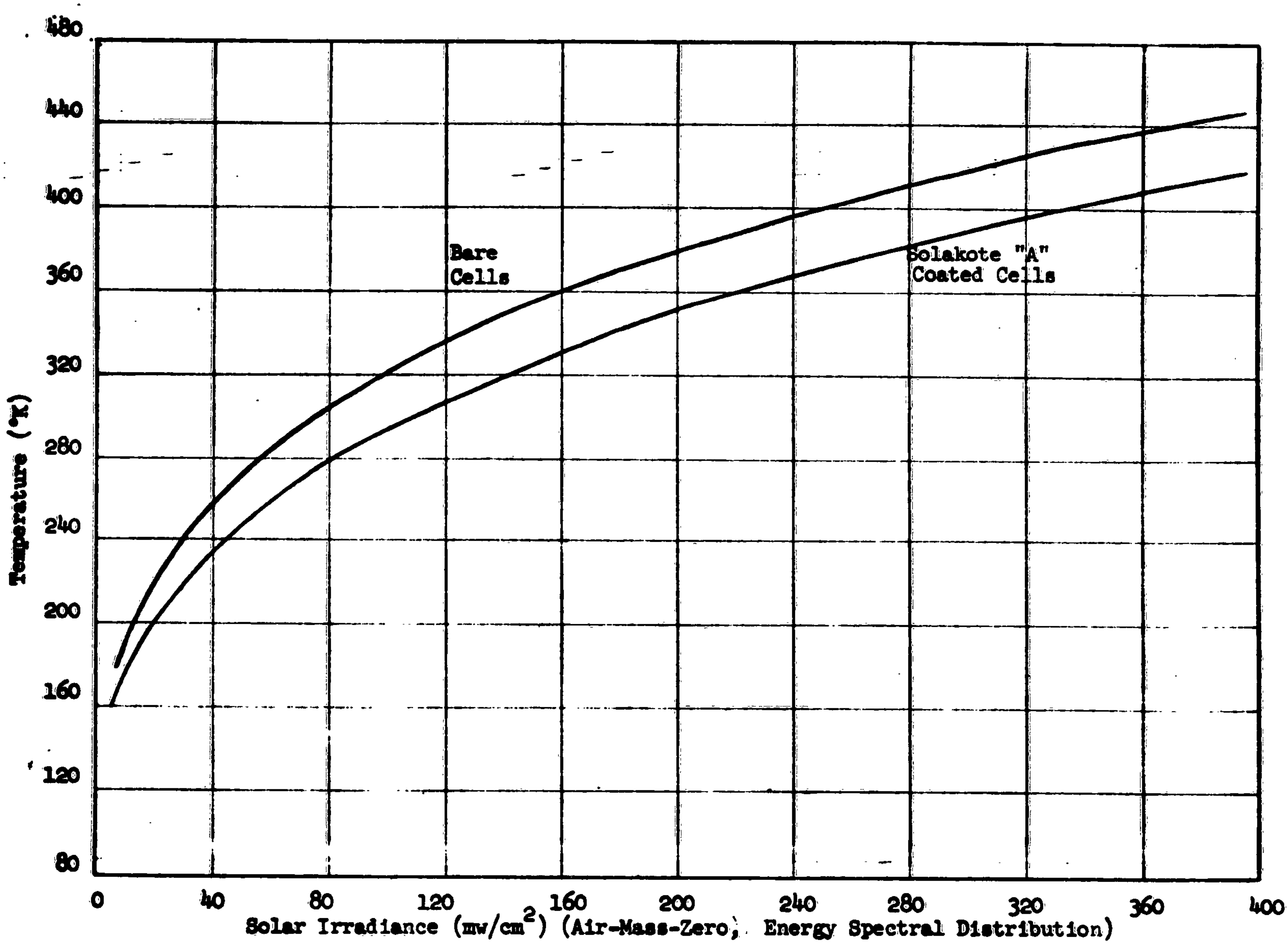

Figure 4. Equilibrium Temperature vs Solar Irradiance for 1960 Non-Gridded "Red" Cells.

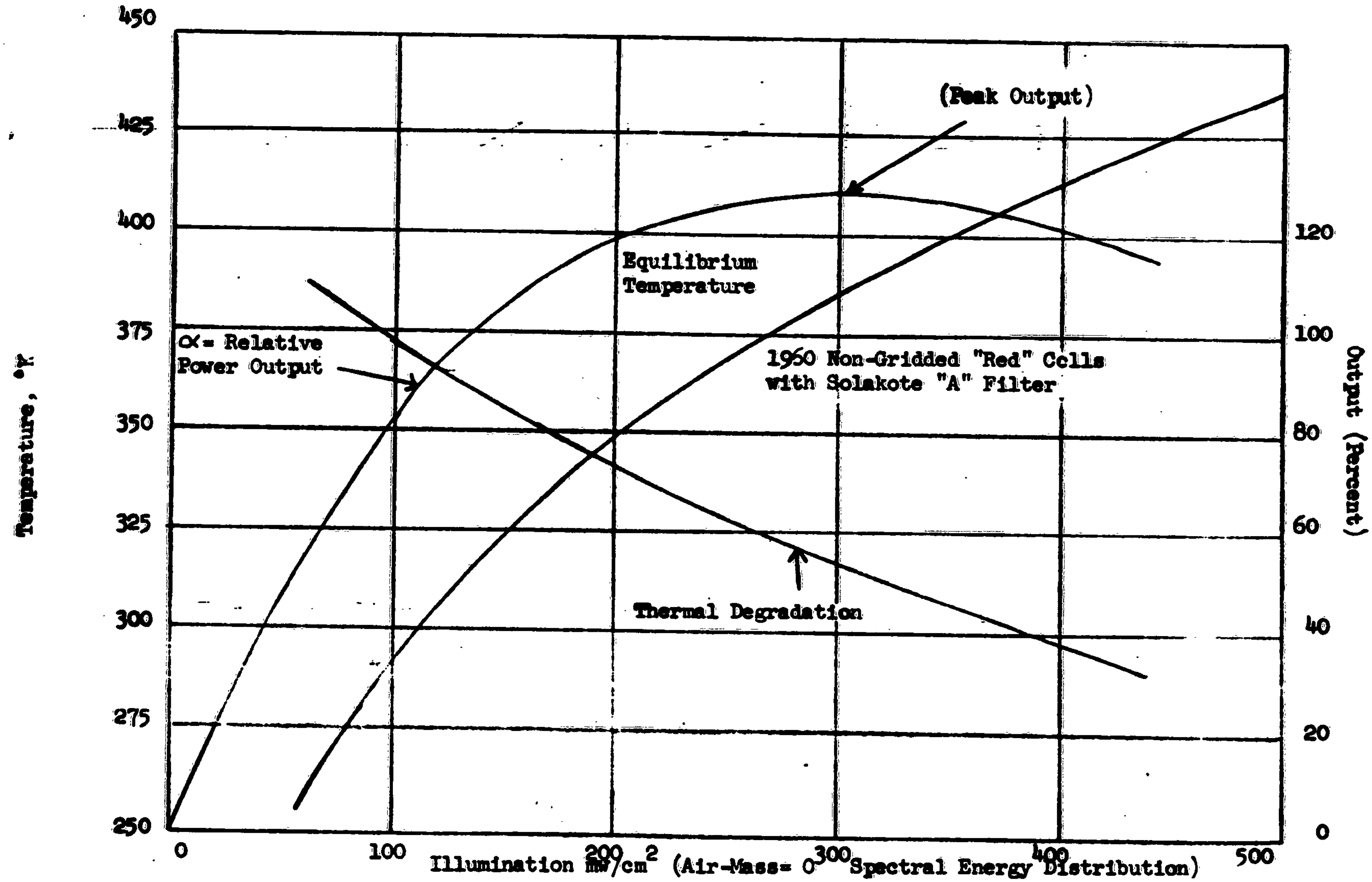

Figure 5. Equilibrium Temperature, Thermal Degradation Factor and Relative Output of Cell Array vs. Illumination.

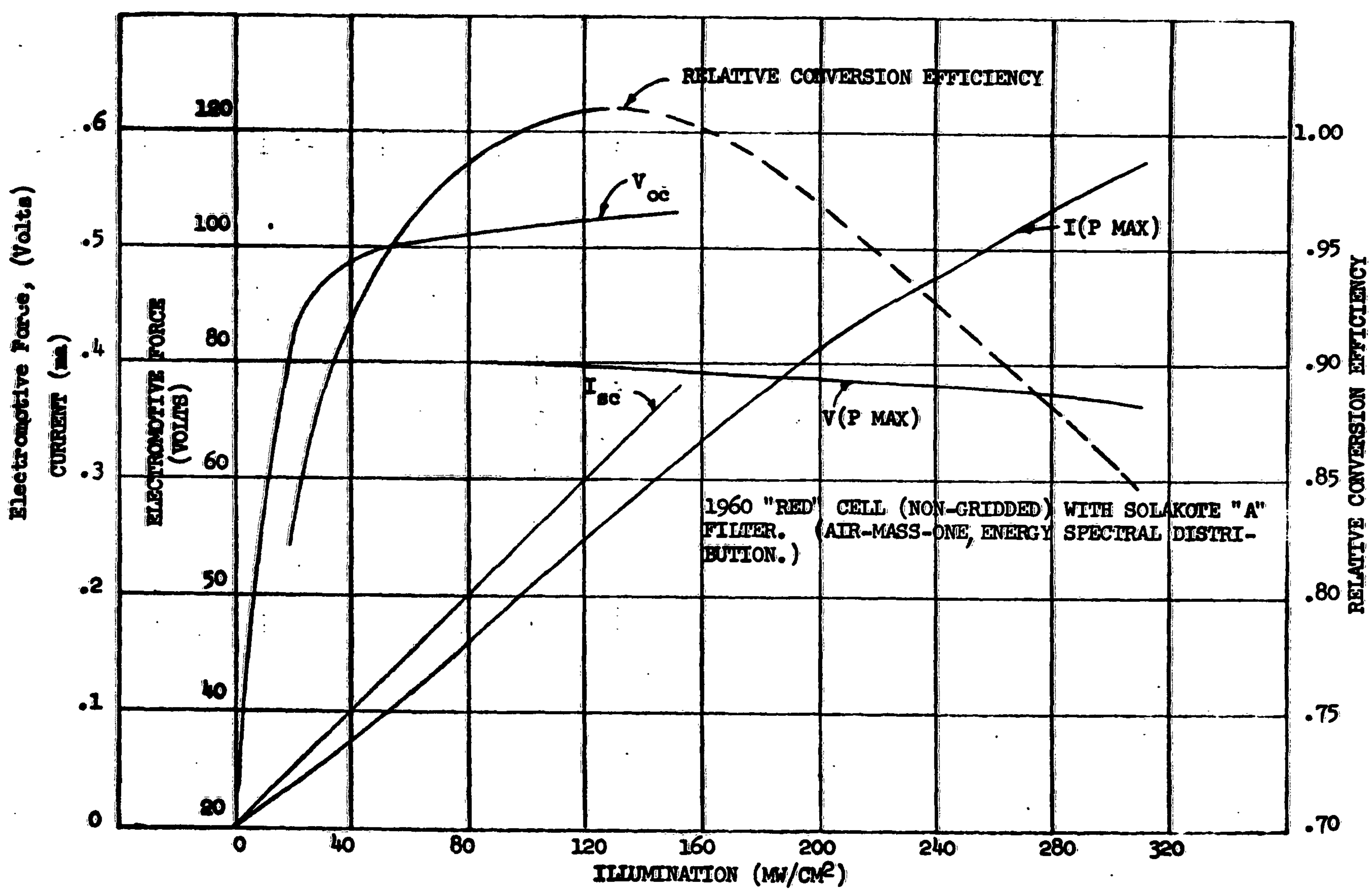

FIGURE 6. EFFECT OF ILLUMINATION LEVEL ON OPEN CIRCUIT VOLTAGE, SHORT CIRCUIT CURRENT, VOLTAGE AND CURRENT AT MAXIMUM POWER, AND RELATIVE CONVERSION EFFICIENCY FOR TYPICAL SILICON SOLAR CELL.

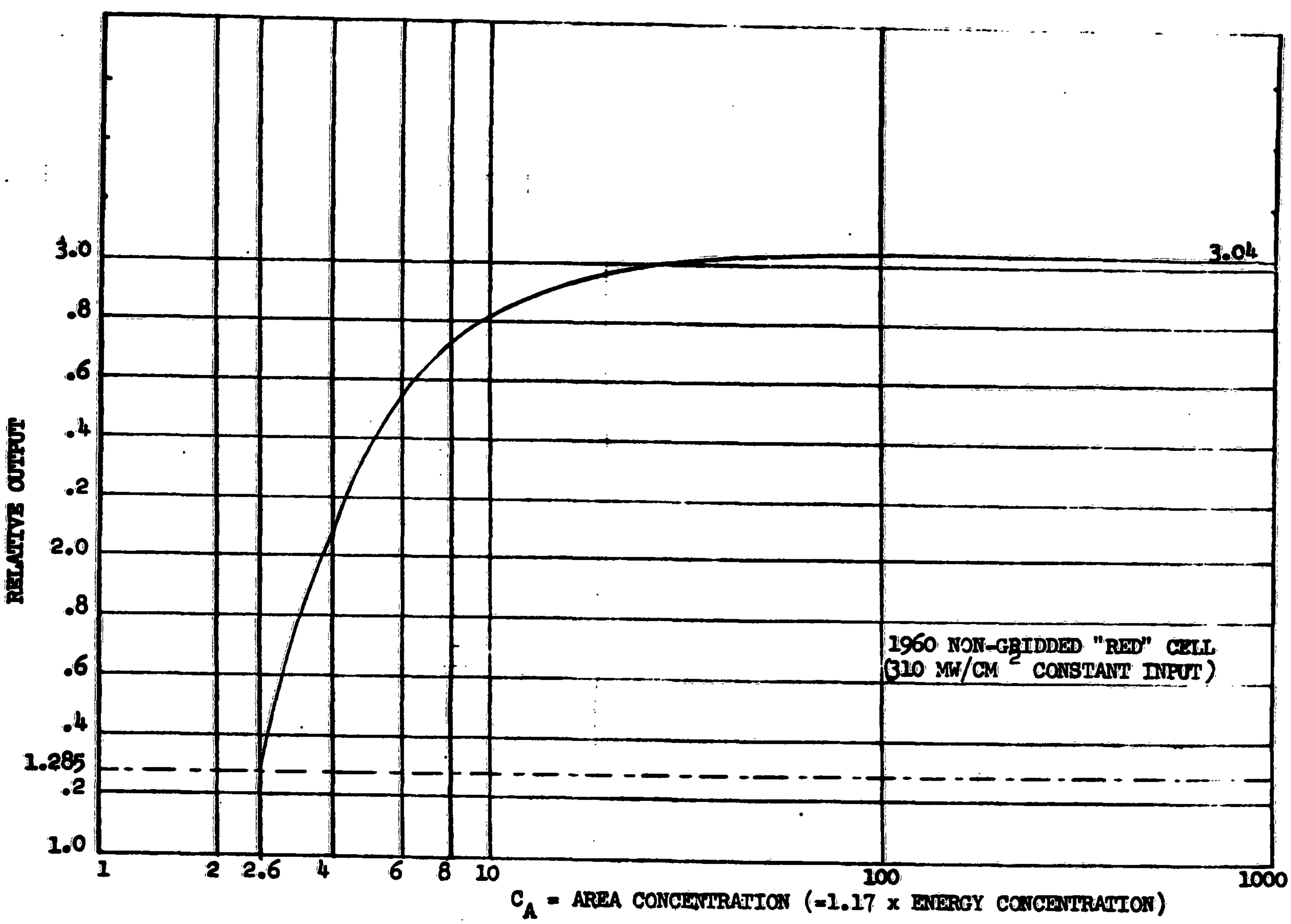

FIGURE 7. OUTPUT PER CELL RELATIVE TO COATED (SOLAKOTE "A") CELL WITHOUT CONCENTRATION VS. AREA CONCENTRATION

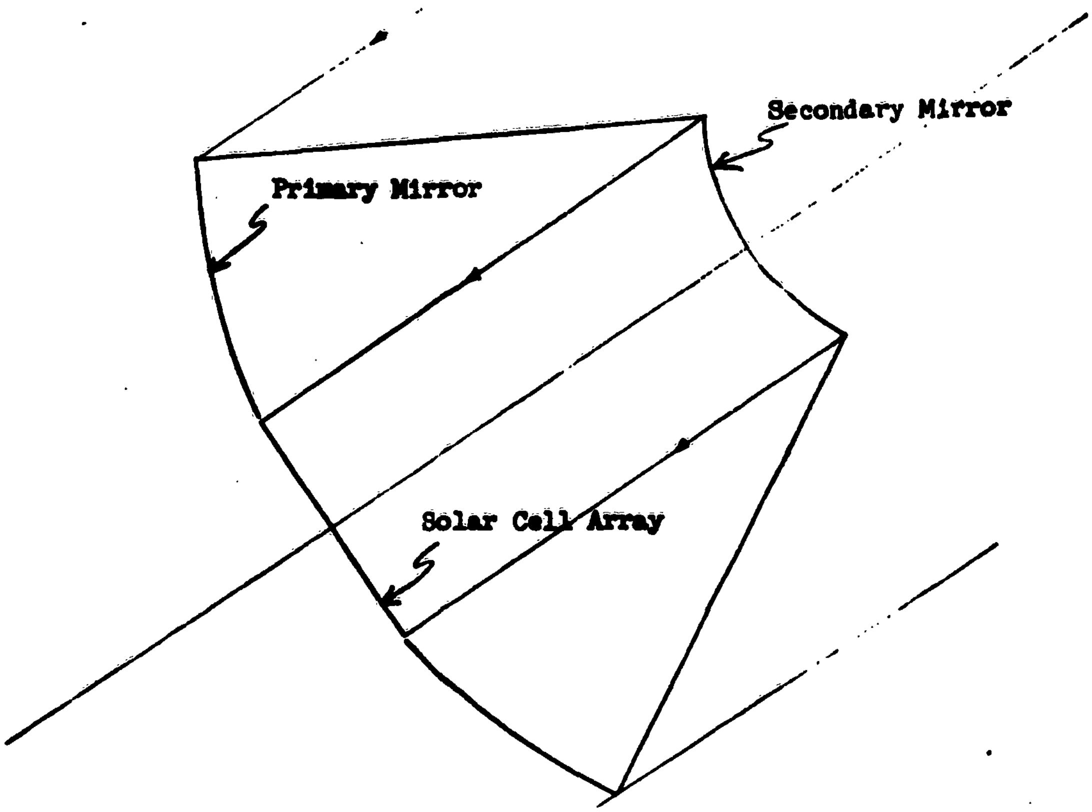

(A) Solar Power System I
(Cassegrainian Mirror System)

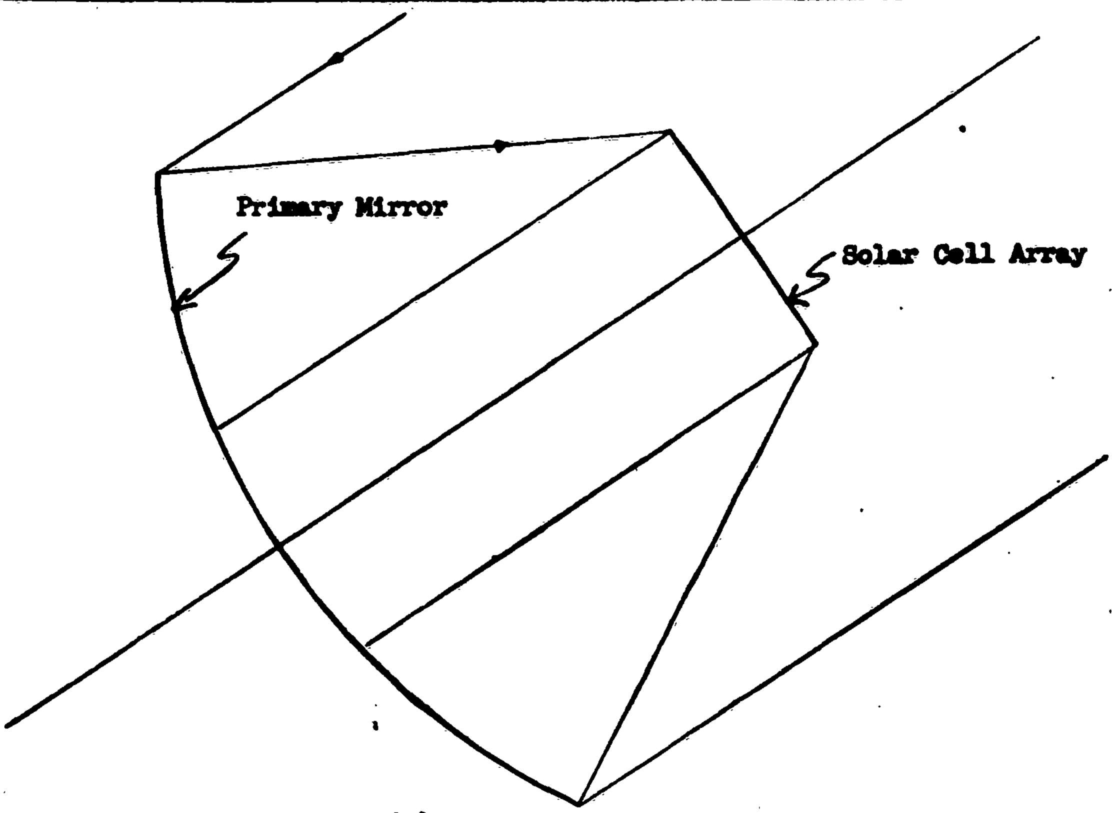

(B) Solar Power System II

Figure 8. Solar Concentrator Configuration.

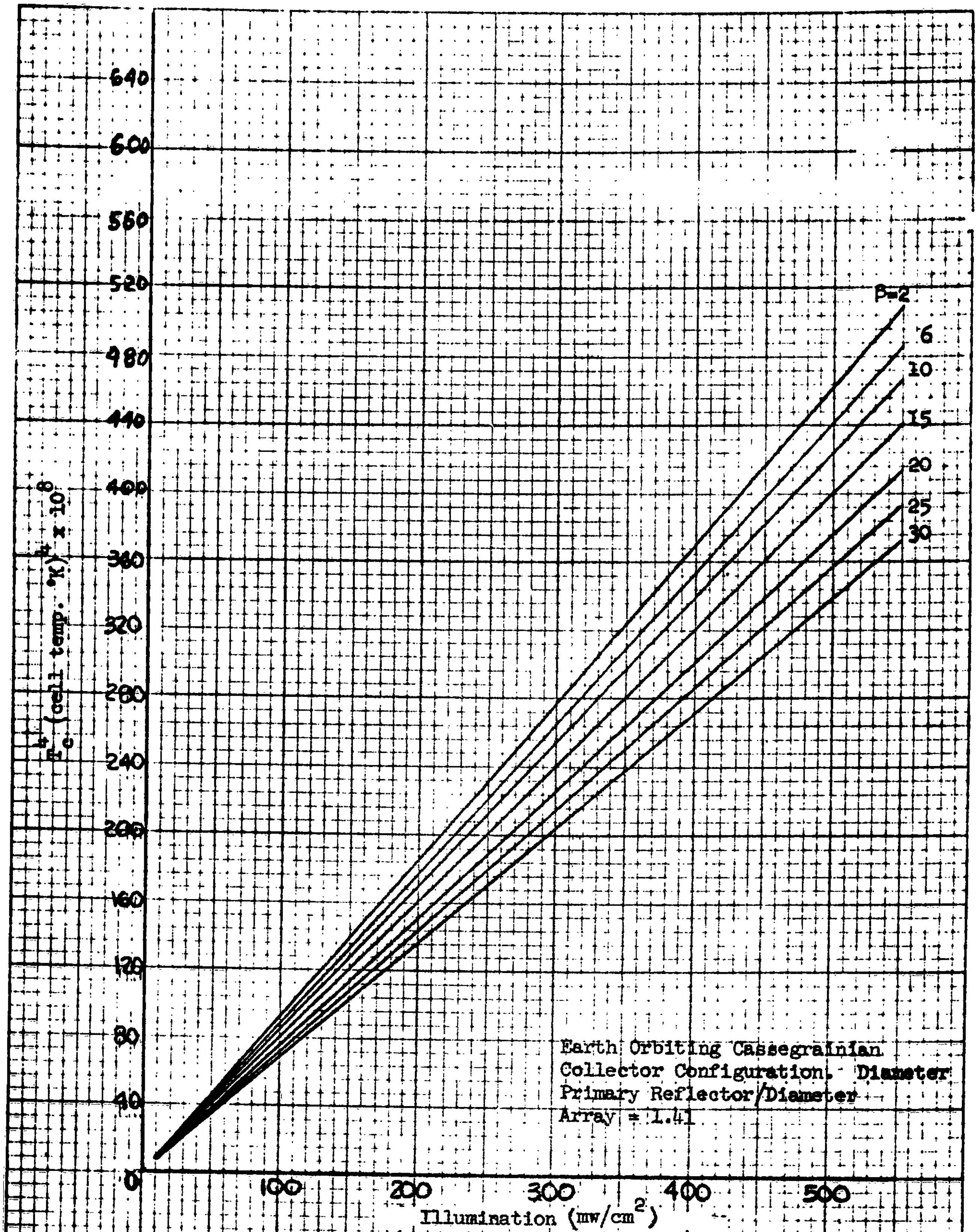

Figure 9. **Solar Cell Temperature as a Function of Illumination on the Cell for C_R = 1.0.**

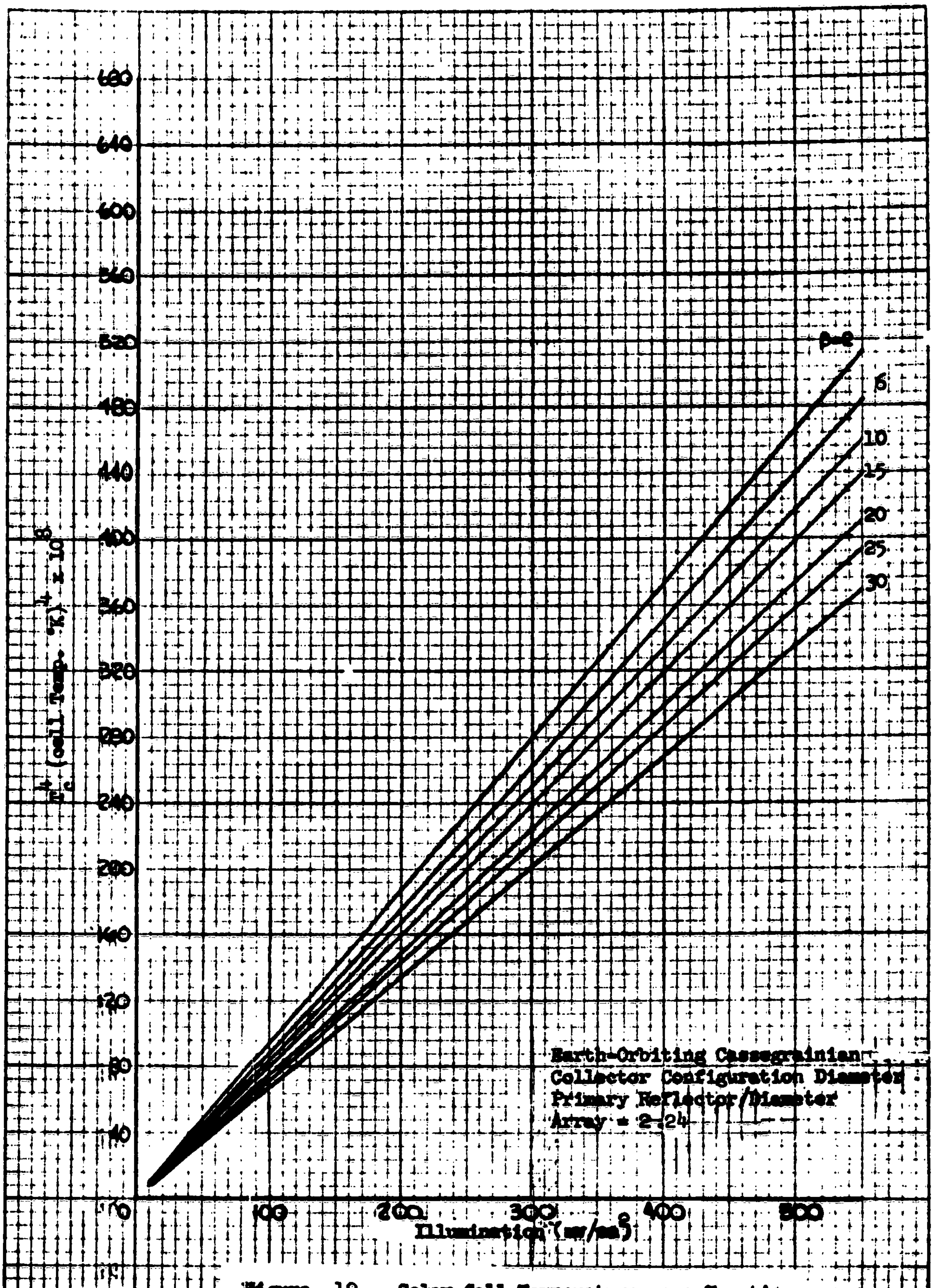

Figure 10. Solar Cell Temperature as a Function of Illumination on the Cell for C_R = 4.

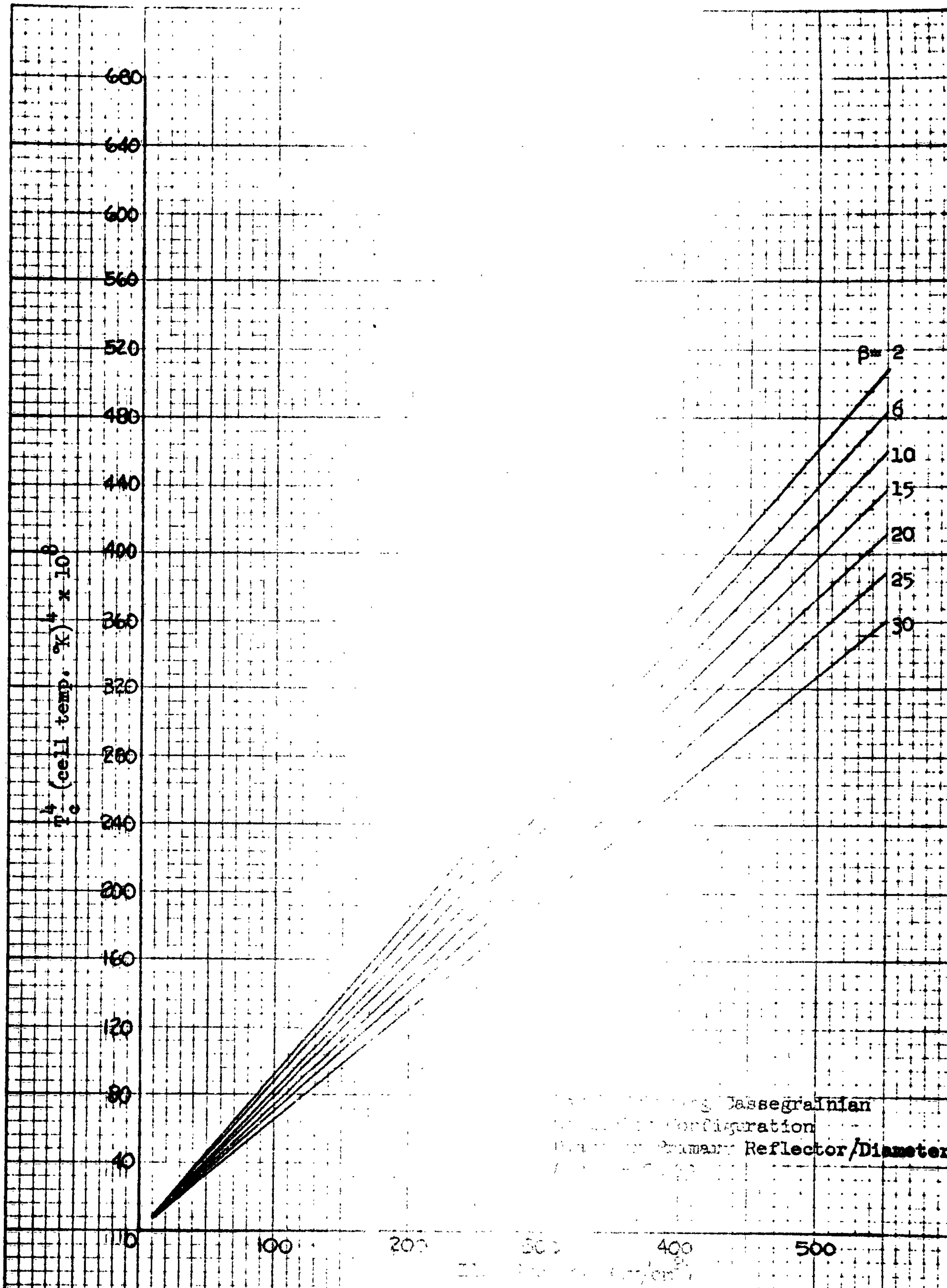

Figure 11. Solar Cell Temperature as a Function of Illumination on Cell for C_p = 6.25.

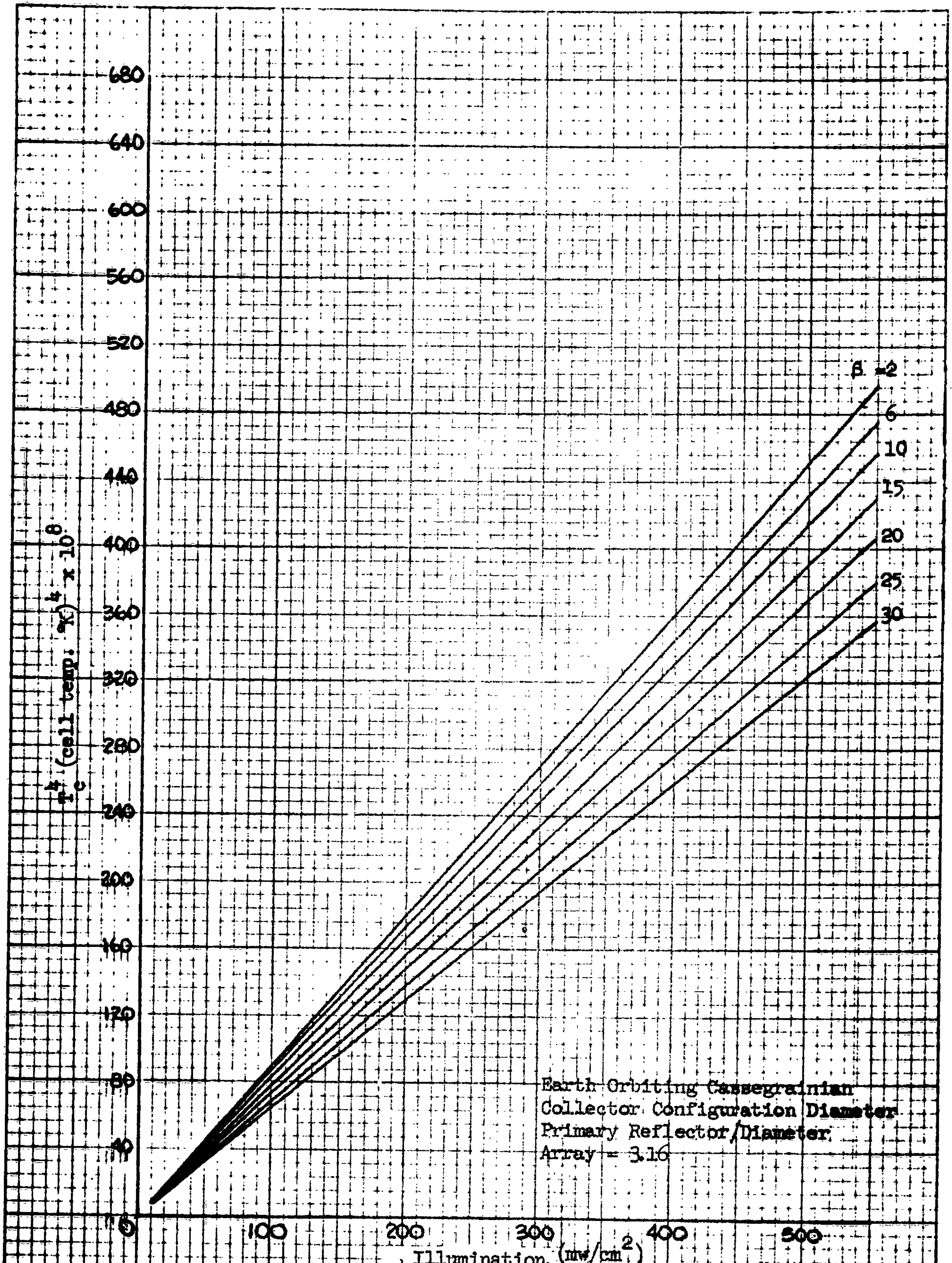

Figure 12. Solar Cell Temperature as a Function of Illumination on the Cell for C_R = 9.

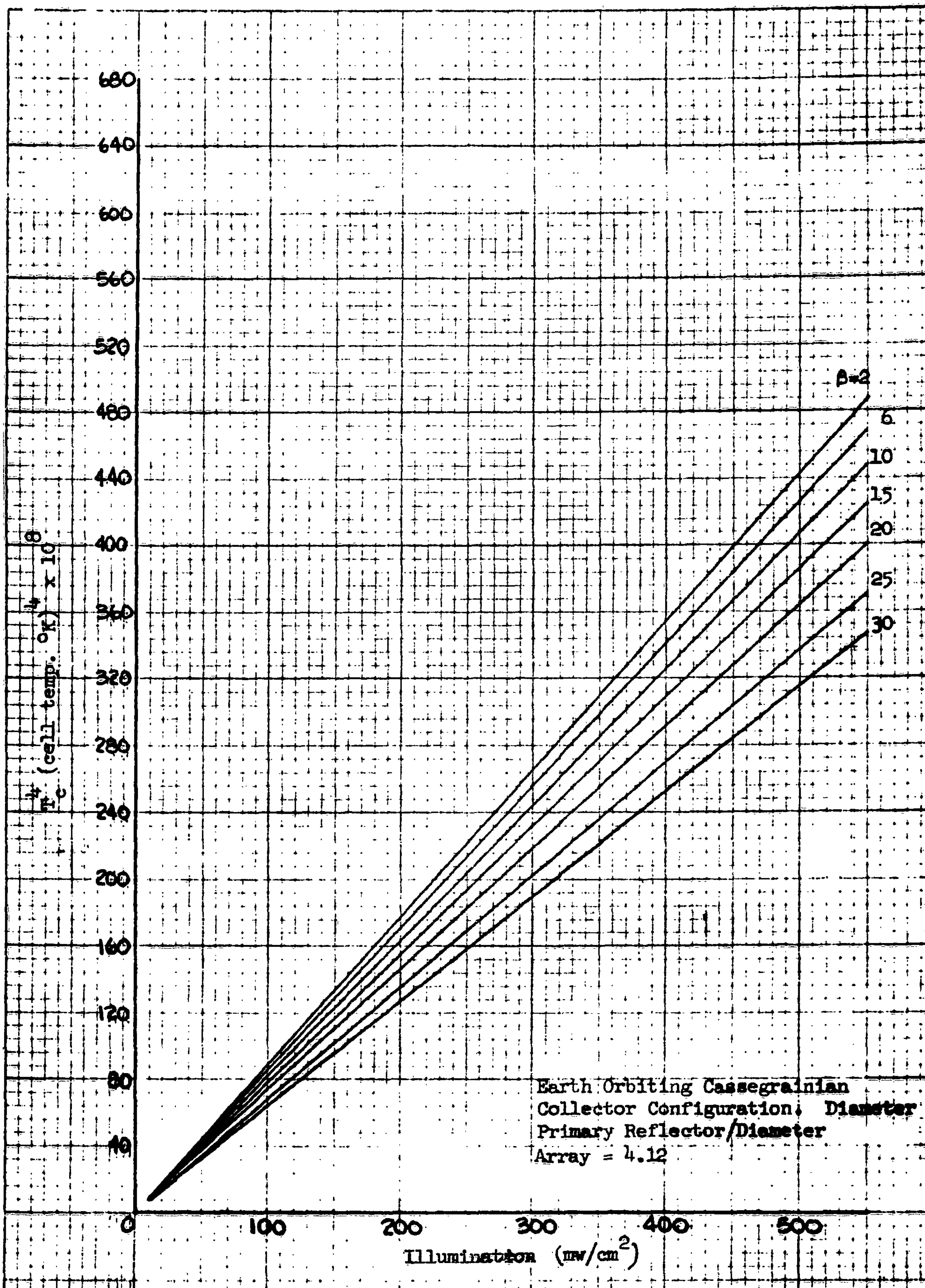

Figure 13. Solar Cell Temperature as a Function of Illumination on Cell for $C_R = 16$.

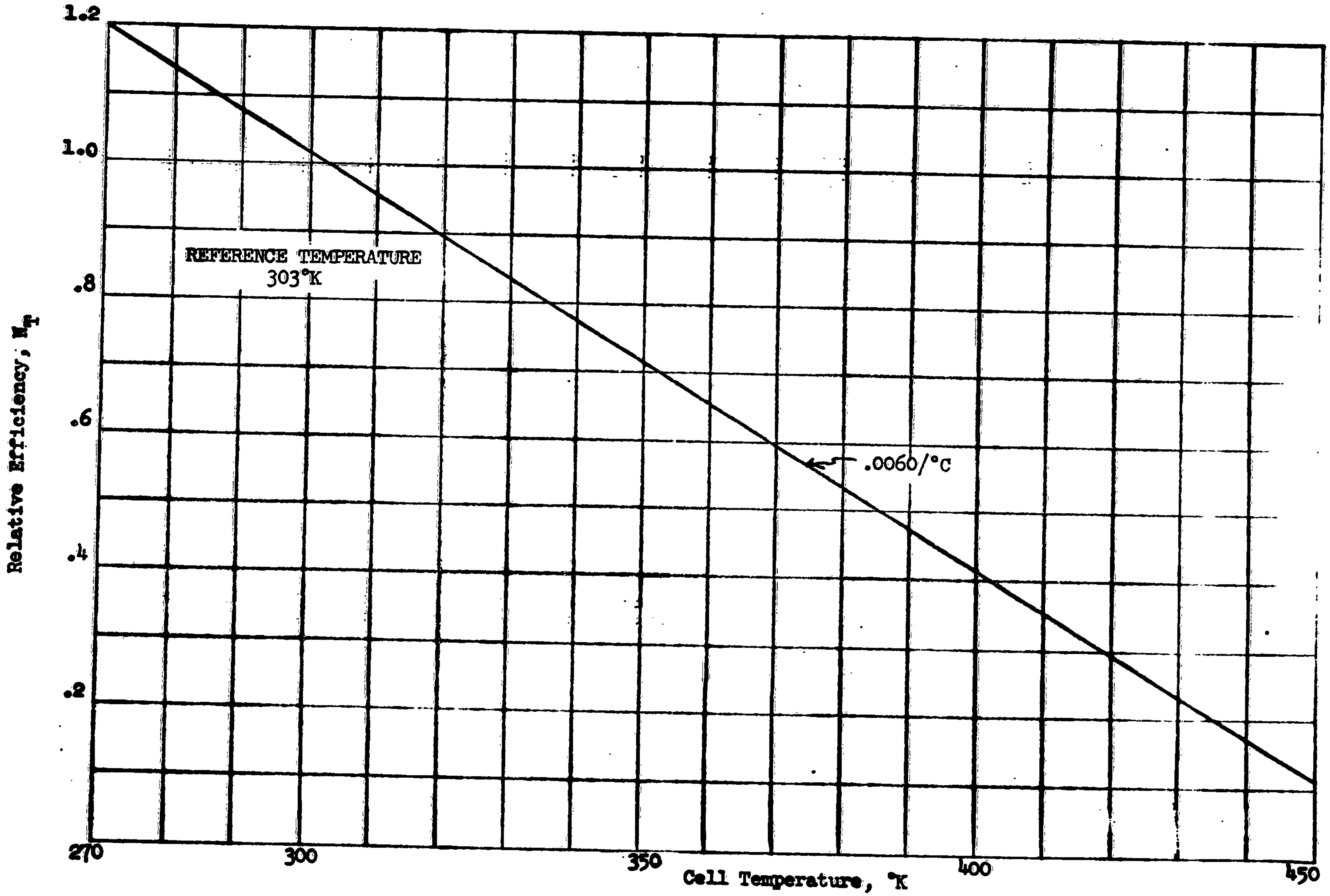

Figure 14. **Typical Temperature Characteristic of An Experimental Gridded "Red" Silicon Solar Cell.**

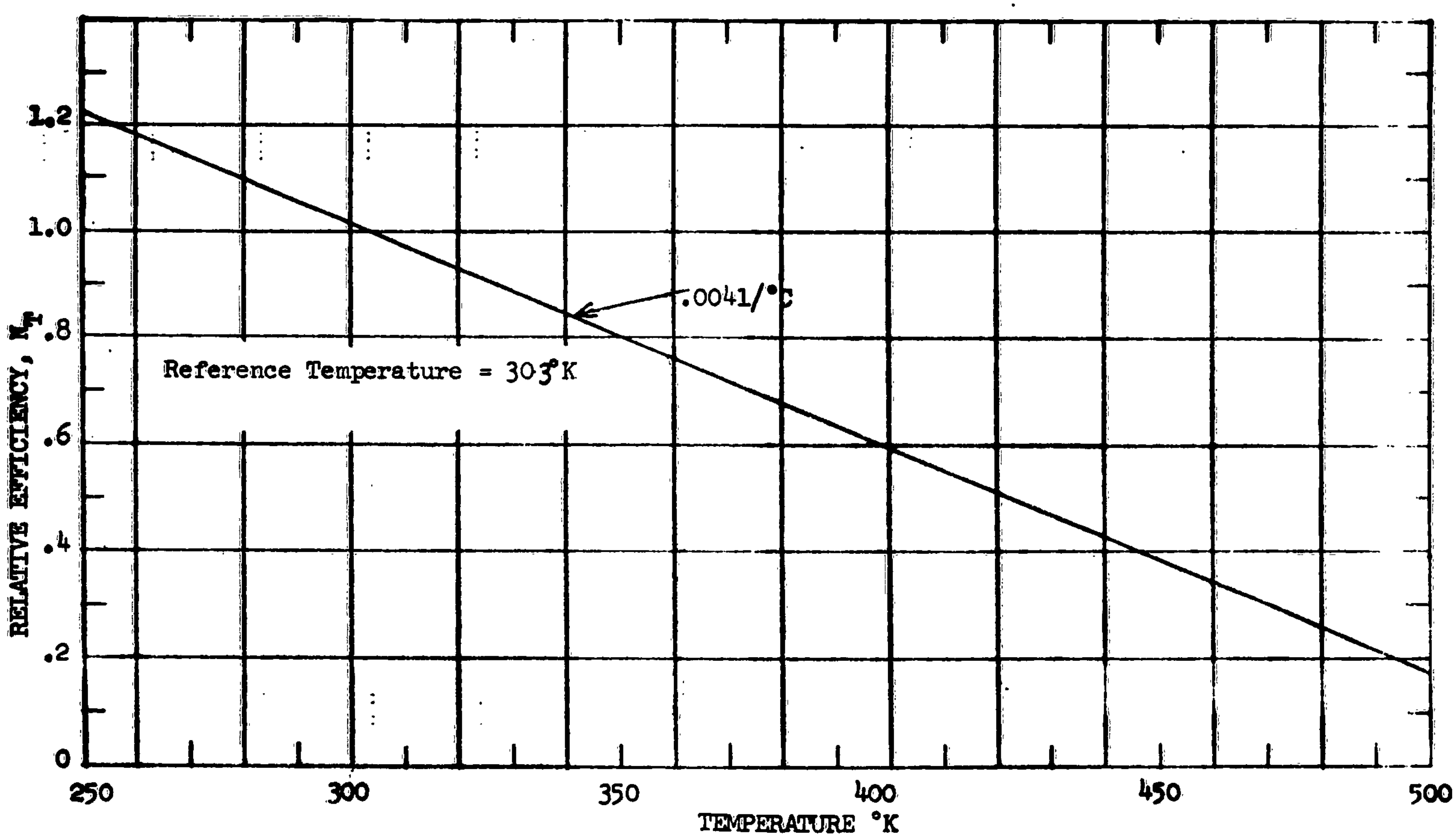

FIGURE 15. **TYPICAL TEMPERATURE CHARACTERISTIC OF A HELIOTEK GRIDDED "BLUE" CELL.**

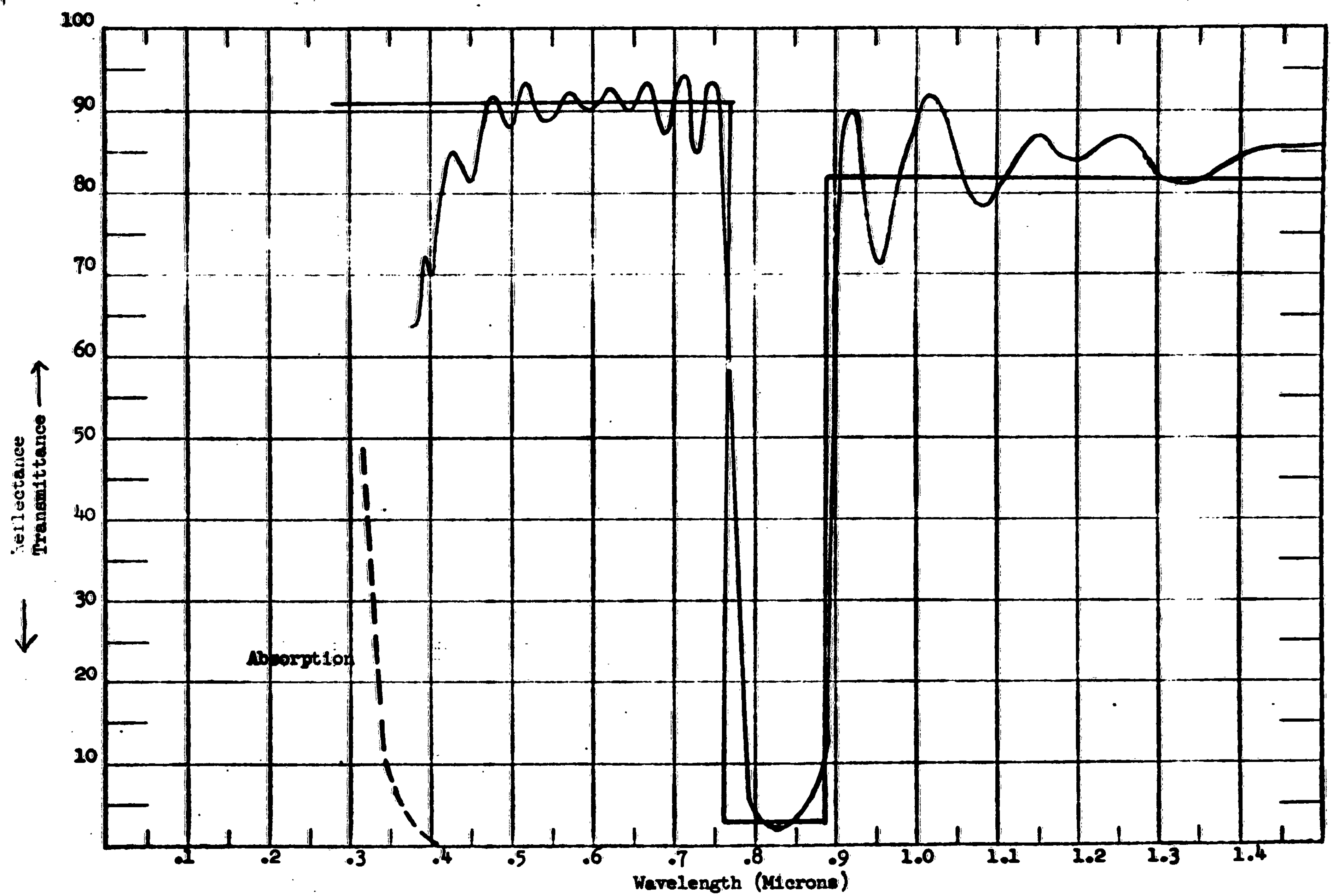

Figure 16. Concentrator Filter of "Red" Cells - Type SL 120/83.

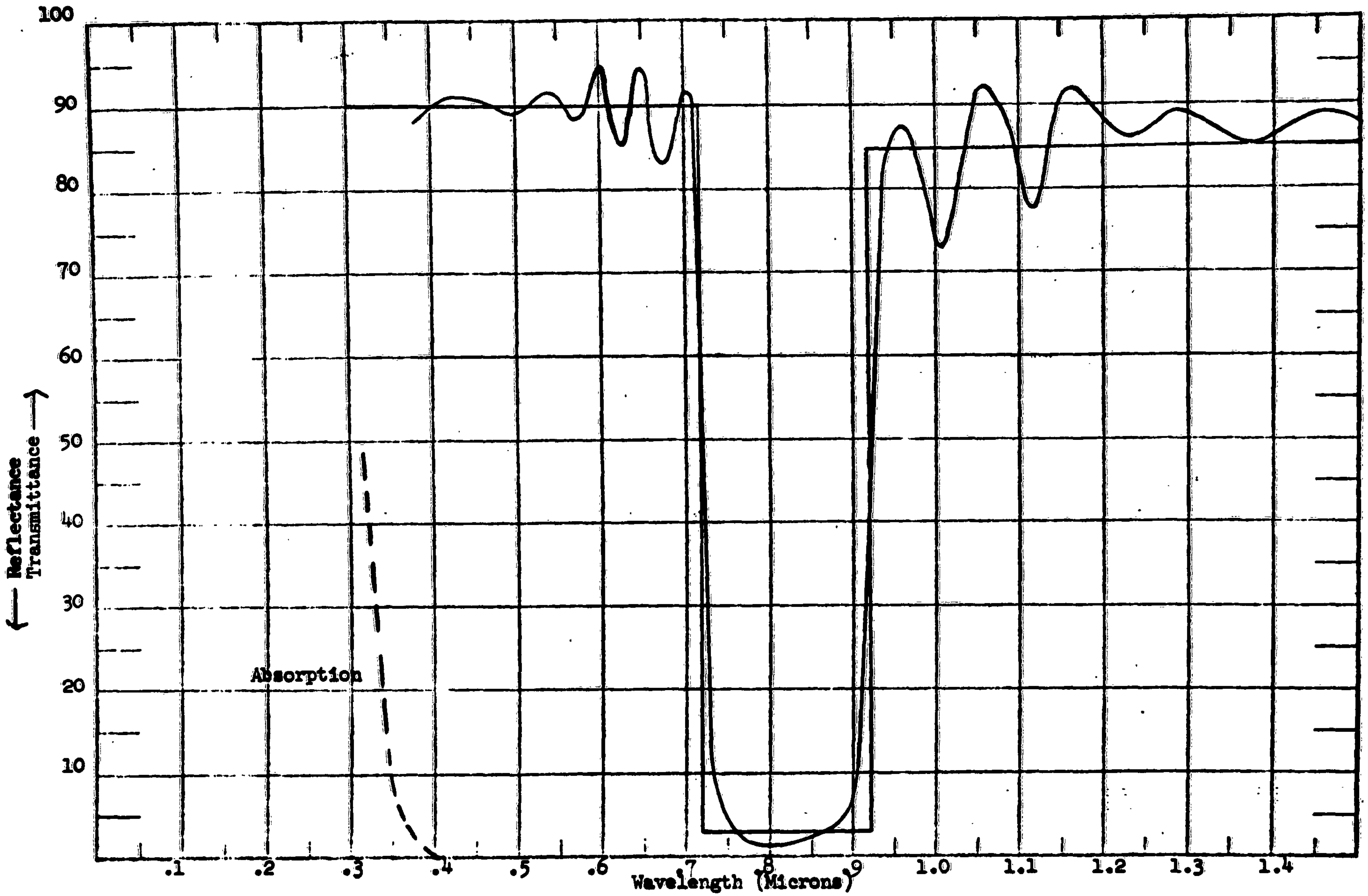

Figure 17. Concentrator Filter for "Red" Cells - Type SL 200/82.

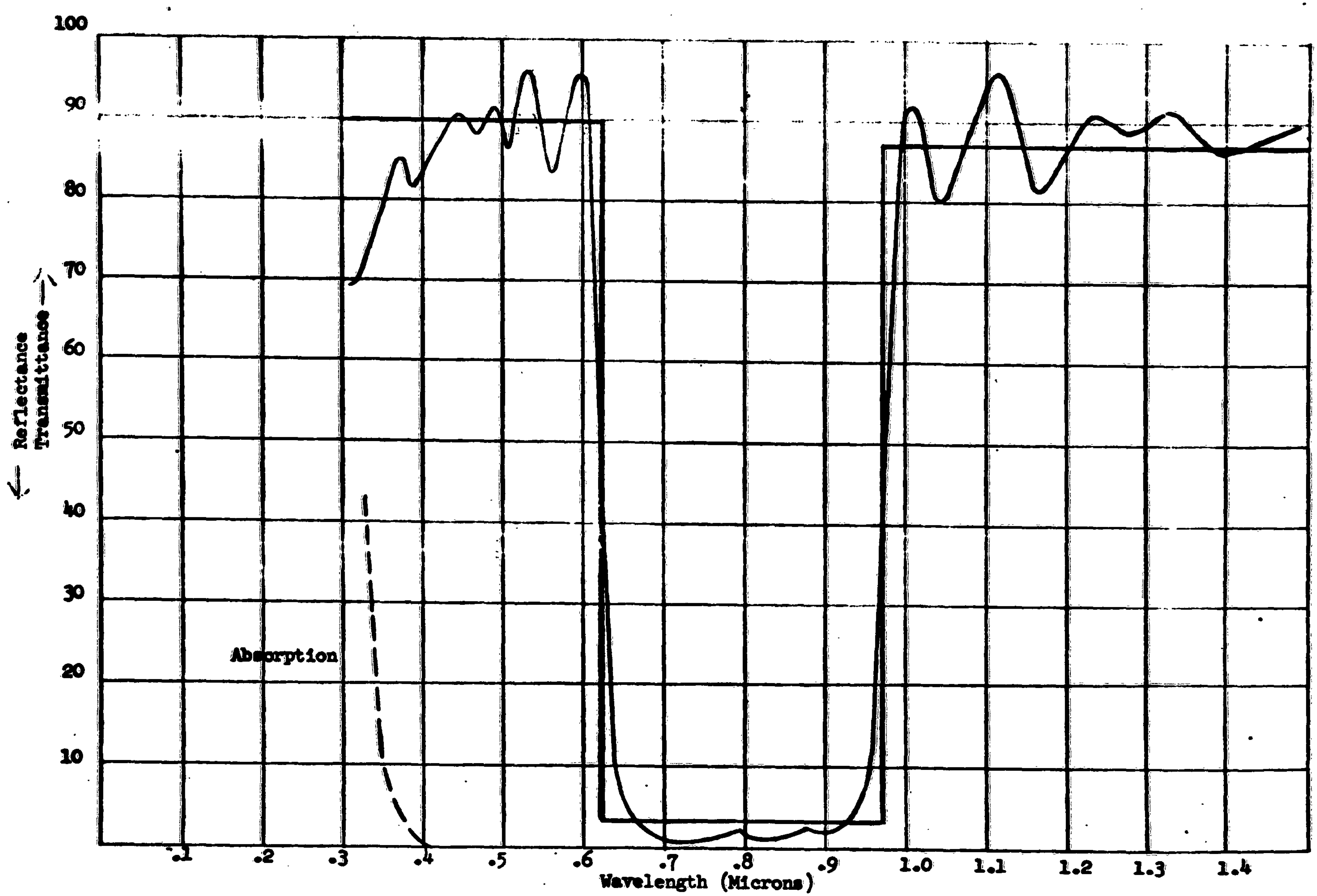

Figure 18. Concentrator Filter for "Red" Cells - Type SL350/80.

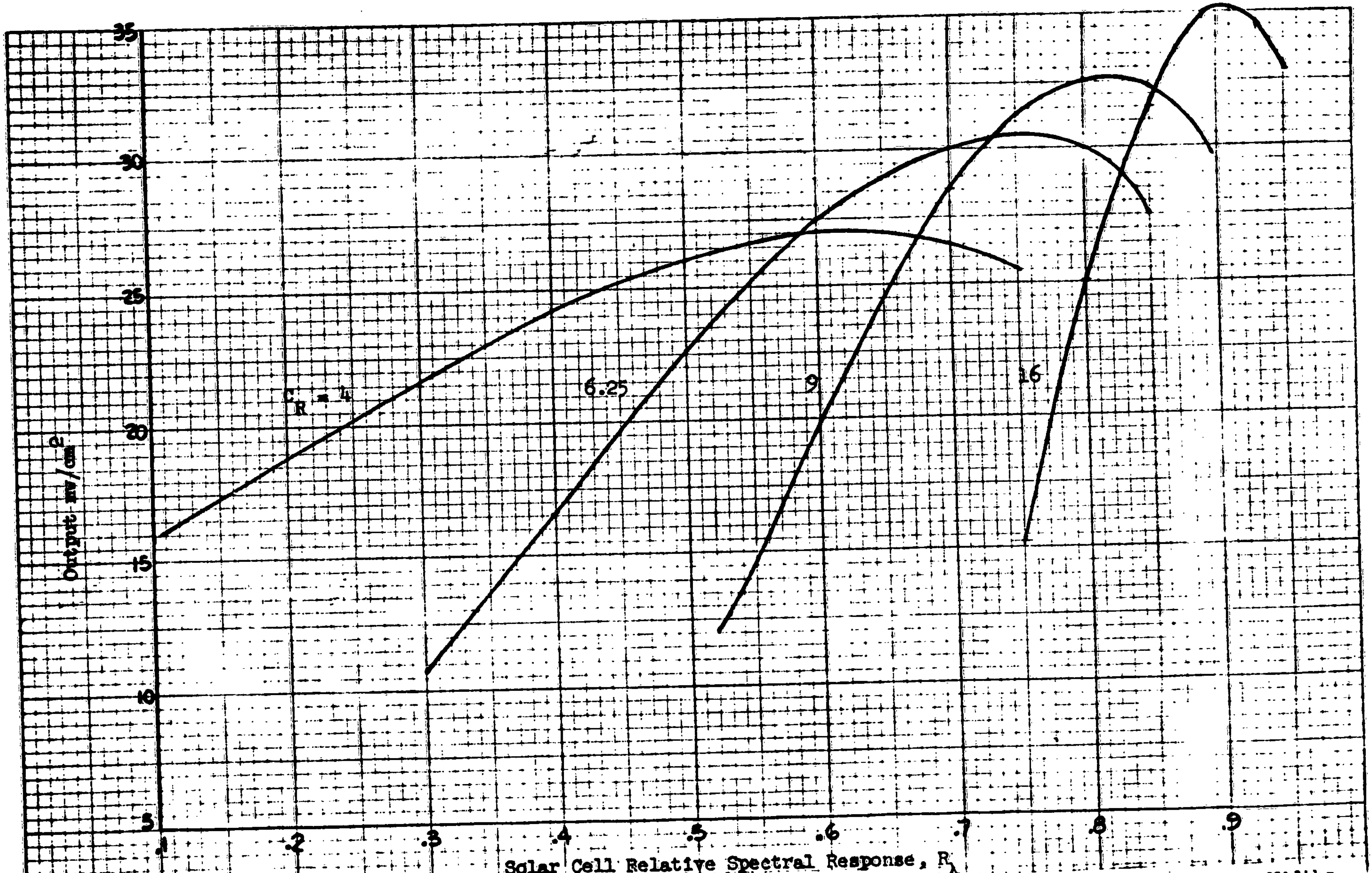

Figure 19. Power Output of Array for Varying Concentration Ratios and Ideal Filter Band-Pass Widths in the Cassegrainian Collector Configuration with Experimental Gridded "Red" Cell with "Red" Cell Temperature-Power Degradation Coefficient = 0.0061 / °C.

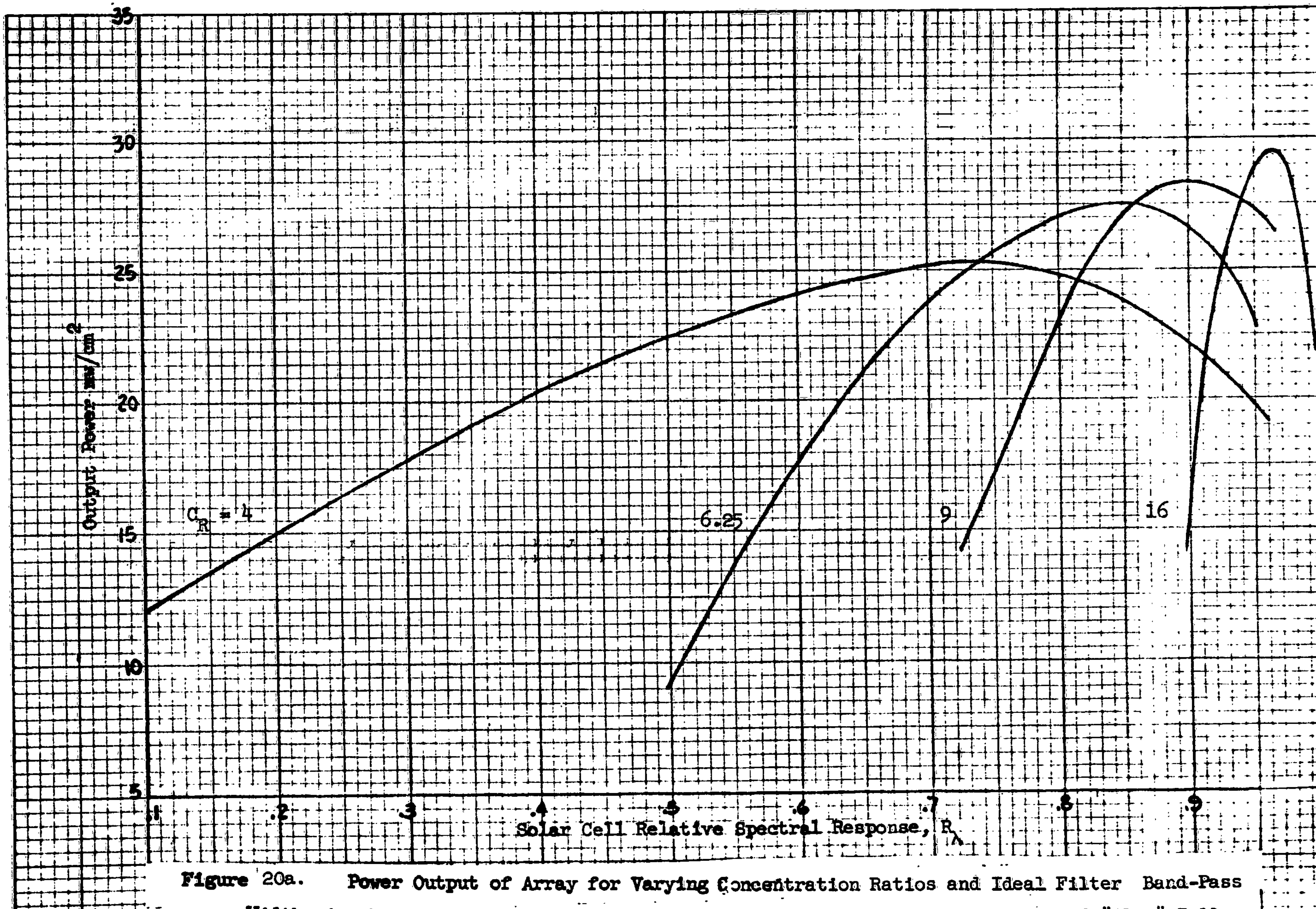

Figure 20a. **Power Output of Array for Varying Concentration Ratios and Ideal Filter Band-Pass Widths in the Cassegrainian Collector Configuration With Hypothetical Gridded "Blue" Cell with "Red" Cell Temperature-Power Degradation Coefficient = 0.0060 /°C.**

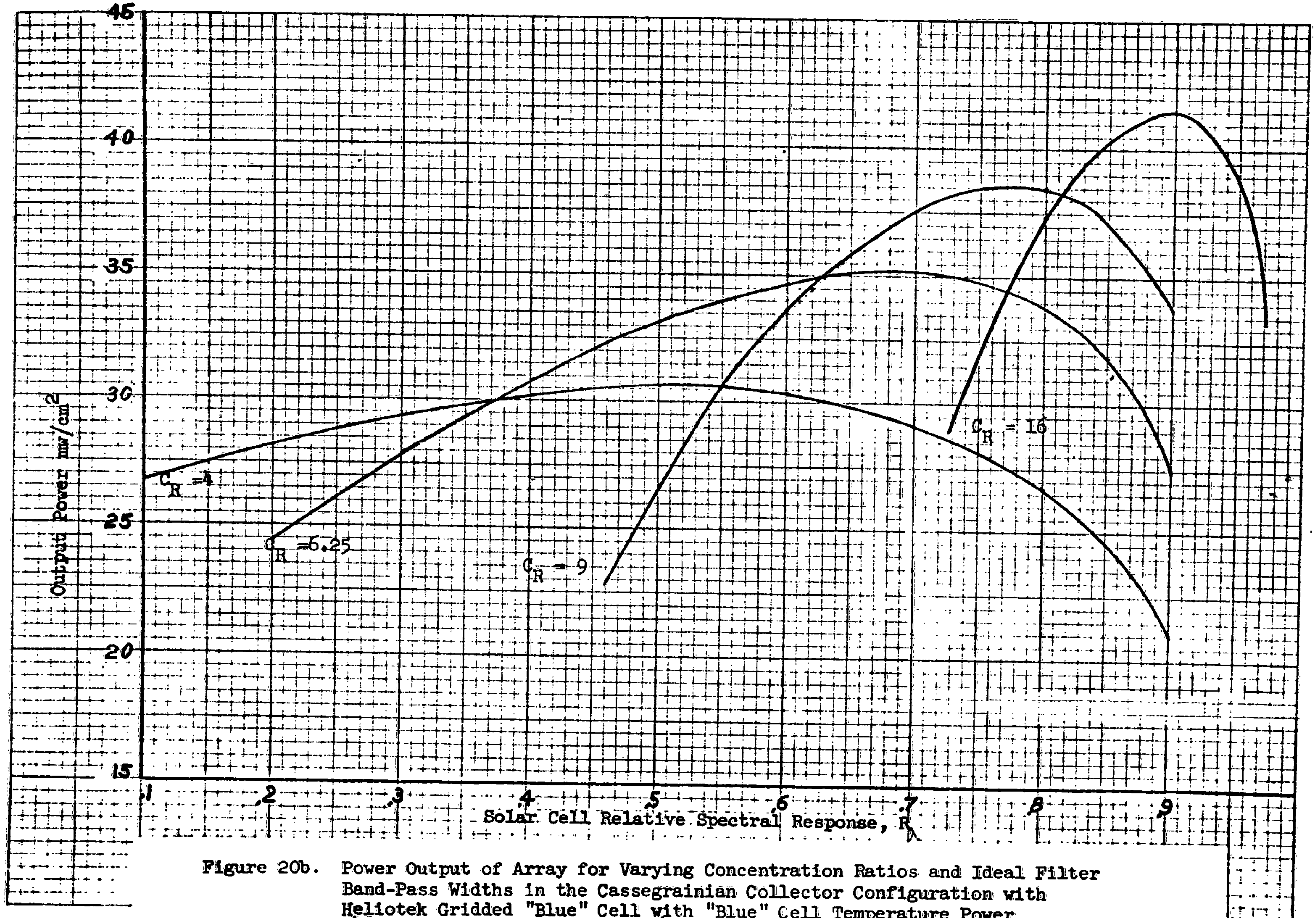

Figure 20b. Power Output of Array for Varying Concentration Ratios and Ideal Filter Band-Pass Widths in the Cassegrainian Collector Configuration with Heliotek Gridded "Blue" Cell with "Blue" Cell Temperature Power Degradation Coefficient = .0041°C.

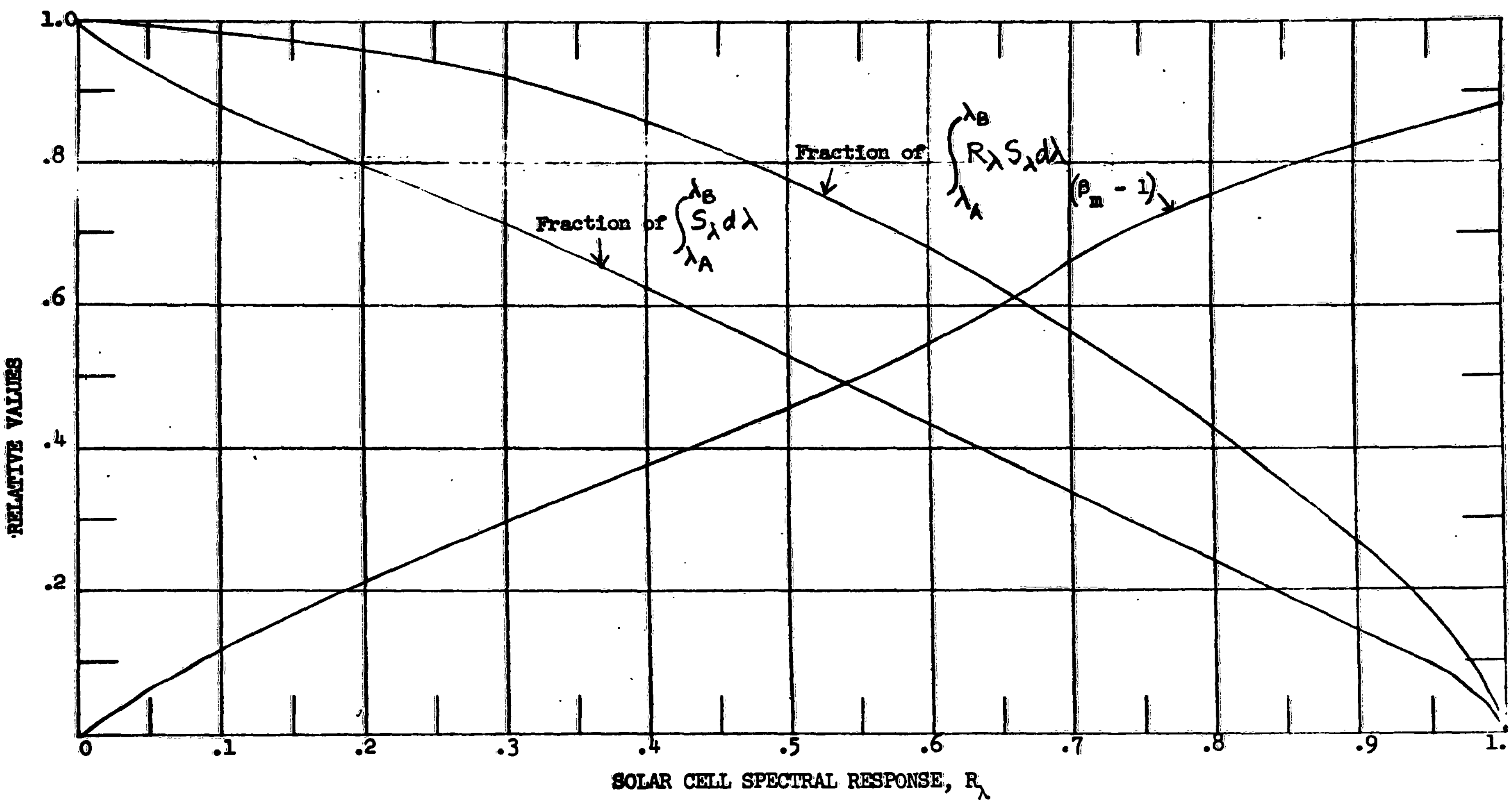

FIGURE 21. FRACTION OF THE SOLAR ENERGY AND CELL POWER OUTPUT OCCURRING IN REGION FOUND BY CHOOSING FILTER BAND-PASS LIMITS AT EQUAL HEIGHT ON THE RESPONSE CURVE OF THE EXPERIMENTAL GRIDDED "RED" SILICON SOLAR CELL. ALSO, $(\beta_m - 1)$, WHERE β_m IS THE MULTIPLIER OF THE AVERAGE ABSOLUTE EFFICIENCY (AT THE REFERENCE TEMPERATURE) BETWEEN λ_A AND λ_B TO GIVE THE AVERAGE EFFICIENCY WITHIN THE R_λ LIMITS.

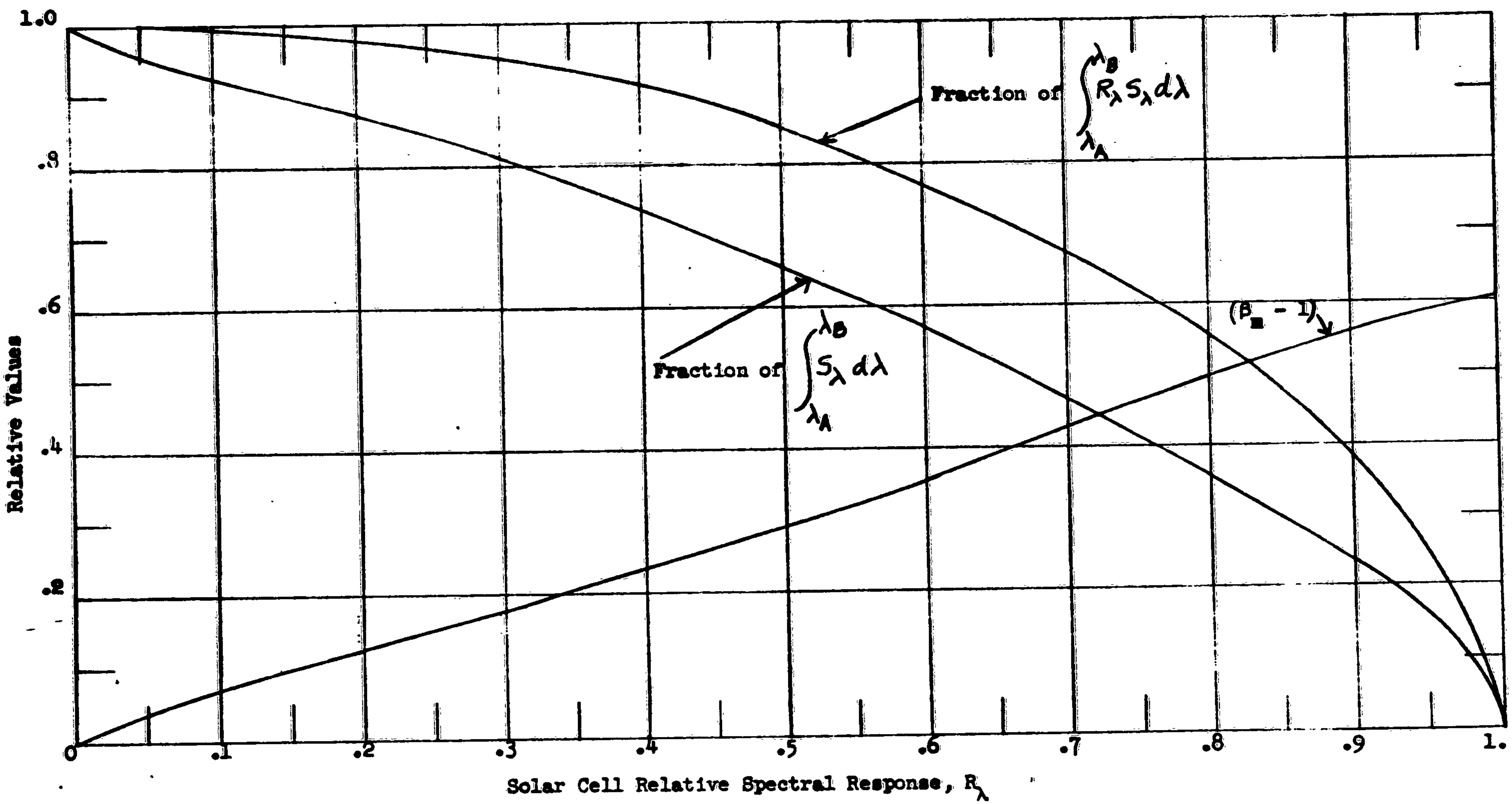

Figure 22. Fraction of the Solar Energy and Cell Power Output Occurring in Region Found by Choosing Filter Band-Pass Limits at Equal Height on the Response Curve of the Heliotek Gridded "Blue" Silicon Solar Cell. Also, $(\beta_m - 1)$, where β_m is the Multiplier of the Average Absolute Efficiency (at the Reference Temperature) Between λ_A and λ_B to Give the Average Efficiency Within the R_λ Limits.

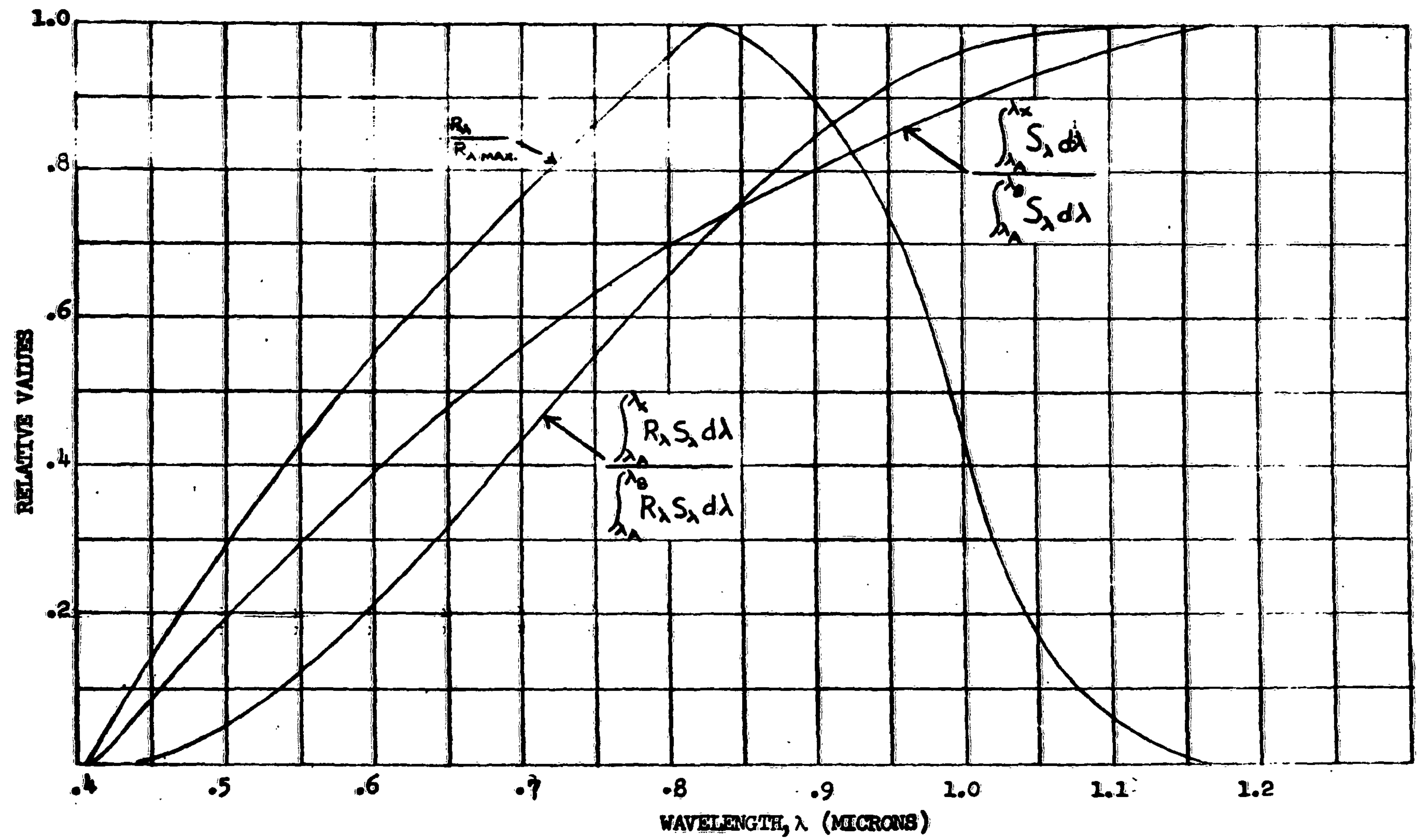

FIGURE 23. NORMALIZED RESPONSE AND CUMULATIVE SOLAR ENERGY AND POWER OUTPUT OF EXPERIMENTAL GRIDDED "RED" SILICON SOLAR CELL AS A FRACTION OF THE TOTAL BETWEEN λ_A AND λ_B.

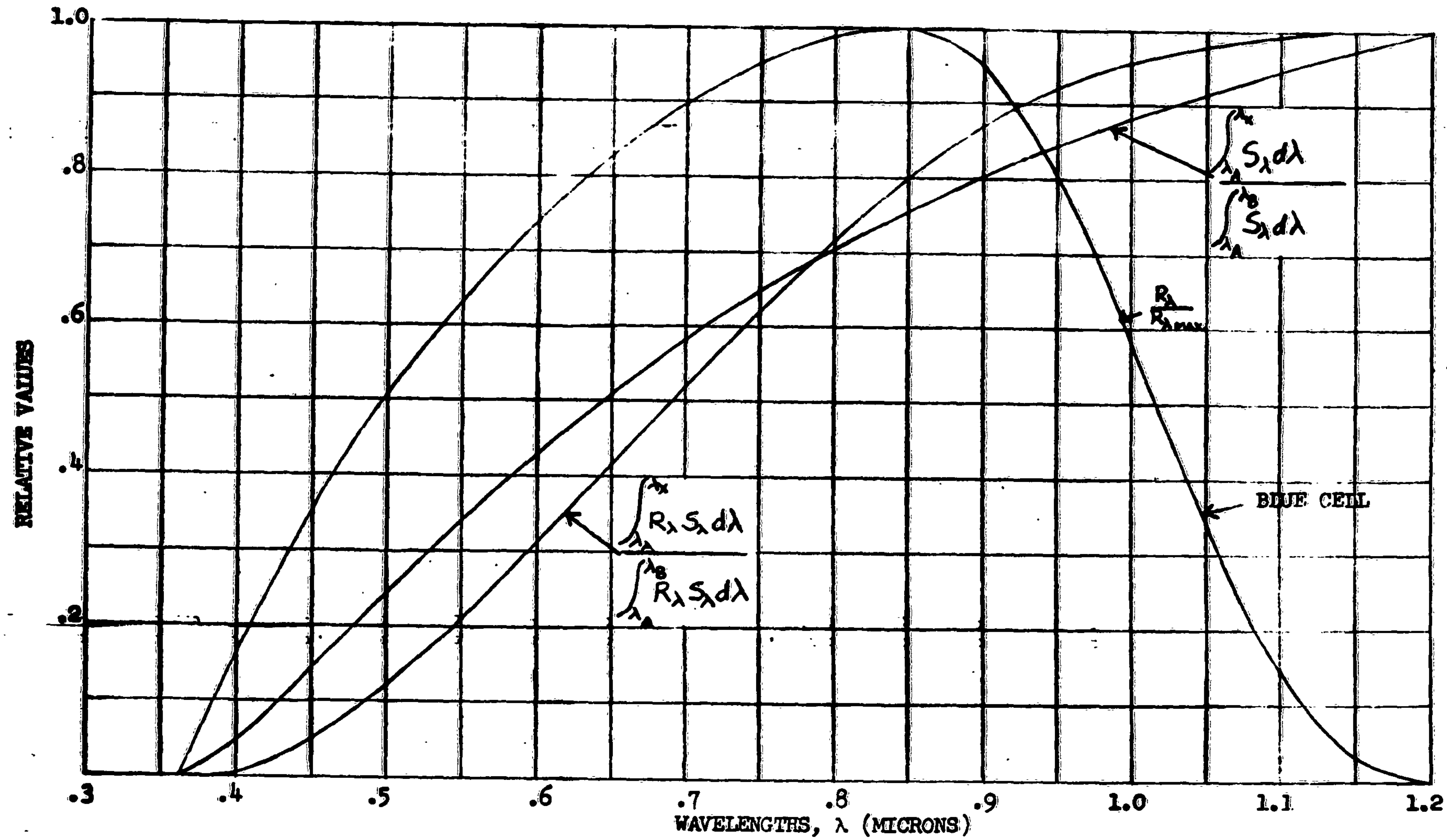

FIGURE 24. NORMALIZED RESPONSE AND CUMULATIVE SOLAR ENERGY AND POWER OUTPUT OF HELIOTEK GRIDDED "BLUE" SILICON SOLAR CELL AS A FRACTION OF THE TOTAL BETWEEN λ_A AND λ_B.

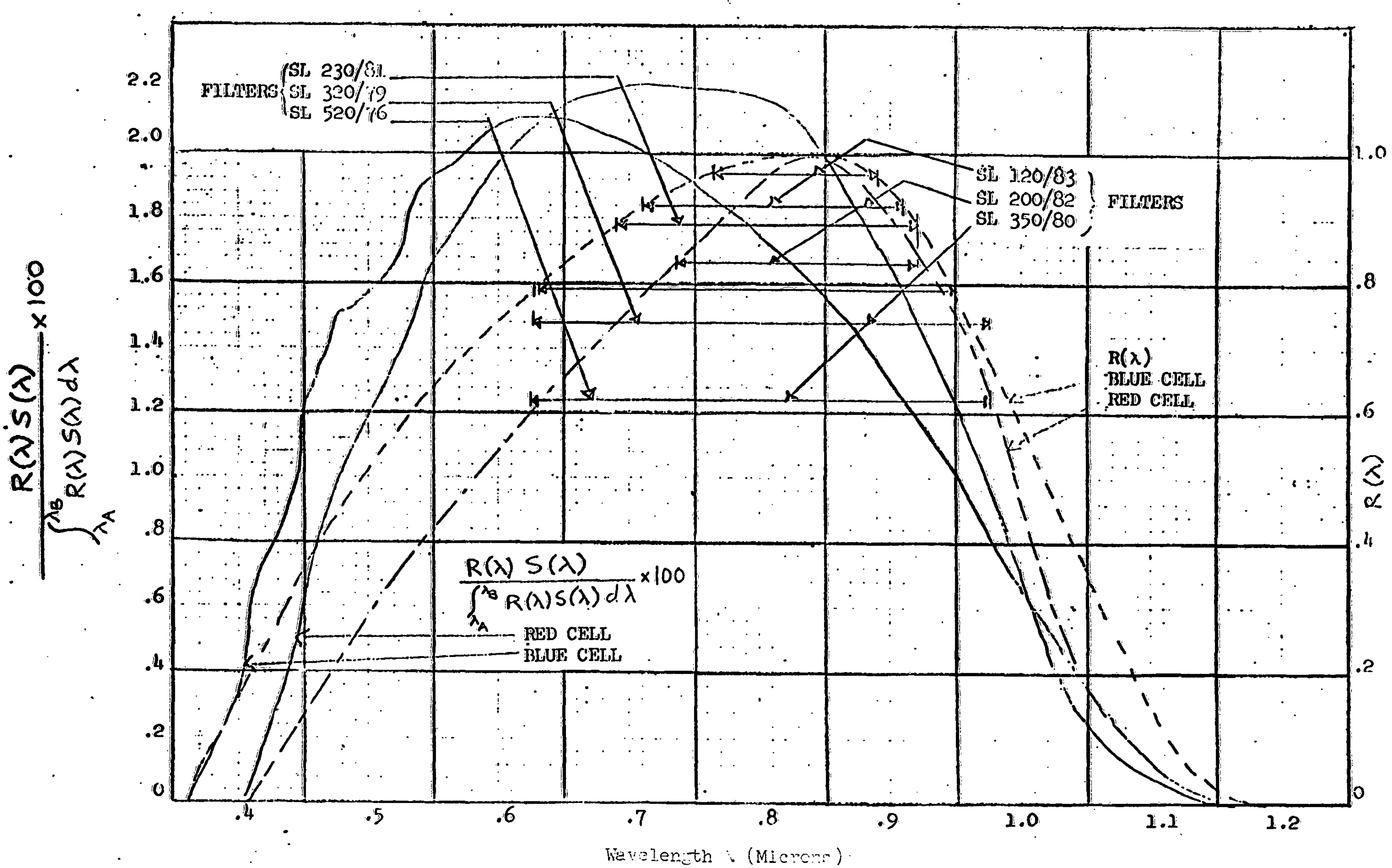

FIGURE 25. SPECTRAL DISTRIBUTION OF SOLAR CELL RESPONSE AND FILTER TRANSMISSION.

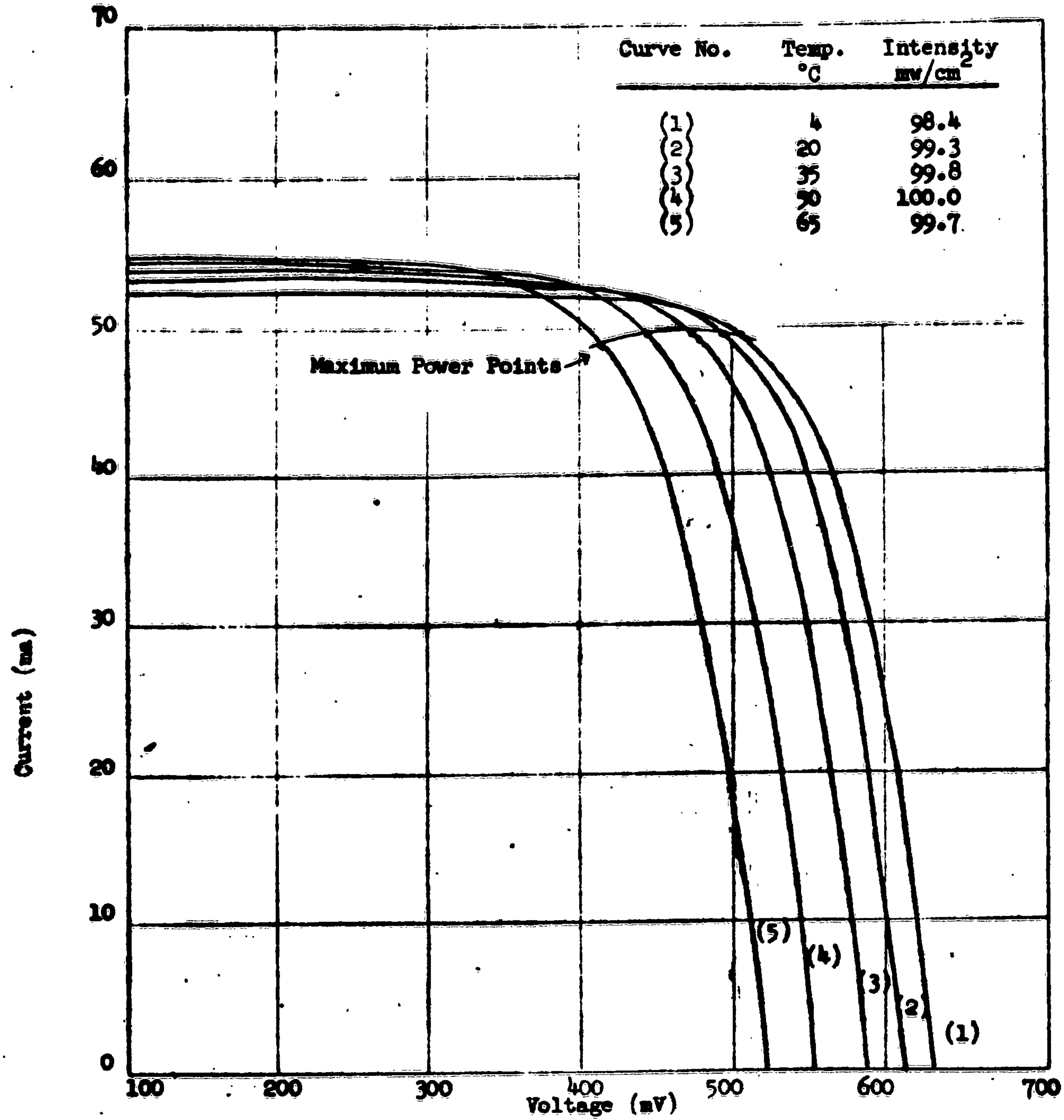

Figure 26. Solar Cell Power Output vs Temperature and Incident Energy for Heliotek Gridded "Blue" Cell (Sunlight at Table Mountain).

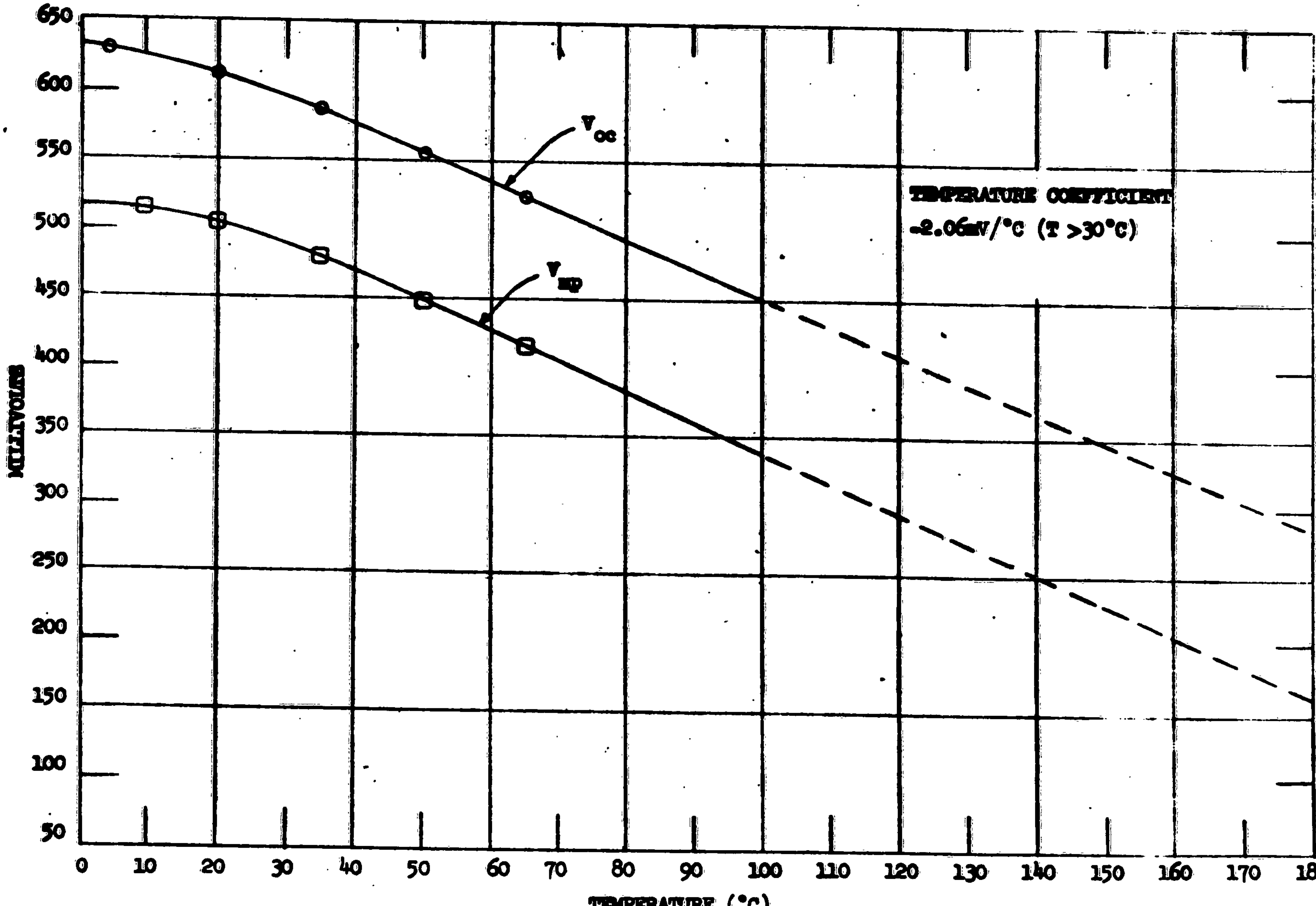

FIGURE 27. SOLAR CELL MAXIMUM POWER VOLTAGE AND OPEN CIRCUIT VOLTAGE VS. TEMPERATURE (SUNLIGHT ON TABLE MTN) FOR HELIOTEK GRIDDED "BLUE" CELL.

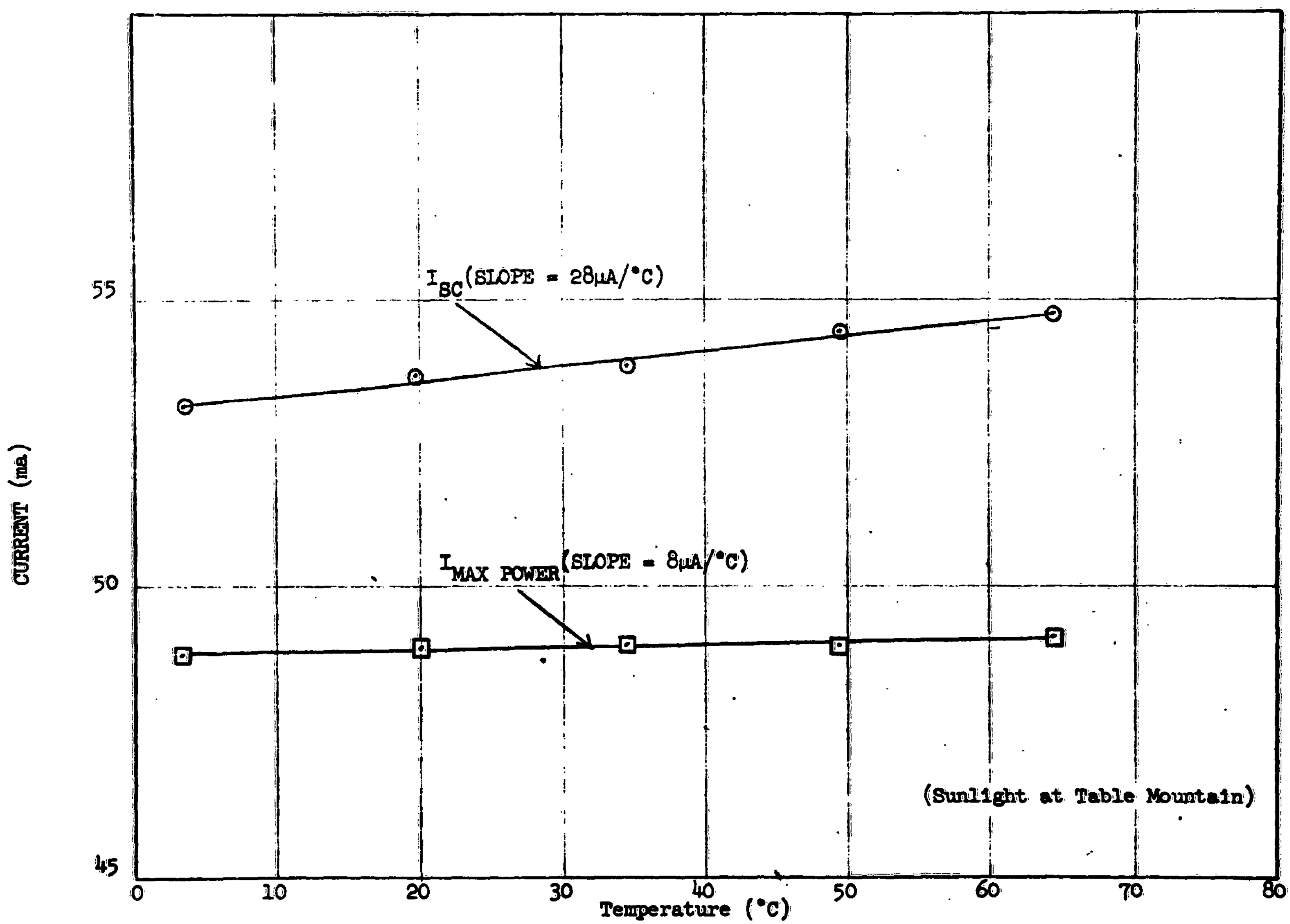

Figure 28. SOLAR CELL CURRENT vs TEMPERATURE FOR HELIOTEK GRIDDED "BLUE" CELL.

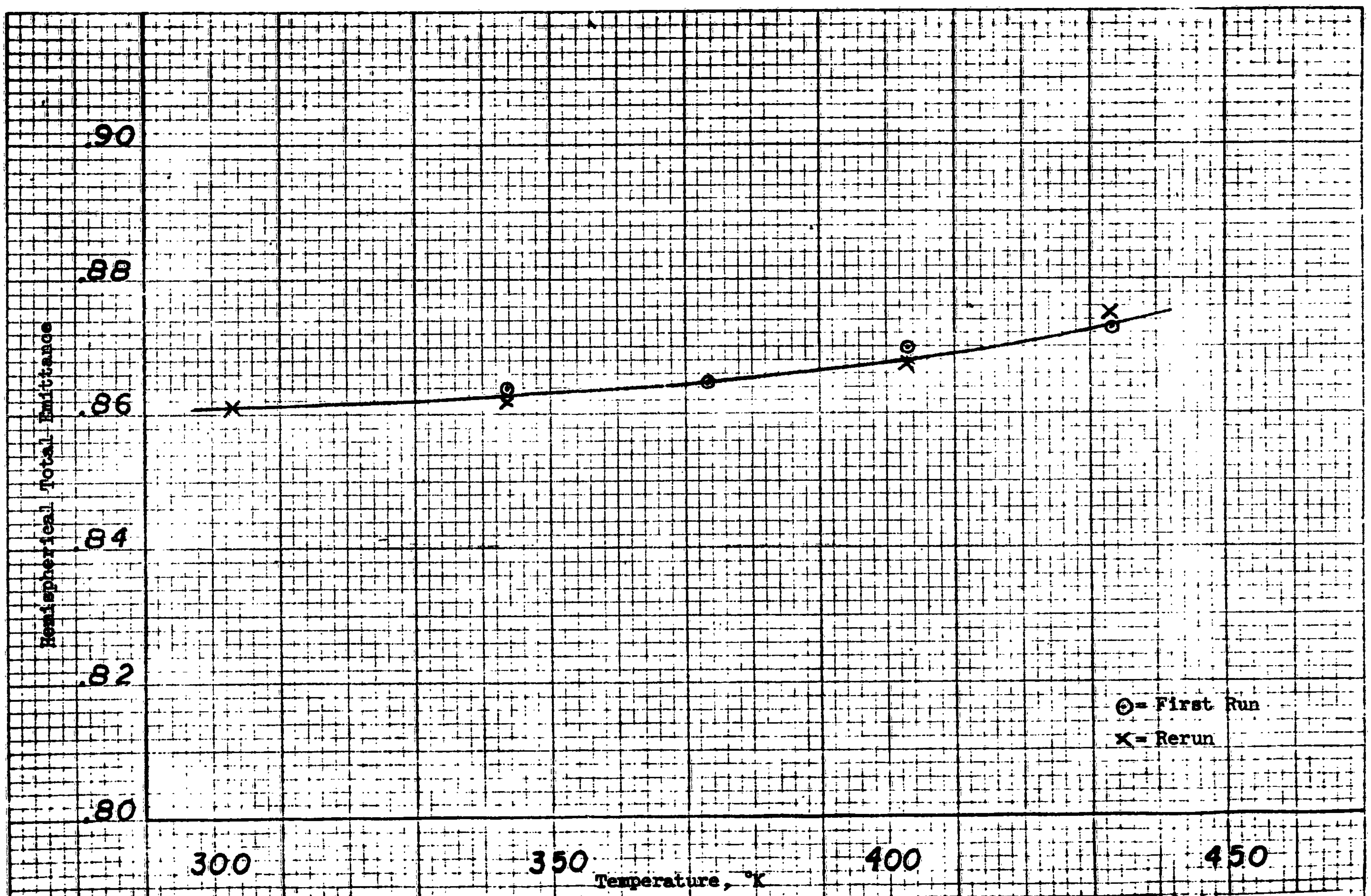

Figure 29. Hemispherical Total Emittance of Heliotek Gridded "Blue" Cell with Solakote "B" Filter.

APPENDIX

SERIES RESISTANCE EFFECTS ON SOLAR CELL MEASUREMENTS

By

MARTIN WOLF

and

HANS RAUSCHENBACH

This paper was presented at the 1961 Pacific General Meeting of the AIEE at Salt Lake City, Utah, August 23-25; 1961 and is to be published in ADVANCED ENERGY CONVERSION by Pergamon Press.

SUMMARY

Current-voltage characteristics of photovoltaic solar energy converter cells are obtainable by three methods, which yield different results due to the effects of the cell internal series resistance. The three resultant characteristics are: (1) the photovoltaic output characteristic, (2) the p-n junction characteristic, and (3) the rectifier forward characteristic. Choice of the proper method is necessary for obtaining the correct information for the individual application.

Most frequently used, e.g. for the determination of solar converter performance, is the photovoltaic output characteristic. A quick way is described for deriving such a characteristic for any light level from a corresponding characteristic obtained at a different light level. This method involves two translations of the coordinate system and requires only the knowledge of the series resistance and the difference in light intensities or short circuit currents.

An inversion of this method permits an easy determination of the series resistance, involving measurements at two arbitrary light levels of unknown magnitude.

The effects of series resistance consist at high light levels in a flattening of the photovoltaic output characteristic and a related drop in the maximum power point voltage. The resultant decrease in efficiency has to be overcome by series resistance reduction for solar cell applications with optical concentrators or for space missions in closer sun-proximity. At very high light levels, the cell series resistance leads to a deviation from the normal proportionality between short circuit current and light intensity; also a "current cutoff" is experienced due to attainment of open circuit condition in a portion of the cell.

The direct measurability of the p-n junction characteristic at high current densities without series resistance effects by the second method provides a powerful tool to the device development engineer, besides yielding a second method for the determination of the series resistance. Results from the application of this method indicate that, in the current density range as used in solar energy conversion, the silicon solar cell characteristic is much more closely described by the diffusion theory for p-n junctions than was previously believed.

1. INTRODUCTION

Like all other known generators of electrical power, solar cells possess some internal series resistance. This internal series resistance is so important as to determine the current-voltage characteristic of most of these power generators. This is, however, not the case with the solar cells. Rather a p-n junction, internally contained in the solar cell, determines the current-voltage characteristic of the device, with the series resistance contributing only in a secondary manner. Nevertheless, the internal series resistance is of sufficient importance as to have caught the attention of the device development engineers, which led to its reduction through decrease of contact resistance and through application of grid-shaped contacts. Also the power systems engineer concerned with the application of solar cells has to pay attention to the cell series resistance for the proper evaluation of current-voltage characteristics, for the matching of cells and for the prediction of solar cell output at differing light intensities. In order to further spread the knowledge about the various effects of the internal series resistance and about their proper interpretation, a summary of the series resistance effects on solar cell measurements and applications is presented in the following paragraphs.

2. THE THREE CURRENT-VOLTAGE CHARACTERISTICS OF SOLAR CELLS

Current-voltage characteristics for solar cells can and have in the past been obtained by three different methods.

The most commonly used method applies a fixed illumination, usually of known intensity, and a resistive load which is varied between short circuit and open circuit conditions, while measuring the voltage across the solar cell terminals and the current out of these terminals.[1] This method of measurement applies the solar cell in its normal photovoltaic mode of operation, and the current-voltage characteristic obtained in this manner is therefore called the "photovoltaic output characteristic." Figure 1a top shows the circuit diagram for this type of measurement, including the generally applied equivalent circuit diagram for the solar cell.[2) 3) 4)] Since this paper is primarily concerned with measurements for applications of photovoltaic cells at relatively high current densities, effects of shunt resistance can be neglected and are therefore not even mentioned in most cases discussed. The following equation is frequently used to describe the current-voltage characteristic obtained by this method:

$$I = I_o \left\{ \exp\left[\frac{q}{AkT}(V - IR_s)\right] - 1 \right\} - I_L \qquad 1)$$

This equation reproduces the obtained characteristics sufficiently well for most cases. Since a solar cell acts as a generator in this test, the current-voltage characteristic is obtained in the fourth quadrant of the current-voltage plane. The quantity I_L, called the light generated current, is proportional to the incident light intensity, if the spectral distribution of the radiation is not varied. The magnitude of this current is further determined by material and geometry factors of the solar cell, but is independent of the current-voltage characteristics. Other quantities of equ. (1) are the terminal current and voltage, I and V respectively, and the internal series resistance R_s; I_o is the diode saturation current determined by material properties; q and k are the electronic charge and the Boltzmann constant, respectively, while T is the absolute temperature and A a dimensionless constant between 1 and 5, but in most solar cells near 2.5 to 3.

The second method tests the solar cell like a diode without application of any illumination, but by supplying DC power from an external bias supply (see Fig. 1a center). The current-voltage characteristic obtained in this manner is therefore called the "diode forward characteristic." Again the voltage across the solar cell terminals and the current into these terminals are measured. The characteristic obtained by this method falls into the first quadrant of the current-voltage plane. It is described by:

$$I = I_b \left\{ \exp\left[\frac{q}{AkT} (V - IR_s)\right] - 1 \right\}. \qquad 2)$$

The diode forward characteristic differs from the photovoltaic output characteristic described by equ. (1) by the absence of the light generated current I_L and by the resulting positive direction of the terminal current I.

The third method for obtaining current-voltage characteristics from a solar cell appears more sophisticated than the previous two. The solar cell is again illuminated, but in this case with variable light intensity. The amount of the illumination does not have to be known, if the value of the light generated current I_L can be determined. This condition is fulfilled when the magnitude of the cell series resistance is sufficiently small so that the output current I of the device, when measured by the photovoltaic output method, is constant for all terminal voltage between 0 and 0.1 volts. In this case the measuring circuit may consist of a switch, a high resistance volt-meter and a low resistance milliamperemeter, arranged as shown in the circuit diagram (Fig. 1a bottom). The voltage drop across the milliamperemeter should be less than 50 millivolts and the resistance in the volt-meter circuit more than 100 kilo-ohms. The measurement consists of determining the short circuit current, I_{sc}, which under the presented conditions for every light intensity setting equals the light generated current I_L, and the open circuit voltage V_o, for every light intensity setting. Each pair of corresponding short circuit current and open circuit voltage values is plotted as one point in the first quadrant of the current-voltage plane. Through the variation of the light intensity, a succession of such points is obtained which presents the desired current-voltage characteristic. A method very similar to the one described here was first applied by Heeger and Nisbet for the matching of solar cells[5], and was again used independently from the investigations described later in this paper for similar studies by Queisser.[6] Should at higher light intensities the condition of flatness of the photovoltaic output characteristic near zero voltage not be fulfilled, then the light intensity will have to be measured independently, its value expressed in equivalent light generated current, and in this form entered into the graph. The measurement of light intensity can be performed by means of a more suitable solar cell, or of other photometric devices. The current-voltage characteristic obtained by this method is described by equ. (3):

$$I_L = I_o \left[\exp \left(\frac{q}{AkT} V_o \right) - 1 \right] \qquad 3)$$

It is derived from equ. (1) for the photovoltaic output characteristic by setting $I = 0$ and replacing V by the open circuit voltage V_o. In this case the term containing the internal series resistance R_s vanishes. The resultant expression is identical to that for the diode forward characteristic except for the absence of the series resistance term.

Figure 1b shows the current-voltage characteristics obtained on the same solar cell by applying the three methods described. A translation $I' = I + I_L$ has, however, been applied to the photovoltaic output characteristic in order to move it into the first quadrant of the current-voltage plane and to make it pass through the origin of this plane, thus facilitating comparison with the other two characteristics. The observed differences between the three characteristics are readily understandable from the previous description of the three methods for their generation. In the photovoltaic output characteristic, a current is generated internally in the cell, giving rise to a voltage across the p-n junction in the forward bias direction and causing current flow through this p-n junction. The difference in current between the light generated current I_L and the forward current through the p-n junction flows through the device terminals, but also results in a voltage drop across the internal series resistance. The measured terminal voltage is therefore smaller than the voltage across the p-n junction by the amount of this voltage drop. In the diode forward characteristic, the current is supplied from an external power supply, not using the internal generator. All of the current passing the solar cell terminals flows through the p-n junction, but it passes the internal series resistance in the opposite direction than it does in the case of the photovoltaic output characteristic. Therefore the voltage across the p-n junction is smaller than the terminal voltage V. In the p-n junction characteristic finally a case is obtained in which the effect of the internal series resistance is eliminated. In the open circuit voltage condition, the terminal voltage is identical to the voltage existing across the p-n junction, while the short circuit current measures the light generated current directly as long as the voltage drop across the internal series resistance is sufficiently small as to cause only a negligibly small current to flow through the p-n junction in the forward direction.

The curves of Fig. 1b substantiate this explanation. The photovoltaic output characteristic exhibits terminal voltages which are smaller than those of the p-n junction characteristic by the voltage drop over the internal series resistance caused by the current flowing through this part of the circuit. Conversely, the diode forward characteristic exhibits voltage values higher than those of the p-n junction characteristic by the voltage drop caused by the current flow through the internal series resistance.

The foregoing discussions also outline the range of application for the different types of characteristics. Whenever the performance of a solar cell as a photovoltaic energy converter is concerned, be it for the determination of its power output, for the matching of different solar cells into a system, or for the extrapolation of the cell output from one intensity level to a different one, then one has to use the photovoltaic output characteristic. If the characteristic of the p-n junction itself is to be studied, then the p-n junction characteristic obviously has to be obtained. If the solar cell is to be used as a passive device and its performance without illumination is to be studied, then the diode forward characteristic has to be taken.

3. THE EFFECT OF SERIES RESISTANCE ON THE RELATIONSHIP BETWEEN SHORT-CIRCUIT CURRENT AND LIGHT INTENSITY

The light generated current I_L is proportional to the intensity of the incident radiation up to extremely high light intensities. Numerous measurements undertaken in order to check this relationship appeared to show deviations at light intensities orders of magnitude below those where deviations can be expected. These supposed deviations were caused by the effect of the series resistance on the short circuit current which had been measured instead of the light generated current. Such a substitution can properly be made on ideal solar cells with zero series resistance, and on real solar cells at sufficiently low light intensities only. At light intensities high enough so that the product of internal series resistance and terminal current exceeds 250 millivolt, the short circuit current can no longer be considered identical to the light generated current.

Figure 2 illustrates this fact on the photovoltaic output characteristics of two different solar cells taken at five values of solar irradiance between 50 milliwatts cm^{-2} and 400 milliwatts cm^{-2}. One of these solar cells is a gridded solar cell with a series resistance of .38 ohms, while the other solar cell is a nongridded cell having a series resistance of about 3.5 ohms. The low-series resistance cell exhibits rather square characteristics up to 400 milliwatts cm^{-2} of solar irradiance, with the terminal current staying constant for variations of the terminal voltage from 0 to 200 millivolts. This means that the short circuit current is identical to the light generated current throughout this irradiance range. The high-series resistance cell, however, exhibits successively more rounded characteristics at increasing light intensities, and the short circuit current deviates from the light generated current already at 200 milliwatts cm^{-2} of solar irradiance. At larger values of solar irradiance, the terminal current does not reach its maximum value at zero terminal voltage, but continues to increase with increasing negative terminal voltages, until it finally reaches its maximum value and equals the light generated current. The photovoltaic output characteristic can readily be extended into the third quadrant of the current-voltage plane, if the resistive load is provided by an external source which permits the simultaneous application of negative voltages.

Figure 3 presents a plot of the short circuit current as a function of solar irradiance for the two cells used for the measurements presented in Fig. 2. This plot shows that the low series resistance cell exhibits a linear relationship between short circuit current and solar irradiance up to 400 milliwatts cm^{-2} which is identical to four times the maximum solar irradiance reached at the earth's surface at sea level at noon time on a clear day. The graph also shows the considerable deviation from linearity for the solar cell withthe high internal series resistance.

The foregoing discussion emphasizes the caution which has to be used in the application of the short circuit current of a solar cell for light metering purposes at high light intensities. The amount of internal series resistance in the cell has to be determined and the region of deviation from the linearity be established before a cell can be confidently applied for such purposes.

4. THE EFFECTS OF INTERNAL SERIES RESISTANCE ON SOLAR CELL PERFORMANCE

The curves of Fig. 2 indicate that the internal series resistance can severely affect the performance of photovoltaic cells as solar energy converters. The maximum power output of a solar cell is given by the area of the largest rectangle that can be drawn inside the photovoltaic output characteristic. The area of such a rectangle increases with increasing "sharpness" of the knee in the photovoltaic ouput characteristic. Internal series resistance causes a successively larger "rounding" of the characteristic at increasing light intensities. Solar cells are normally designed for best performance at radiation intensities as obtained at the earth's surface. Such cells may therefore not give optimum performance at increased light intensities as may be encountered in space vehicle applications in closer proximity to the sun or in the use of solar cells combined with radiation concentrating devices.

Figure 4 presents three sets of curves, calculated for a solar cell with $I_o = 6.9 \times 10^{-12}$ amp, $I_L = 5.5 \times 10^{-2}$ amp, and $\frac{q}{AkT} = 38.6$ Volt $^{-1}$, and with assumed internal series resistance values of 0, 0.5 and 1.0 ohms. The curves give the maximum power output into a matched load, the maximum power point voltages and the efficiencies for values of solar irradiance between 50 and 350 milliwatts per square centimeter. The zero-resistance solar cell shows monotonously increasing power output with increasing light intensity. Finite values of the series resistance cause the maximum power output to increase less rapidly at the higher light intensities. This effect becomes progressively larger with increasing series resistance and light intensity.

The maximum power point voltage, which steadily increases with increasing light intensity for the zero-series resistance cell, starts to decrease at higher light intensities for the cell with 0.5 ohms series resistance, and shows continuous and larger decrease at a series resistance value of 1.0 ohm through the intensity range of 50 to 400 mW cm^{-2}. The maximum power point voltage which steadily increases with light intensity for the zero-series resistance cell starts to decrease at the higher light intensities for the cell with 0.5 ohms series resistance, and shows a continuous drop at a series resistance value of 1.0 ohm.

The dotted curves in Figure 4 present the conversion efficiency. The curve for the zero-series resistance cell hows a monotonous rise toward the higher solar irradiance values while the curves for the 0.5 and the 1.0 ohm cells exhibit progressive efficiency decreases toward the higher light intensities.

Also presented in Figure 4 are experimental curves obtained on two solar cells with 0.38 and 3.5 ohms series resistance, respectively. It is interesting to note that the shape of the experimental curve for the 0.38 ohm cell fits perfectly into the system of the theoretical curves although its absolute values are somewhat lower due to deviations of other device parameters from those assumed for the theorectical evaluation. The information presented in this paragraph leads to the conclusion that for high power output and high efficiency at high light intensities, and for a minimum change of the maximum power point voltage with increasing light intensities, solar cells with progressively smaller internal series resistance will have to be selected or be specifically developed.

5. A METHOD FOR THE PREDICTION OF THE PHOTOVOLTAIC OUTPUT CHARACTERISTIC FOR DIFFERENT LIGHT LEVELS

The photovoltaic output characteristic as described by equ. (1) permits an easy prediction of the corresponding current voltage characteristic for a given light level which differs from the one at which the original characteristic has been measured.

In the case of the solar cell with zero-series resistance, the exponent of equ. (1) contains only the independent variable, that is the terminal voltage. For any fixed light level only the exponential term is variable on the right hand side of equ. (1). Any change in the light intensity enters then into the relationship through the light generated current I_L. A change in the light intensity results, at constant terminal voltage V, in a change of the terminal current I equal to the difference of the light generated currents ΔI_L. This means that the shape of the curve, which is determined by the exponential term, is invariant with respect to light intensity. The mathematical derivation for this is presented in Appendix A of this paper. The photovoltaic output curve for a different value of light intensity can readily be obtained by translating the original curve parallel to the ordinate of the IV coordinate system by an amount equal to the difference in the light generated currents, which is proportionate to the difference of the light intensities.

The method outlined in the previous paragraph is valid for solar cells with small values of series resistance or at sufficiently low light levels so that the effects of the series resistance can be neglected. This is expressed in the condition that the product IR_s has to be negligibly small compared to the terminal voltage V. If this condition is not fulfilled, then a second translation parallel to the abscissa has to be performed on the photovoltaic output characteristic for the transformation to a second light intensity. The second translation consists in a decrease of the terminal voltage by an amount equal to the product of the internal series resistance R_s and the difference in the light generated currents, ΔI_L. A formal derivation for this case is also given in Appendix A.

For a change of the photovoltaic output characteristic from the light intensity L_1 with the light generated current I_{L_1} to the light intensity L_2 generating the current I_{L_2}, the two translations

$$I_2 = I_1 - \Delta I_L \qquad 4)$$

and

$$V_2 = V_1 - \Delta I_L R_s \qquad 5)$$

have therefore to be performed. Since I_L is proportional to the light intensity $I_L = CL$, ΔI_L can be expressed through relationship between the light intensities:

$$\Delta I_L = C(L_2 - L_1) \qquad 6)$$

Since I_{L_1} can be readily obtained from the photovoltaic output characteristic, measured at light intensity L_1, ΔIL is more conveniently related to the difference in light intensities through the form:

$$\Delta I_L = I_{L_1} \frac{L_1 - L_2}{L_1} \qquad 7)$$

A previously expressed note of caution in the substitution of the short circuit current I_{sc} for the light generated current I_L at high light intensities or large value of series resistance should be observed.

Figure 5 illustrates the two translations of the coordinate system to be performed by going from a light intensity L_1 at which the photovoltaic output characteristic has been measured, to a higher light intensity L_2 at which this characteristic is desired to be known.

Figure 6 presents experimental data to demonstrate the correctness of this procedure. The photovoltaic output characteristics from Figure 2 for the low series resistance solar cell, measured at five different light levels between 50 and 400 mW cm^{-2}, are reproduced in Figure 6. After performing the translations of the coordinate system for the four photovoltaic output curves obtained at the lower light intensities to the 400 mW cm^{-2} level, they are found to all fall on top of each other as well as on the experimental curve for this intensity. The experimentally obtained curves are given in solid lines, while the transformed curves are presented by squares, circles, and triangles, corresponding to the different original intensities.

6. A METHOD FOR THE DETERMINATION OF THE INTERNAL SERIES RESISTANCE

An inversion of the method described in Section 5 permits the easy and accurate determination of the internal series resistance of any solar cell. For this purpose the photovoltaic output characteristic has to be measured at two different light intensities, the magnitudes of which does not have to be known. The two characteristics are translated against each other by the amounts ΔI_L and $\Delta I_L \times R_s$ in the y- and the x-direction, respectively. Two corresponding points on the two characteristics show a displacement with respect to each other, which is identical to the two translations of coordinate systems. The displacement parallel to the ordinate gives the value of ΔI_L. Since the displacement parallel to the abscissa equals $\Delta I_L R_s$, the value of the internal resistance R_s is readily obtained.

One practical approach to this procedure is to choose an arbitrary interval ΔI from the short circuit current I_{sc}, which determines the first characteristic. It is frequently found convenient to choose ΔI

so as to obtain a point in or near the knee of the characteristic. The same ΔI value is used for the finding a second corresponding point on the second characteristic. An illustration of the procedure is presented in Fig. 7.

This method was first suggested in 1960 by Swanson.[7]

7. EXPERIMENTALLY FOUND DEVIATIONS FROM THE LUMPED CONSTANT MODEL

It has been found that the measured current-voltage characteristics of many solar cells cannot be very accurately described by the equivalent circuit model of Fig. 1 and by equ. (1). These deviations have been found to be due to two separate effects: one involving the p-n junction characteristic, and the other the internal series resistance. The effect involving the p-n junction characteristic will be discussed in Section 8, while in this section attention will be directed to the effect of the internal series resistance.

If the model discussed in the previous sections is valid, then the same value of internal series resistance R_s will be obtained by application of the method described in Section 6, independent of the chosen value of ΔI. Also, a sequence of photovoltaic output characteristics obtained at different light levels, and transformed to any one of these curves by the method described in Section 5 will show perfect agreement between the individual curves as illustrated in Fig. 6. Equality of the series resistance values obtained from different parts of the characteristic, and agreement between transformed curves is, however, not found on all solar cells measured. The high series resistance cell A-N-16 used for obtaining data for Fig. 2 through 4 shows such deviations. These observations are not only made on cells with high internal series resistance, although the deviations found in low series resistance cells are generally substantially smaller.

Fig. 8a presents two curves obtained on a low series resistance gridded solar cell at two different light intensities. Marked in this figure are the series resistance values obtained at different portions of the characteristics. These values range from 0.5 to 0.7 ohms. It has been observed, that the limits of the range of series resistance values are rather independent of the amount of light intensity and of the difference in light intensities used for this evaluation, except for the fact that at high light intensities a different portion of the curve can be evaluated which is not available at the low intensities. This is demonstrated by the data contained in Table I, which were obtained on cell A-G-43.

The reasons for the deviations are to be found in the physical configuration of the solar cell. Major contributions to the internal series resistance come from the sheet resistance of the p-layer, the bulk resistance of the n-layer, and the resistance between the semiconducting material and the metallic contacts. While the contact series resistance can properly be represented by a lumped resistance, the sheet resistance and the bulk resistance are distributed throughout the device. Fig. 9 shows the transition from the physical configuration of the solar cell to the distributed constants model. The cell is imaginarily divided into many elements, each one containing a p-n junction, which acts as a source and a shunting diode simultaneously. These junction elements are inter-connected by the distributed resistances. This model was studied in 1958 by the first author as the proper representation for the current flow and voltage distribution in a solar cell, but has been discarded because of the enormous complexity of its evaluation. A similar, slightly simplified model has been proposed by Wysocki, Loferski and Rappaport in 1960,[8)] but was apparently also not evaluated. Because of the rather small values of internal series resistance encountered in the modern gridded solar cells, an intermediate model is proposed here. It represents the next refinement step from the lumped constants model of Fig. 1. Instead of dividing the cell into many elements, it splits the solar cell into two equal parts and adds the bulk resistance, the contact resistance, and a portion of the sheet resistance into a lumped element next to the terminal. The other portion of the sheet resistance is placed in the connection between the two parts of the cell. The ratio between the values of the two resistance elements has been found to vary between individual cells.

Fig. 11 presents the p-n junction characteristic of a silicon solar cell obtained by the third method described in Section 2. It also presents theoretical points obtained by the lumped constants model according to Fig. 1a, and by the improved lumped constants model of Fig. 9. Also presented is the experimentally obtained photovoltaic output characteristic which demonstrates good agreement between the experimental data and the improved lumped constants model. A resistance ratio of 9 to 1 has been found to be appropriate for the cell evaluated for this figure.

8. APPLICATION OF THE P-N JUNCTION CHARACTERISTIC FOR DEVICE STUDIES

The diode forward characteristic has long been used for the investigation of device parameters like the saturation current, the constant A in the exponent of the diode characteristic, the temperature dependence of these characteristics, and for the interpretation of the physical mechanism causing the observed device behavior. The p-n junction characteristic, described as method 3 in Section 2, provides a very useful supplement to the diode forward characteristic for such studies. The usefulness of the p-n junction characteristic stems from the severe effect which the series resistance has on the diode forward characteristic at high injection levels, and which is not present in the p-n junction characteristic.

At sufficiently low injection levels where series resistance effects become negligible the two characteristics become identical. Fig. 10 contains a diode forward characteristic and a p-n junction characteristic obtained at 23° C on the gridded solar cell A-N-12 which was used for the previously described measurements. The graph shows excellent agreement obtained between the two different methods at injection levels below 10^{-3} Amp on the 2 cm^2 cell. Experimentally obtained points of the p-n junction characteristic, given by circles superimposed on the also experimentally obtained diode forward characteristic which is presented by the solid curve, demonstrate this agreement. Above 2×10^{-3} amperes, however, divergence between the two curves is observed. The difference between the p-n junction characteristic and the diode forward characteristic at high injection levels corresponds to a series resistance of 0.33 ohms, which differs from the 0.38 ohms value obtained from the photovoltaic output characteristic according to Section 6.

Evaluation of the reverse characteristic yields a shunt resistance value of 13.8 kilo ohms, and a saturation current $I_o = 6.5 \times 10^{-6}$ Amp. The current conducted through such a shunt resistance is shown in Fig. 10 by the curve marked "$I = \frac{V}{R_{sh}}$". By subtracting the current conducted through this shunt resistance from the current values of the diode forward characteristic, a new curve is obtained which deviates from the experimentally obtained characteristic at the low injection levels. The curve thus obtained is the true p-n junction characteristic without resistive shunt effects. The curve is matched by a diode equation of the form of equ. (2) with a saturation current $I_o = 5.5 \times 10^{-6}$ Amp and constant A = 2.86 at a device temperature of 296° K. At the high injection levels, however, a deviation from the exponential is observed. This deviation is in the diode forward characteristic partially hidden by the effect of the series resistance, but can be clearly observed and evaluated from the p-n junction characteristic.

The p-n junction characteristic at high injection levels asymptotically approaches a second exponential curve which in the semi-log plot of Fig. 10 is represented by a straight line. The transition region between the two pure exponential portions of the curve is very accurately described by the sum of the two exponential terms. It is interesting to note that on all solar cells thus investigated, the second exponential term has an A value of 1 and saturation currents of 10^{-12} to 10^{-11} amperes for the 2 cm^2 junction. Such values are to be expected from a device following the carrier diffusion theory of a p-n junction as described by Shockley.[9)]

Also shown in Fig. 10 is a diode forward characteristic obtained on the same cell at a device temperature of 417° K. At the high injection level a series resistance voltage drop corresponding to the series resistance value of 0.33 ohms was found in the room temperature curve. This voltage drop was subtracted from the diode forward characteristic and, again, was found to lead to a good match to the p-n junction characteristic. The very highest current values, which were obtained by the diode forward method only, appear too high, probably due to thermal runaway during the measurements.

The resultant characteristic for the p-n junction at 417° K can also be best described by the super-position of two exponential terms. Like in the room temperature case, the curve approaches asymptotically the exponential represented by a straight line in the semi-log plot at the high injection levels, while the transition region is accurately described by the sum of the two exponentials.

The remarkable finding is, that the exponential for the higher injection levels has the constant A = 1. Using the carrier diffusion theory for p-n junctions as described by Shockley, and the experimental value for $I_o = 3.3 \times 10^{-12}$ amp at 296° K, one arrives at a saturation current $I_o = 8 \times 10^{-6}$ amp for the same junction at 417° K. This is in very good agreement with the experimental finding of 7×10^{-6} amperes.

While extremely good correlation between the p-n junction characteristic at high injection levels and the carrier diffusion theory for p-n junction behavior could repeatedly be established, no correlation to a theoretical behavior could be found for the lower injection level part of the characteristic. A considerable spread of values for the constant A and for the saturation current were found for the lower injection level exponential. Still more non-uniformity was observed in the temperature dependence of this portion of the curve. Since no pattern could yet be established in these findings, a hypothesis shall not be advanced for the physical nature of the characteristics at the lower current levels.

The foregoing discussions lead to a replacement of equ. (1) by the following form:

$$I = I_{o1} \left[\exp \left(\frac{q}{AkT} V \right) - 1 \right] + I_{o2} \left[\exp \left(\frac{q}{kT} V \right) - 1 \right] - I_L \qquad 8)$$

with $A = A(T)$.

According to this description, a new equivalent circuit diagram evolved containing two separate forward biased diodes connected in parallel. This new model resembles one advanced earlier by Watson.[10] Watson, however, assigned identical exponents to both junctions, and described only a relatively small difference in the saturation currents. A separation of the two p-n junctions by the series resistance is not necessary, because the p-n junction characteristic alone exhibits the property of the super-position of the exponentials, and at high injection levels where the series resistance becomes most effective the characteristic is dominated by only one of the two exponentials.

The knee of the I-V characteristic, however, is most heavily affected by the transition region between the two exponentials. This is demonstrated in Fig. 11 which shows an exponential curve with $A = 1$ and $I_o = 1.6 \times 10^{-12}$ Amp together with the experimentally obtained p-n junction characteristic for cell A-G-43. In the portion of the characteristic nearer the open circuit voltage point, which is the high injection region, close approximation between the two curves can be noticed. In the knee of the curve, however, which falls into the transition between the two exponentials, the experimental curve appears much more rounded than the single exponential with $A = 1$. In the part of the curve approaching the short circuit current, the difference between the two exponentials is not concernable because of the scale of the plot.

The sum of two exponentials, for which the saturation currents and A-values have been obtained from a semi-log plot for cell A-G-43 similar to Fig. 10, has been calculated and its results are superimposed on the experimentally obtained p-n junction characteristic, illustrating the good agreement.

Finally, the photovoltaic output characteristic is shown, obtained experimentally at a light intensity equivalent to about 500 mW cm^{-2} of solar irradiance. Shown with this curve as circles are values calculated by using the "sum-of-two-exponentials" model together with a single lumped series resistance corresponding to the original model of Fig. 1a. The points obtained in this manner show a fair approximation to the experimental curve, with the largest deviations at the knee of the curve which is of greatest interest for maximum power output considerations.

A further calculation has been carried out using the improved lumped constants model described in Section 7 and Fig. 9 together with the "sum-of-two-exponentials" model. The results are presented in the form of squares superimposed on the experimental curve. They prove the very close approximation to the actual cell characteristic obtained by the use of this model. The equivalent circuit diagram of this model is shown in Fig. 12, and the equation describing it has the following form:

$$
\begin{aligned}
I = {} & I_{o_1}\left\{\exp\left[\frac{q}{kT}\left(V - IR_{s_2}\right)\right] - 1\right\} + I_{o_2}\left\{\exp\left[\frac{q}{AkT}\left(V - IR_{s_2}\right)\right] - 1\right\} \\
& + I_{o_1}\left\{\exp\left[\frac{q}{kT}\left[V - IR_{s_2} - \left(I - \frac{1}{2}I_L + I_{D_3} + I_{D_4}\right) R_{s_1}\right]\right] - 1\right\} \\
& + I_{o_2}\left\{\exp\left[\frac{q}{AkT}\left[V - IR_{s_2} - \left(I - \frac{1}{2}I_L + I_{D_3} + I_{D_4}\right) R_{s_1}\right]\right] - 1\right\} - I_L
\end{aligned}
\tag{9}
$$

Although this model is only the next improvement step after the original lumped constants model, it exhibits already considerable complexity, but yields also much more satisfactory results.

It will be interesting to note that for cell A-G-43 the values for R_{s_1} and R_{s_2} which were found to give best results were 0.265 and 0.30

respectively. This compares to a single lumped resistance of $R_s = 0.36$ ohms for the old model. The values indicate a larger contribution from the sheet resistance than from the bulk and contact resistances.

The foregoing discussions shed light on the importance of the p-n junction characteristic to the device development engineer, who can by applying this method study the device parameters without being hindered by the overshadowing effects of series resistence.

9. CONCLUSION

The foregoing discussions illuminates the effect of series resistance on solar cell measurements and the caution to be taken in their interpretation. The reduction of efficiency at high light intensities due to high values of series resistance was analyzed with the conclusion that for advantageous application of solar cells at high light intensities emphasis has to be placed on the reduction of series resistance. Finally, new features of the p-n junction characteristic were discussed.

These were previously hidden due to the modification of the current-voltage characteristic by series resistance effects. New lumped constants models were developed which more closely approximate the characteristics measured on the solar cells.

10. ACKNOWLEDGEMENT

Special appreciation shall be expressed to Messrs. P. Goldsmith and W. Schaefle of the Jet Propulsion Laboratory, Pasadena, California, for their mentioning of observed discrepancies between measured photovoltaic output characteristics and the theoretical curves as described by the older lumped constants model.

REFERENCES

1. Rauschenbach, H., "Understanding Solar Measurements", March-April and May-June issues of SPAN.
2. Pfann, W. G., and van Roosbroeck W., J. Appl. Phys. 25, 1422 (1954)
3. Prince, M. B., "Silicon Solar Energy Converters", J. Appl. Phys. 26, 534-540, May, 1955.
4. Wolf, M. and Prince, M. B., "New Developments in Silicon Photovoltaic Devices and Their Application in Electronics," published in "Solid State Physics in Electronics and Telecommunications," Proceedings of an International Conference held in Brussels, Belgium, June 2-7, 1958, 2, 1180-1196, Academic Press, London and New York, 1960.
5. Heeger, A. J., and Nisbet, T. R., "The Solar Cell Diode Curve -- A Crucial Design Parameter", Lockheed Missile Systems Division, Sunnyvale, California, LMSD No. 310003.
6. Queisser, H. J., "Forward Characteristics and Efficiencies of Silicon Solar Cells", Submitted for publication in "Solid State Electronics", (Pergamon Press).
7. Swanson, L. D. (Private Communication)
8. Wysocki, J. J., Loferski J.J., and Rappaport, "Research on Photovoltaic Converters", Radio Corporation of America.
9. Shockley, W., "Electrons and Holes in Semiconductors", Van Nostrand, New York, 1950.
10. Watson, R. H., "Equivalent-circuit Characteristics of the Solar Cell"., Presented at the 1960 Pacific General Meeting of the AIEE at San Diego, California, August 11, 1960.

TABLE I

Series Resistance Values Obtained On Solar Cell A-G-43 At Different Correlation Points and Light Intensities

* * *

Initial Solar Irradiance $mWcm^{-2}$	Initial Light Generated Current ΔI_{L_1} mA	Final Solar Irradiance $mWcm^{-2}$	Final Light Generated Current I_{L_2} mA	Light Generated Current Difference ΔI_L mA	Correlation Current Difference ΔI mA	Measured Series Resistance R_s Ohms
~50	25.1	100	50.1	25	2.7	0.4
					5.6	0.4
					12.1	0.4
					20.2	0.36
					25.1	0.36
~100	50.1	200	100.0	49.9	10.0	0.36
					20.0	0.34
					30.0	0.36
					40.0	0.36
					49.9	0.32
~100	50.1	300	150.0	100	5.0	0.58
					10.0	0.42
					25.0	0.37
					50.0	0.34
~100	50.1	400	199	148.9	5.0	0.43
					25.0	0.37
					50.1	0.34
~100	50.1	500	249.5	199.4	5.0	0.38
					25.0	0.39
					50.1	0.36
~300	150.0	400	199	49	25	0.36
					150	0.30
~300	150.0	500	249.5	99.5	25	0.42
					50	0.39
					75	0.37
					100	0.36
					125	0.34
					150	0.32

THREE METHODS FOR OBTAINING CURRENT-VOLTAGE CHARACTERISTICS ON SOLAR CELLS

1. PHOTOVOLTAIC OUTPUT (CONSTANT ILLUMINATION)

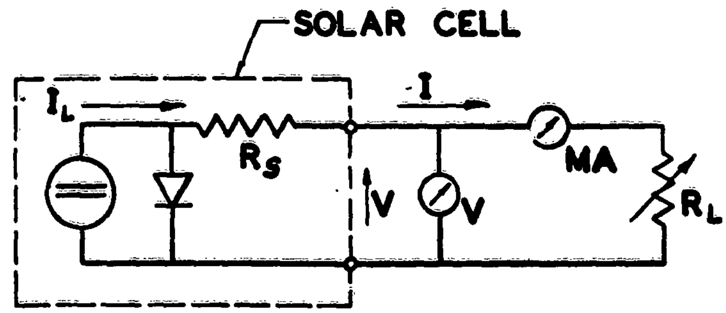

$$I = I_0\left\{\mathrm{EXP}\left[\frac{q}{AkT}\,(V - IR)\right] - 1\right\} - I_L \qquad I < 0 \qquad V \geq 0$$

2. DIODE FORWARD (WITHOUT ILLUMINATION)

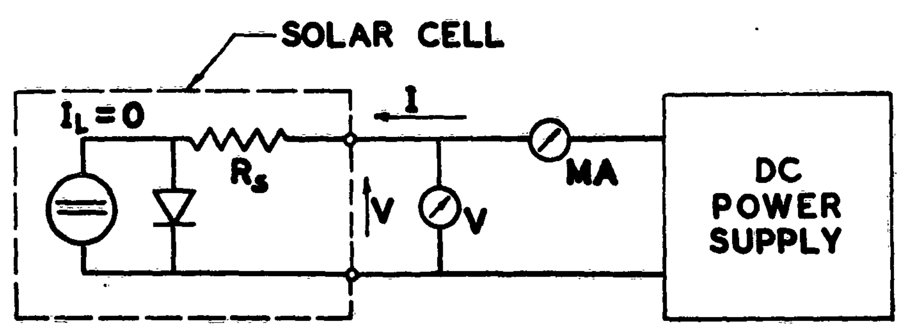

$$I = I_0\left\{\mathrm{EXP}\left[\frac{q}{AkT}\,(V - IR_S)\right] - 1\right\} \qquad I \geq 0 \qquad V \geq 0$$

3. P-N JUNCTION (VARIABLE ILLUMINATION)

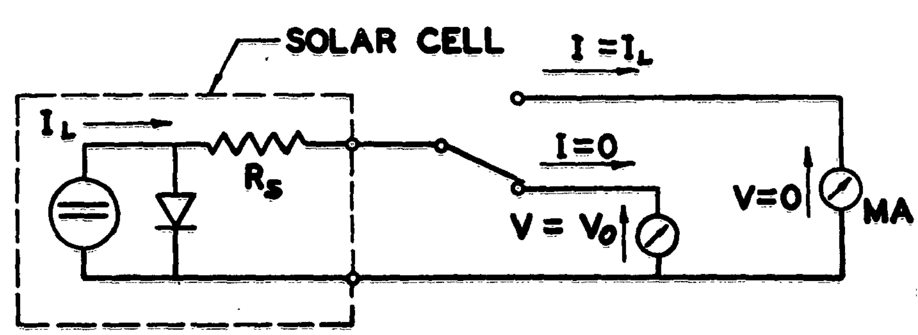

$$I_L = I_0\left[\mathrm{EXP}\left(\frac{q}{AkT}\,V_0\right) - 1\right] \qquad \text{PLOT } I_L \text{ VS. } V_0$$

FIG. 1a.

FIG. 1b.

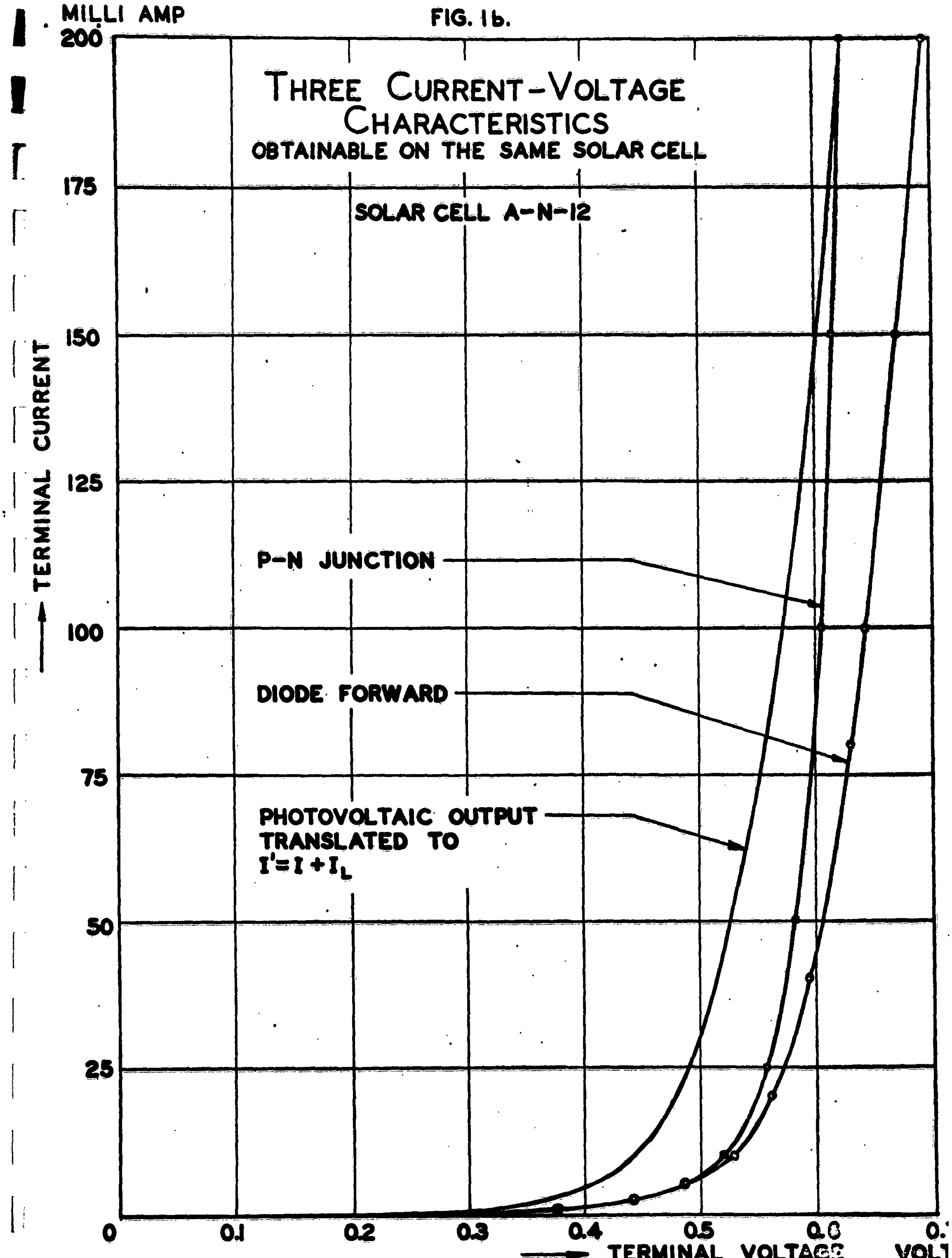

THREE CURRENT-VOLTAGE CHARACTERISTICS
OBTAINABLE ON THE SAME SOLAR CELL
SOLAR CELL A-N-12
MILLI AMP
200
175
150
125
100
75
50
25
0
→ TERMINAL CURRENT
P-N JUNCTION
DIODE FORWARD
PHOTOVOLTAIC OUTPUT TRANSLATED TO $I' = I + I_L$
0.1
0.2
0.3
0.4
0.5
0.6
→ TERMINAL VOLTAGE
VOLT

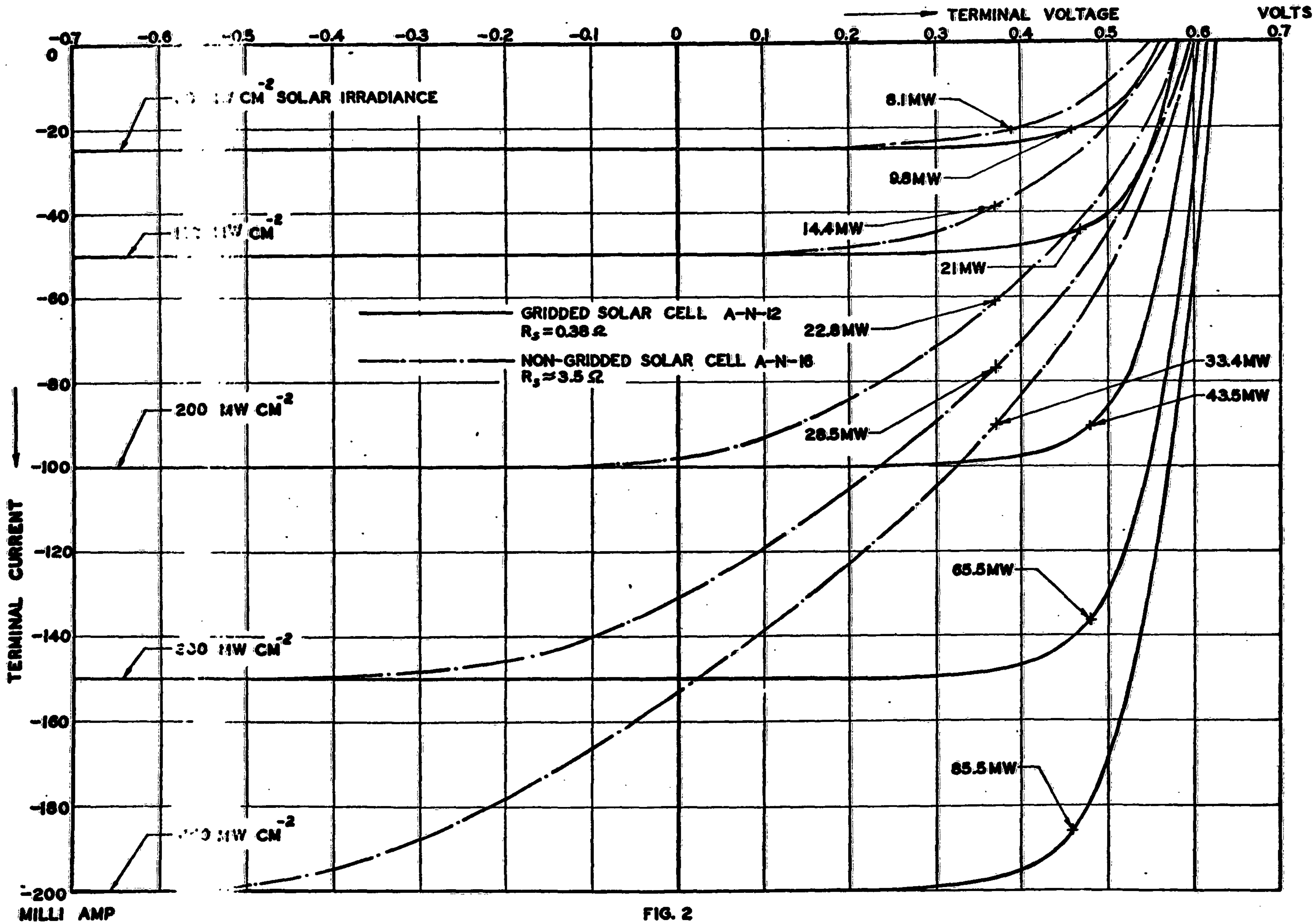

TERMINAL VOLTAGE
VOLTS
-0.7
-0.6
-0.5
-0.4
-0.3
-0.2
-0.1
0
0.1
0.2
0.3
0.4
0.5
0.6
0.7
TERMINAL CURRENT
MILLI AMP
0
-20
-40
-60
-80
-100
-120
-140
-160
-180
-200
CM^{-2} SOLAR IRRADIANCE
CM^{-2}
200 MW CM^{-2}
MW CM^{-2}
MW CM^{-2}
8.1MW
9.8MW
14.4MW
21MW
22.8MW
28.5MW
33.4MW
43.5MW
65.5MW
85.5MW
GRIDDED SOLAR CELL A-N-12
$R_s = 0.38\ \Omega$
NON-GRIDDED SOLAR CELL A-N-16
$R_s = 3.5\ \Omega$

FIG. 2

FIG. 3

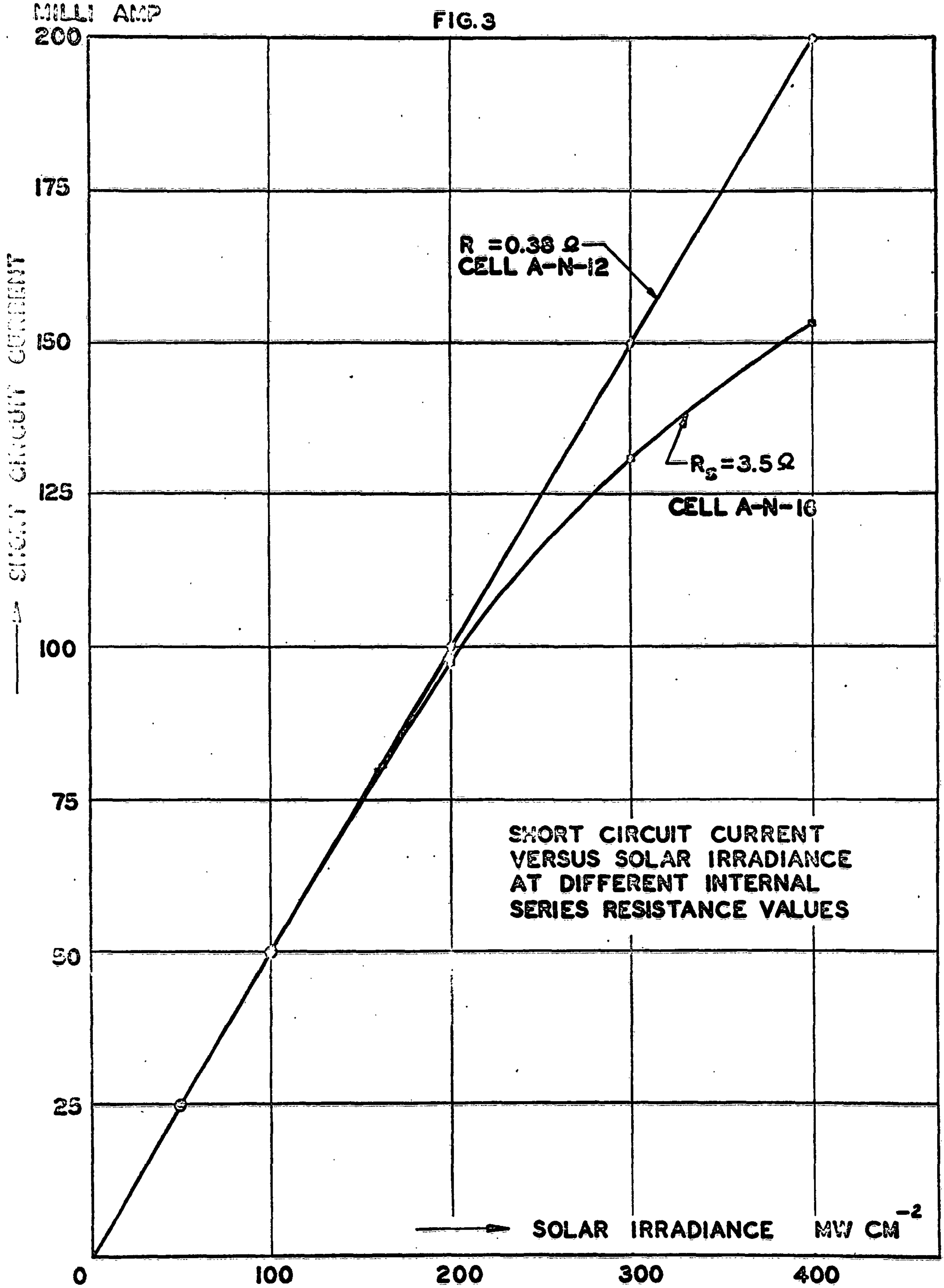
MILLI AMP
200
175
150
125
100
75
50
25
SHORT CIRCUIT CURRENT
R =0.38 Ω
CELL A-N-12
R_S=3.5 Ω
CELL A-N-16
SHORT CIRCUIT CURRENT VERSUS SOLAR IRRADIANCE AT DIFFERENT INTERNAL SERIES RESISTANCE VALUES
SOLAR IRRADIANCE MW CM^{-2}
0
100
200
300
400

FIG. 4

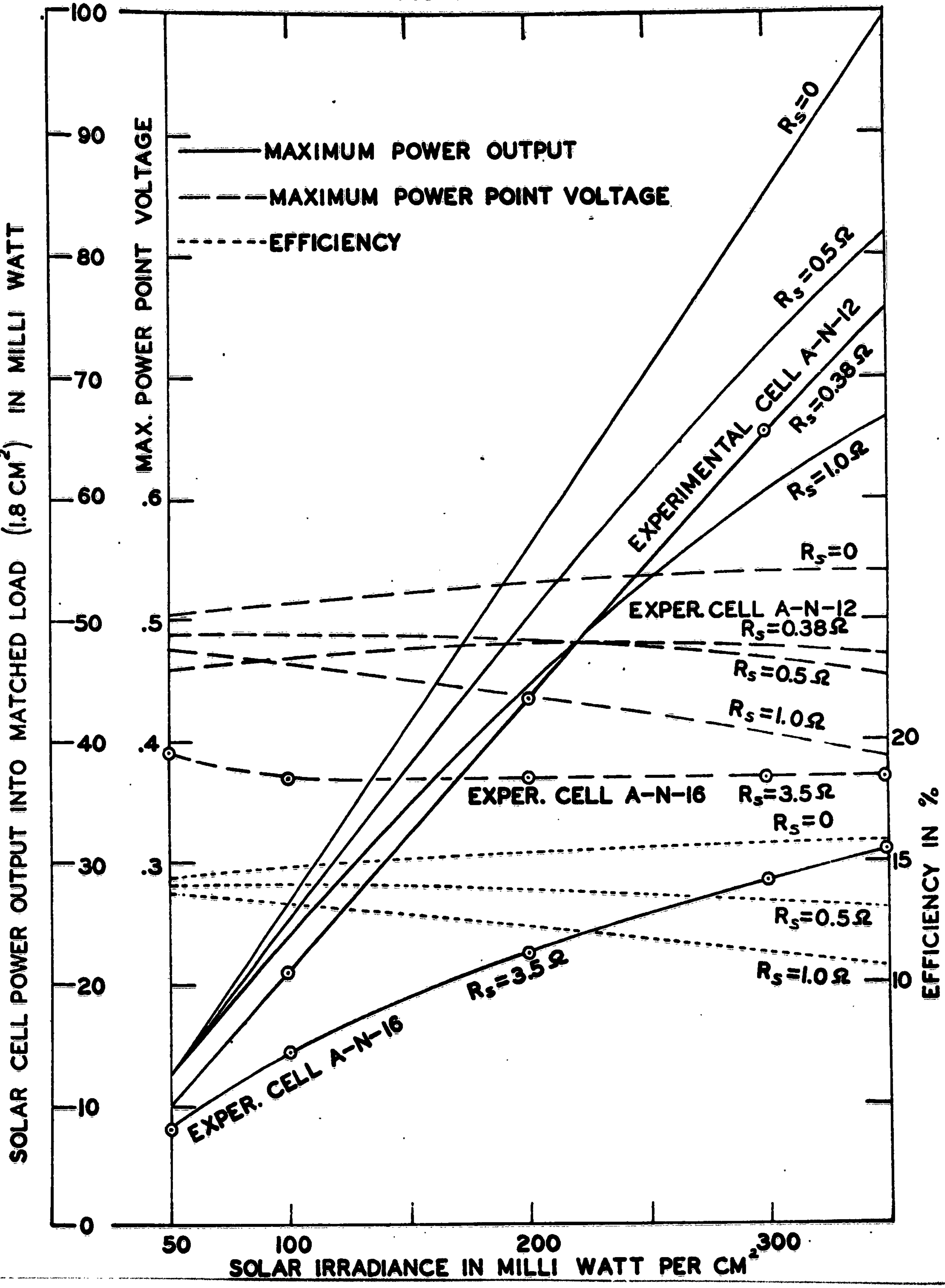
SOLAR CELL POWER OUTPUT INTO MATCHED LOAD (1.8 CM²) IN MILLI WATT
MAX. POWER POINT VOLTAGE
EFFICIENCY IN %
SOLAR IRRADIANCE IN MILLI WATT PER CM²
MAXIMUM POWER OUTPUT
MAXIMUM POWER POINT VOLTAGE
EFFICIENCY
Rs=0
Rs=0.5Ω
EXPERIMENTAL CELL A-N-12
Rs=0.38Ω
Rs=1.0Ω
Rs=0
EXPER. CELL A-N-12
Rs=0.38Ω
Rs=0.5Ω
Rs=1.0Ω
EXPER. CELL A-N-16
Rs=3.5Ω
Rs=0
Rs=0.5Ω
Rs=1.0Ω
Rs=3.5Ω
EXPER. CELL A-N-16
0
10
20
30
40
50
60
70
80
90
100
.3
.4
.5
.6
10
15
20
50
100
200
300

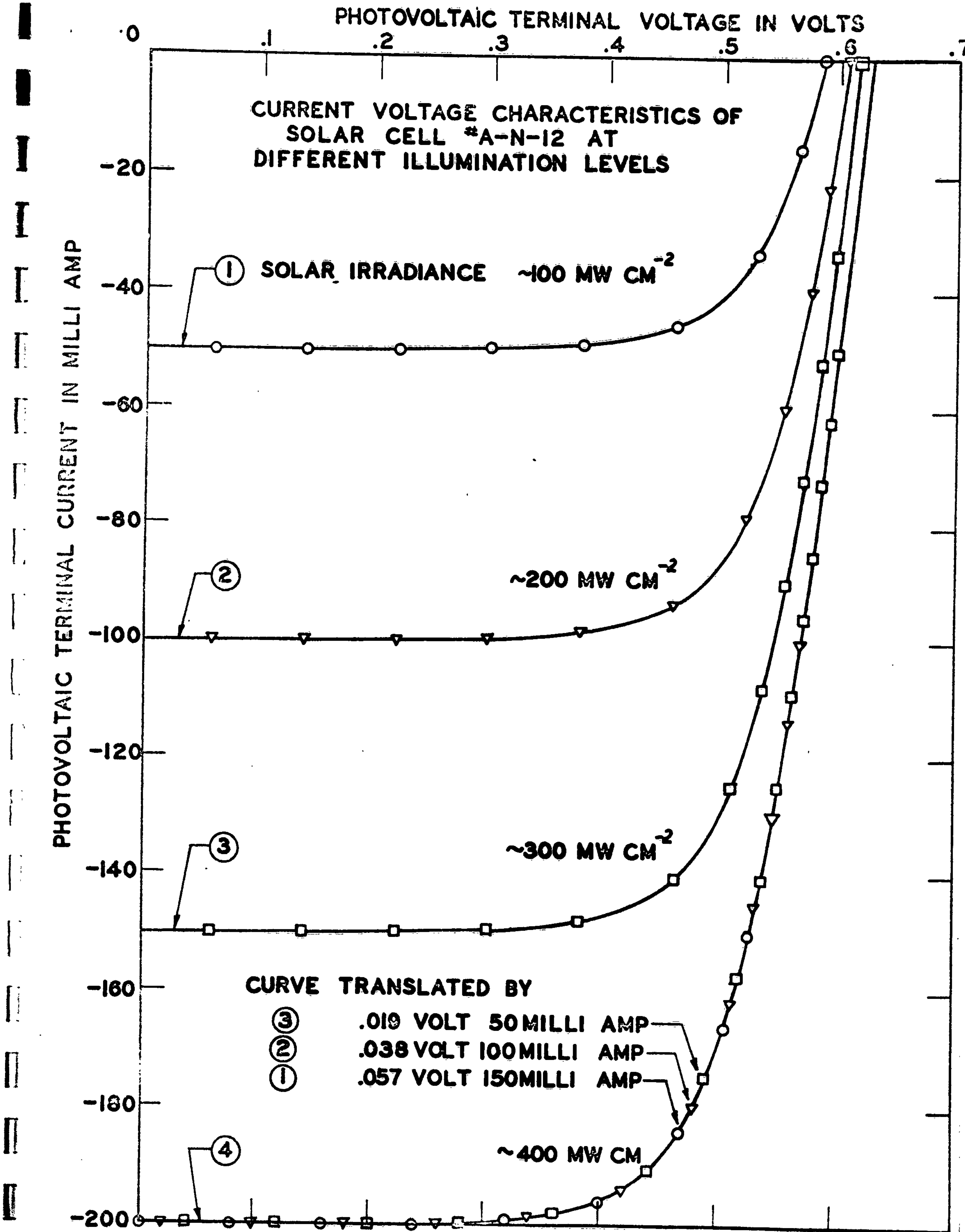
PHOTOVOLTAIC TERMINAL VOLTAGE IN VOLTS
0
.1
.2
.3
.4
.5
.6
.7
CURRENT VOLTAGE CHARACTERISTICS OF SOLAR CELL #A-N-12 AT DIFFERENT ILLUMINATION LEVELS
PHOTOVOLTAIC TERMINAL CURRENT IN MILLI AMP
-20
-40
-60
-80
-100
-120
-140
-160
-180
-200
① SOLAR IRRADIANCE ~100 MW CM-2
②
~200 MW CM-2
③
~300 MW CM-2
④
~400 MW CM
CURVE TRANSLATED BY
③ .019 VOLT 50 MILLI AMP
② .038 VOLT 100 MILLI AMP
① .057 VOLT 150 MILLI AMP

FIG. 6

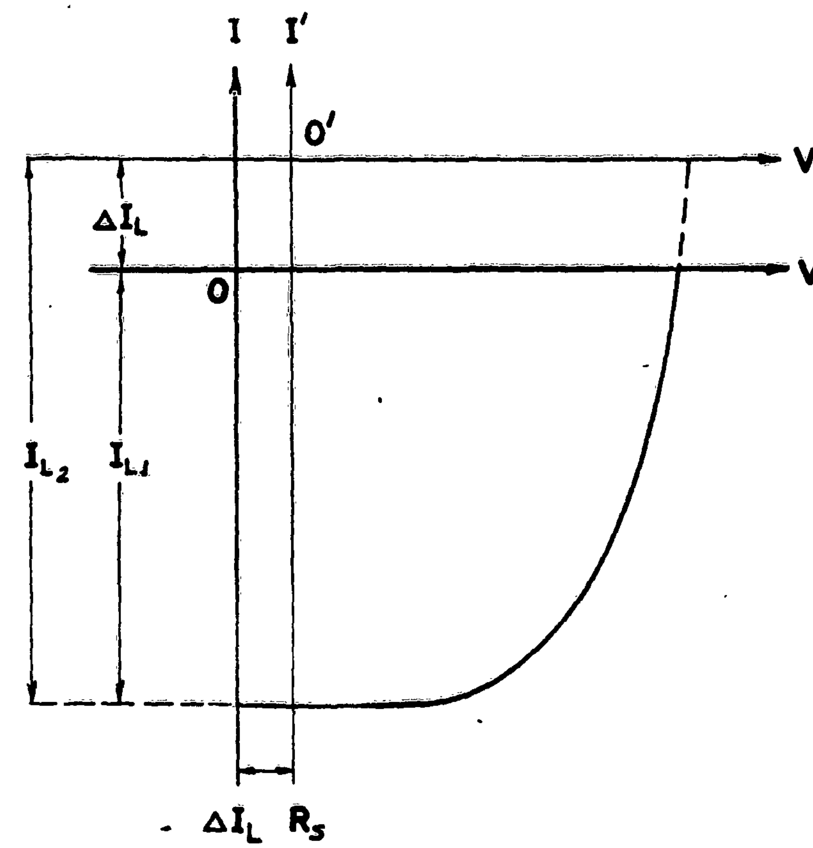

FIG. 5

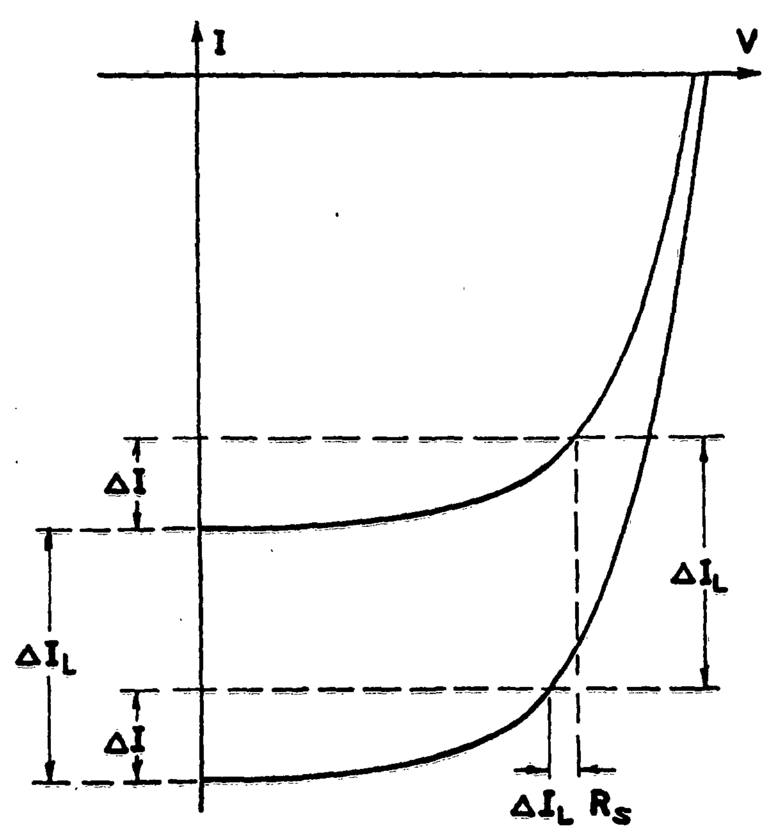

FIG. 7

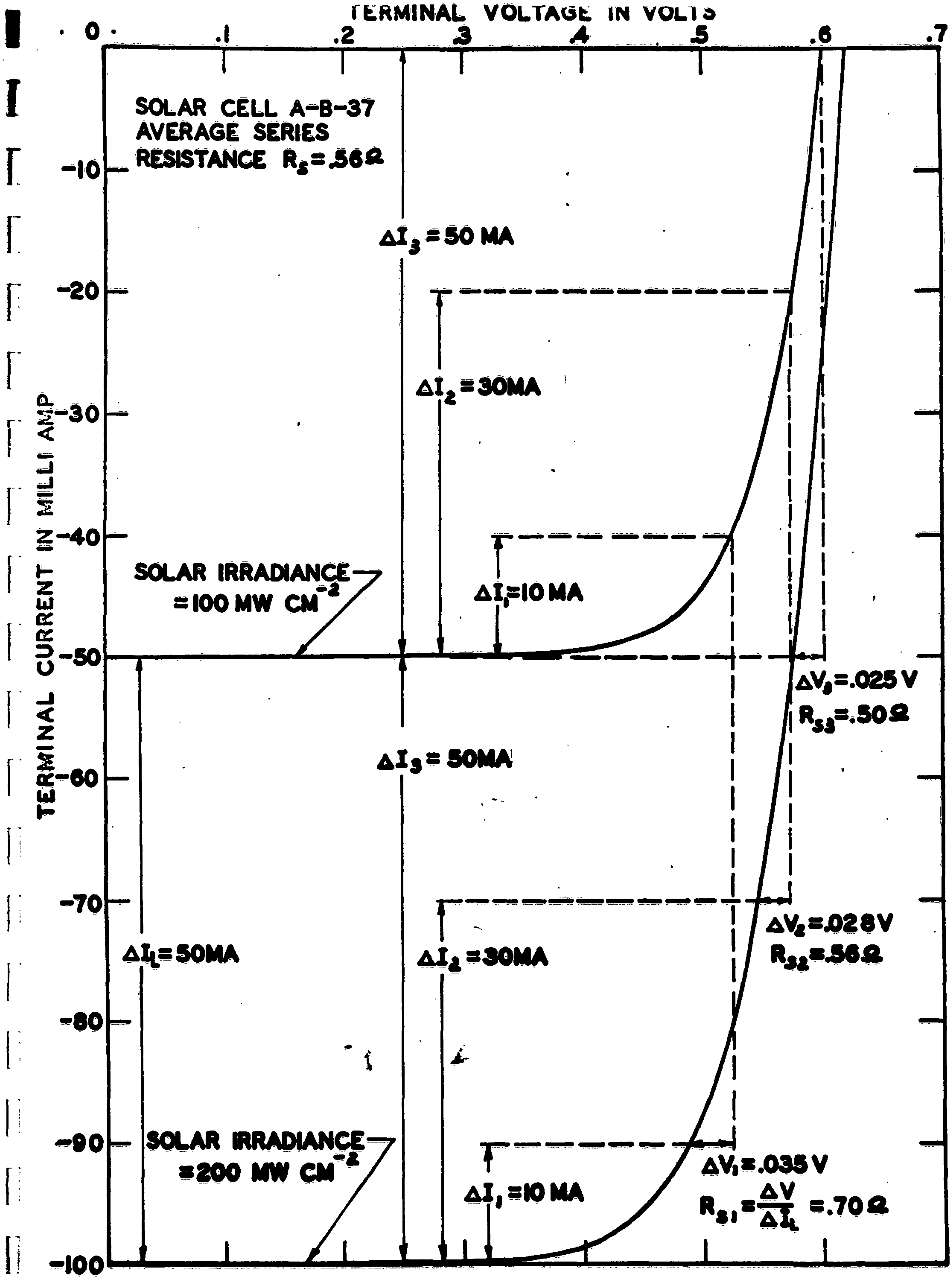

TERMINAL VOLTAGE IN VOLTS
0
.1
.2
.3
.4
.5
.6
.7
TERMINAL CURRENT IN MILLI AMP
-10
-20
-30
-40
-50
-60
-70
-80
-90
-100
SOLAR CELL A-B-37
AVERAGE SERIES
RESISTANCE R_S=.56Ω
ΔI3=50 MA
ΔI2=30MA
ΔI1=10 MA
SOLAR IRRADIANCE =100 MW CM^-2
ΔV3=.025 V
RS3=.50Ω
ΔI3= 50MA
ΔIL=50MA
ΔI2=30MA
ΔV2=.028V
RS2=.56Ω
SOLAR IRRADIANCE =200 MW CM^-2
ΔI1=10 MA
ΔV1=.035V
RS1=ΔV/ΔIL =.70Ω

FIG. 8a

VARIATION OF CURVE SHAPE WITH LIGHT INTENSITY OBSERVED ON CELL A-B-37

CURVE NO.	SOLAR IRRADIANCE MW CM^{-2}	SHIFT ΔI MA	SHIFT $\Delta I_L R_S$ MILLIVOLT
1	50	–	–
2	100	25	13
3	200	75	39
4	300	125	63
5	400	175	90

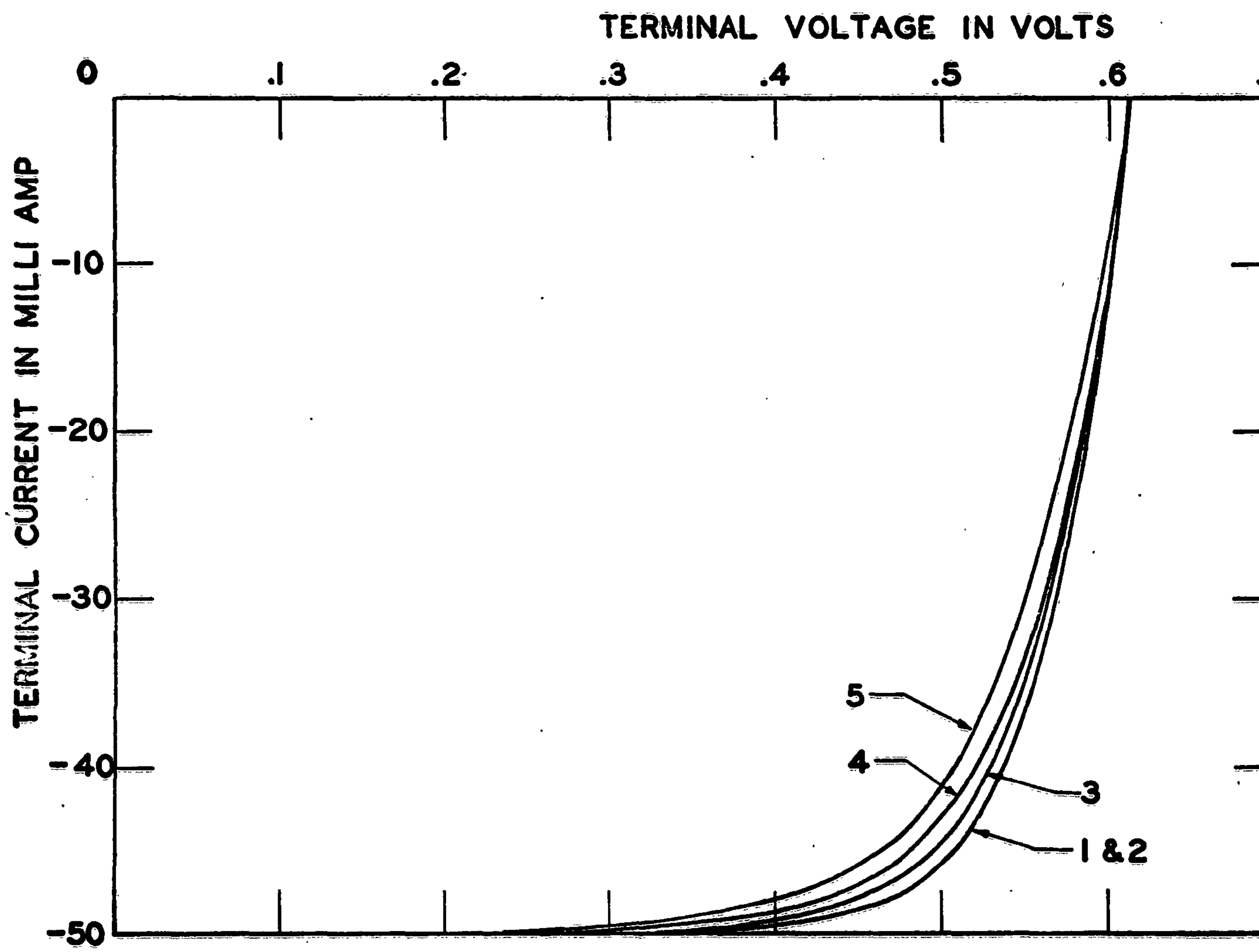

T-2067

FIG. 8b

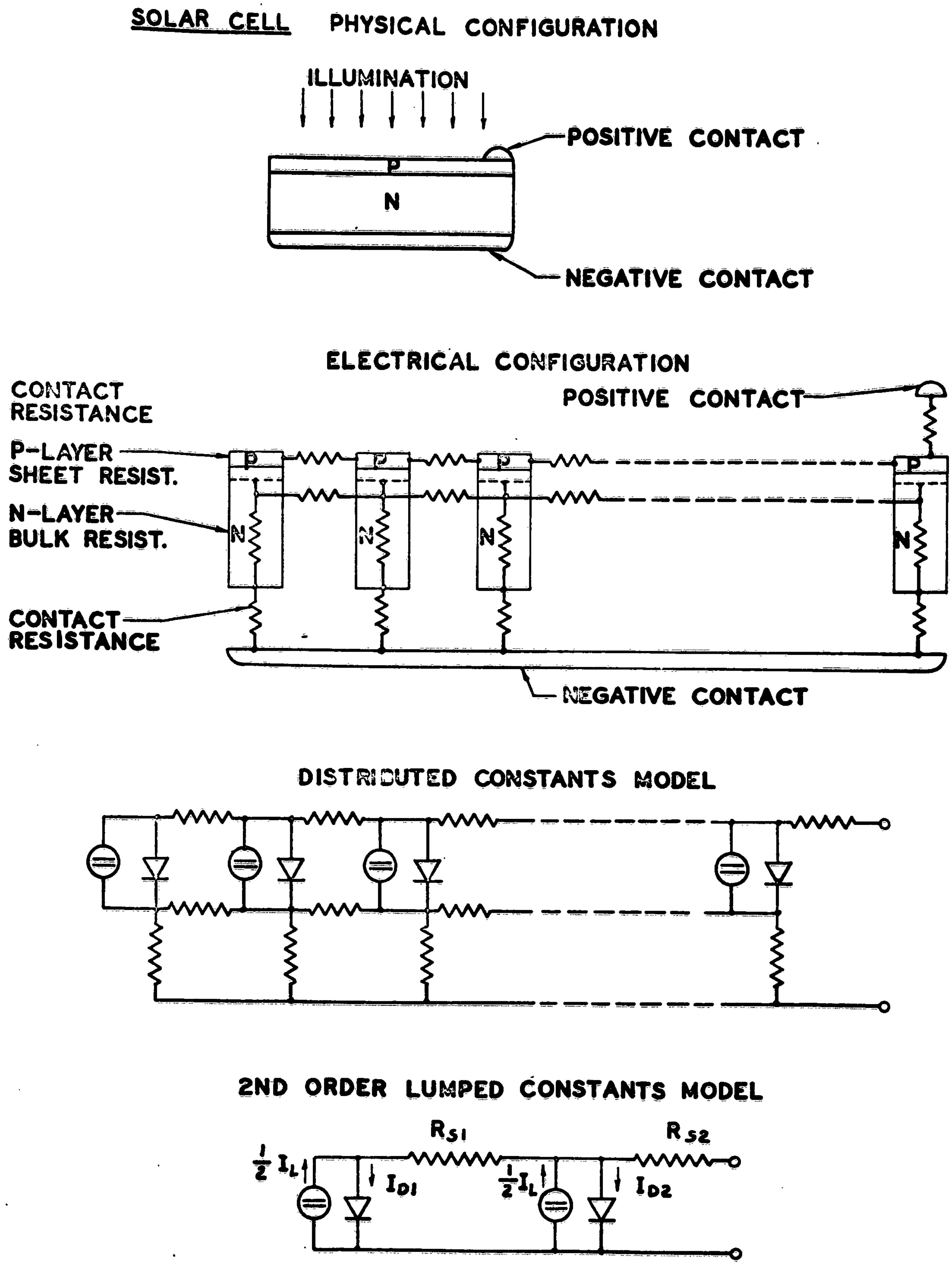
SOLAR CELL PHYSICAL CONFIGURATION
ILLUMINATION
POSITIVE CONTACT
P
N
NEGATIVE CONTACT
ELECTRICAL CONFIGURATION
CONTACT RESISTANCE
POSITIVE CONTACT
P-LAYER SHEET RESIST.
N-LAYER BULK RESIST.
CONTACT RESISTANCE
NEGATIVE CONTACT
DISTRIBUTED CONSTANTS MODEL
2ND ORDER LUMPED CONSTANTS MODEL
R_{S1}
R_{S2}
$\frac{1}{2} I_L$
I_{D1}
$\frac{1}{2} I_L$
I_{D2}

FIG. 9.

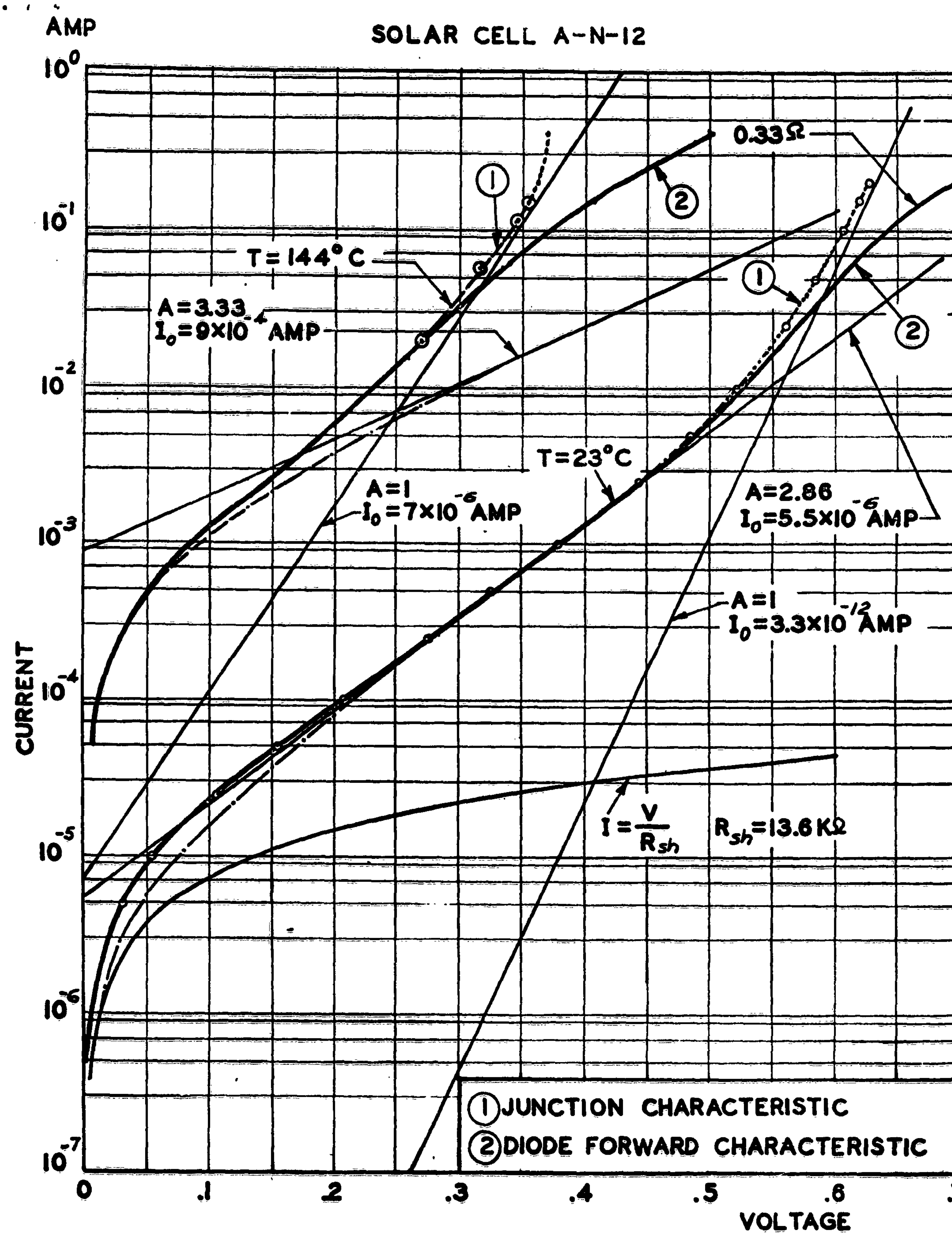
SOLAR CELL A-N-12
AMP
CURRENT
VOLTAGE
0.33Ω
T=144°C
A=3.33
I₀=9×10⁻⁴ AMP
T=23°C
A=1
I₀=7×10⁻⁶ AMP
A=2.86
I₀=5.5×10⁻⁶ AMP
A=1
I₀=3.3×10⁻¹² AMP
I = V/R_sh
R_sh=13.6 KΩ
1 JUNCTION CHARACTERISTIC
2 DIODE FORWARD CHARACTERISTIC

FIG. 10

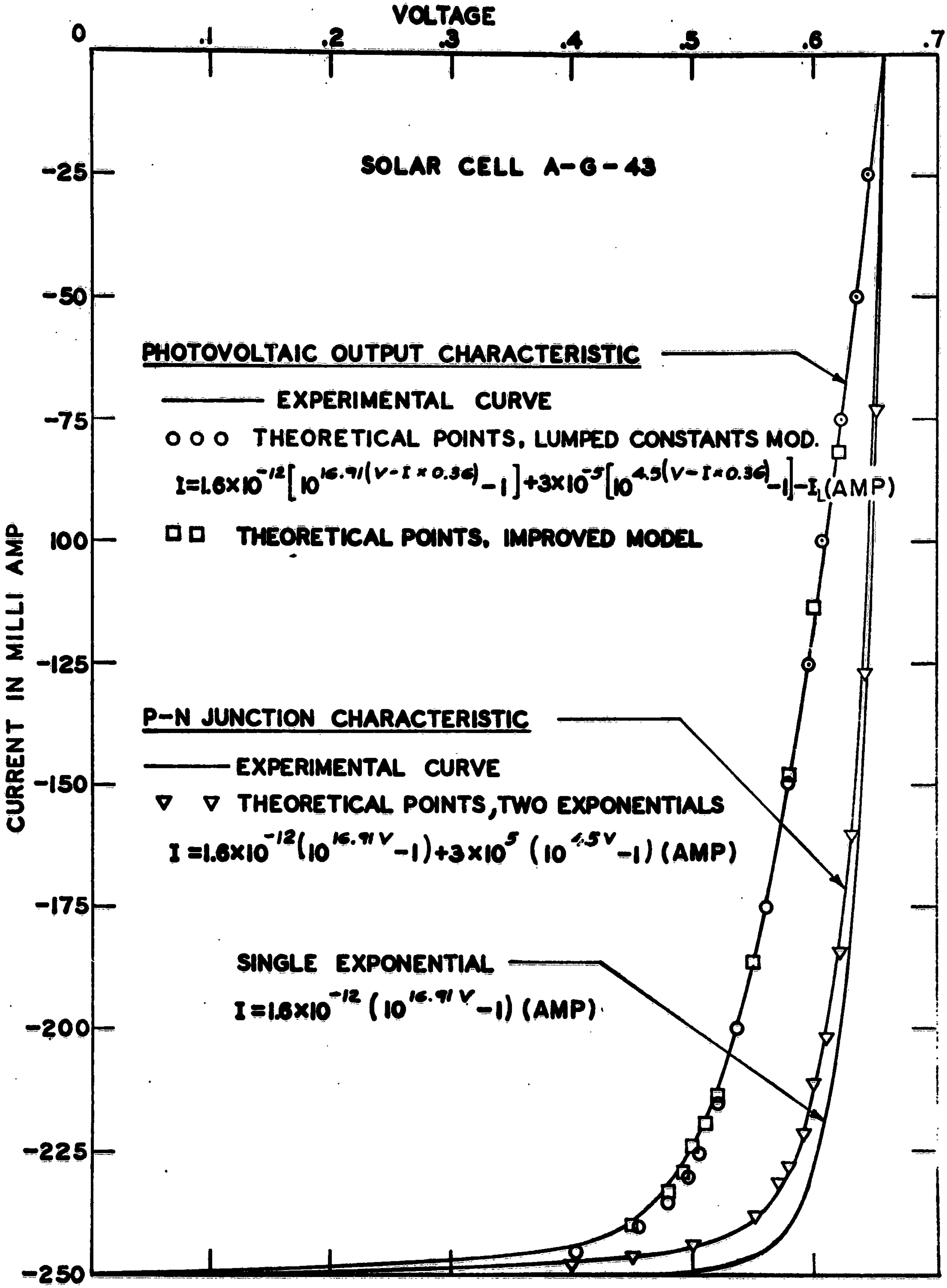
VOLTAGE
0
.1
.2
.3
.4
.5
.6
.7
SOLAR CELL A-G-43
CURRENT IN MILLI AMP
-25
-50
-75
100
-125
-150
-175
-200
-225
-250
PHOTOVOLTAIC OUTPUT CHARACTERISTIC
EXPERIMENTAL CURVE
THEORETICAL POINTS, LUMPED CONSTANTS MOD.
$I=1.6\times10^{-12}\left[10^{16.91(V-I\times0.36)}-1\right]+3\times10^{-5}\left[10^{4.5(V-I\times0.36)}-1\right]-I_L$ (AMP)
THEORETICAL POINTS, IMPROVED MODEL
P-N JUNCTION CHARACTERISTIC
EXPERIMENTAL CURVE
THEORETICAL POINTS, TWO EXPONENTIALS
$I=1.6\times10^{-12}(10^{16.91V}-1)+3\times10^{5}(10^{4.5V}-1)$ (AMP)
SINGLE EXPONENTIAL
$I=1.6\times10^{-12}(10^{16.91V}-1)$ (AMP)

T-2064

FIG. 11

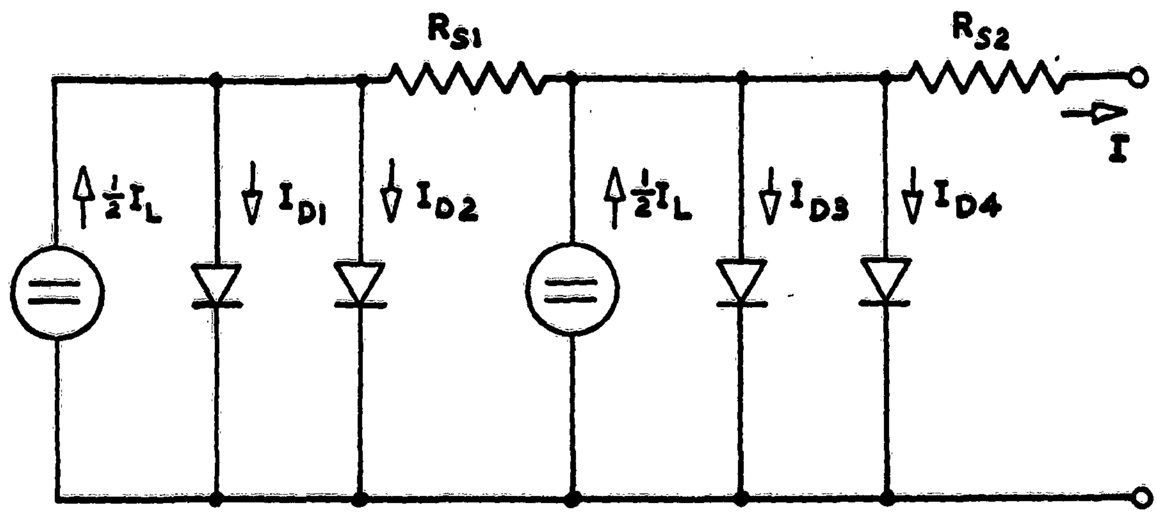

$$I_{D1} = I_{01}\left\{\text{EXP.}\left[\frac{q}{kT}\left[V - IR_{S2} - \left(I - \tfrac{1}{2}I_L + I_{D3} + I_{D4}\right) R_{S1}\right]\right] - 1\right\}$$

$$I_{D2} = I_{02}\left\{\text{EXP.}\left[\frac{q}{AkT}\left[V - IR_{S2} - \left(I - \tfrac{1}{2}I_L + I_{D3} + I_{D4}\right) R_{S1}\right]\right] - 1\right\} \qquad A = f(T)$$

$$I_{D3} = I_{01}\left\{\text{EXP.}\left[\frac{q}{kT}\left(V - IR_{S2}\right)\right] - 1\right\}$$

$$I_{D4} = I_{02}\left\{\text{EXP.}\left[\frac{q}{AkT}\left(V - IR_{S2}\right)\right] - 1\right\} \qquad A = f(T)$$

FIG. 12

APPENDIX A

Finding the proper IV - characteristic for an individual solar cell or a solar cell matrix after a light level change by means to two translations of the coordinate system.

The basic equation describing the current-voltage characteristic of a solar cell neglecting series- and shunt-resistance is:

$$I = I_o \left(e^{BV} - 1\right) - I_L \quad ; \qquad \text{(A1)}$$

where: $B = \frac{q}{AkT}$, and all other quantities as described in Section 2 of the paper.

Let:

$$I_1 = I_o \left(e^{BV_1} - 1\right) - I_{L_1} \quad ; \qquad \text{(A2)}$$

be equ. (A1) at light level L_1 and

$$I_2 = I_o \left(e^{BV_2} - 1\right) - I_{L_2} \quad ; \qquad \text{(A3)}$$

the same equation at light level L_2.
Since V is the independent variable, one can choose:

$$V_2 = V_1 \qquad \text{(A4)}$$

and can set:

$$I_{L_2} = I_{L_1} + \Delta I_L . \qquad \text{(A5)}$$

where ΔI_L is proportional to the difference in light intensity between levels 1 and 2. Subtracting equ. (A2) from equ. (A3) after introducing equ. (A4) and (A5), one obtains:

$$\underline{\underline{I_2 = I_1 - \Delta I_L}} \qquad \text{(A6)}$$

for all choices of $V_2 = V_1$.
Equation (6) describes a translation of the coordinate system parallel to the current axis by the amount ΔI_L on the current axis.

For higher light levels, the effect of series resistance on the IV - characteristic has to be included, due to the increased magnitude of the current I, (see Fig. 1). Here

$$V' = V - IR_s . \qquad \text{(A7)}$$

is the voltage across the p-n junction, which is larger than the terminal voltage V by the voltage drop in the series resistance. (Note that the current I is a negative quantity (see equ. (A1), resulting in V' V for power generation in the solar cell (4th quadrant operation). The IV-characteristic for the equivalent circuit (Fig. 1a) is:

$$I = I_o\,(e^{B(V - IR_s)} - 1) - I_L \quad ; \qquad (A8)$$

$$= I_1\,(e^{BV'} - 1) - I_L \quad ; \qquad (A8a)$$

Introducing again two light levels 1 and 2, one obtains:

$$I_1 = I_1\,(e^{BV_1'} - 1) - I_{L_1} \quad ; \qquad (A9)$$

$$I_2 = I_1\,(e^{BV_2'} - 1) - I_{L_1} - \Delta I_L \quad ; \qquad (A10)$$

Again one chooses:

$$V_2' = V_1' \quad ; \qquad (A11)$$

and obtains the same translation as before:

$$I_2 = I_1 - \Delta I_L \quad ; \qquad (A6)$$

Equation (7) results, however, in two different terminal voltages V_1 and V_2 for the two currents I_2 and I_1. From equ. (11), (7) and (6), follows:

$$V_1 - I_1R_s = V_2 - I_1R_s + \Delta I_LR_s \qquad (A11a)$$

which describes a constant relationship between V_1 and V_2 for any choice of V_1. The constant of this relationship is proportional to the series resistance R_s and to the change in light level. Equation (11a) thus describes a second translation of the coordinate system, this one parallel to the voltage axis by the amount:

$$\underline{\underline{V_2 = V_1 - \Delta I_LR_s}} \qquad (A12)$$

Equations (A6) and (A7) describe the photovoltaic output characteristic as invariant to any change in the light intensity except for two translations of the (current-voltage) coordinate system.

Spectrolab,
North Hollywood, California

INVESTIGATION OF OPTICAL COATINGS FOR SOLAR CELLS, Dr. F.E. Fuller, January 1962. 114 pp. incl.illus. (ARPA Order No. 80-61) Technical Summary Report No. 2 Spectrolab/2004 Contract DA 36-039 SC-87449 Order No. 40647-PM-61-93-93

Unclassified Report

(over)

UNCLASSIFIED

1. Power Supplies
2. Solar Energy - Applications

I. Fuller, Dr.F.E.
II. Spectrolab/2004
III. DA-36-039 SC-87449

UNCLASSIFIED

Spectrolab,
North Hollywood, California

INVESTIGATION OF OPTICAL COATINGS FOR SOLAR CELLS, Dr. F.E. Fuller, January 1962. 114 pp. incl.illus. (ARPA Order No. 80-61) Technical Summary Report No. 2 Spectrolab/2004 Contract DA 36-039 SC-87449 Order No. 40647-PM-61-93-93

Unclassified Report

(over)

UNCLASSIFIED

1. Power Supplies
2. Solar Energy - Applications

I. Fuller, Dr.F.E.
II. Spectrolab/2004
III. DA-36-039 SC-87449

UNCLASSIFIED

Performance analyses are made of silicon cell solar power systems using radiation concentration and filtering. The elementary conditions of system design for optimum performance of such systems are established and a plan is outlined for construction of a prototype system.

UNCLASSIFIED

UNCLASSIFIED

Performance analyses all made of silicon cell solar power systems using radiation concentration and filtering. The elementary conditions of system design for optimum performance of such systems are established and a plan is outlined for construction of a prototype system

UNCLASSIFIED

UNCLASSIFIED

PSD Dist. List A (Mandatory)
September 1962

DISTRIBUTION LIST
Technical Summary Report No. 2
Contract No. DA 36-039 SC-87449

Commanding Officer
U.S.A. Electronics Research
and Development Laboratory
Fort Monmouth, N. J.
ATTN: Logistics Division (MARKED FOR PROJECT ENGINEER) (2)
ATTN: SELRA/SL-P (1)
ATTN: SELRA/SL-LNR (1)
ATTN: SELRA/SL-LNE (1)
ATTN: Dir.of Research/Engineering (1)
ATTN; SELRA/ADJ (1)
ATTN: Technical Document Center (1)
ATTN: Technical Information Div. (UNCLASSIFIED REPORTS ONLY FOR RETRANSMITTAL TO ACCREDITED BRITISH AND CANADIAN GOVERNMENT REPRESENTATIVES (3)

OASD (R and D) Rm.3E1065
ATTN: Technical Library
The Pentagon,
Washington 25, D.C. (1)

Chief of Research and Development
OCS, Dept. of the Army
Washington 25, D.C. (1)

Commanding General
U.S.A. Electronics Command
ATTN: AMSEL-AD
Fort Monmouth, N. J. (1)

Director
U.S. Naval Research Laboratory
ATTN: Code 2027
Washington 25,D.C. (1)

Commanding Officer and Director
U.S. Naval Electronics Laboratory
San Diego 52, California (1)

Commander
Air Force Command and Control
Development Division
ATTN: CRZC
L. G. Hanscom Field
Bedford, Mass. (1)

Commander
Rome Air Development Center
ATTN: RACTL
Griffiss Air Force Base, N. Y. (1)

Commanding General
U.S.A. Electronics Research and
Development Activity
ATTN: Technical Library
Fort Huachuca, Arizona (1)

Commanding Officer
Diamond Ordnance Fuze Laboratories
ATTN: Library, Room 211, Bldg. 92
Washington 25, D.C. (1)

Commanding Officer
U.S.A. Electronics Material Support
Agency
ATTN: SELMS-ADJ
Fort Monmouth, N. J. (1)

Deputy President
U.S.A. Security Agency Board
Arlington Hall Station
Arlington 12, Virginia (1)

Commander
Armed Services Technical Information
Agency
ATTN: TIPCR
Arlington Hall Station
Arlington 12, Virginia (10)

PSD Dist.List A(Mandatory)
September 1962

DISTRIBUTION LIST
Technical Summary Report No. 2
Contract No. DA 36-039 SC-87449

Chief
U.S.Army Security Agency
Arlington Hall Station
Arlington 12, Virginia (2)

Commander
Aeronautical Systems Division
ATTN: ASAPRL
Wright-Patterson Air Force Base
Ohio (1)

Air Force Systems Command
ATTN: AFSC STLO (NARDAE)
Johnsville, Pennsylvania (1)

Commander
Air Force Cambridge Research Laboratory
ATTN: CRXL-R
L. G. Hanscom Field
Bedford, Mass. (1)

Commander
Air Force Command and Control Development Division
ATTN: CCRR (1)
ATTN: CCSD (1)
L. G. Hanscom Field
Bedford, Mass.

Power Information Center
Moore School Building
200 South Thirty-Third Street
Philadelphia 4, Pennsylvania (1)

Headquarters
U. S.Army Material Command
Research and Development Directorate
ATTN: AMCRD-DE-MO
Washington 25, D.C. (1)

Commanding General
U. S. Army Electronics Command
ATTN: AMSEL-RE-A
Fort Monmouth, N. J. (1)

PSD Dist. List B (Steering
Group Members - Mandatory)
July 1962

DISTRIBUTION LIST
Technical Summary Report No. 2
Contract No. DA 36-039 SC-87449

Army Research Office
Office, Chief Research and
Development
Room 3D442, The Pentagon
Washington 25, D.C.
ATTN: Dr. Sidney J. Magram (1)

Director Advanced Concepts Division
Bureau of Ships (Code 350)
Washington 25, D.C.
ATTN: LCDR. Frank W. Anders (1)

Office of Naval Research (Code 429)
Department of the Navy
Washington 25,D.C.
ATTN: Mr. James R. Patton, Jr. (1)

Headquarters
USAF (AFRDR-AS)
Washington 25, D.C.
ATTN: Maj. William G. Alexander (1)

Commander
Aeronautical Systems Division
Wright-Patterson Air Force Base
Ohio
ATTN: Mr. George W.Sherman (1)

Assistant Director, Material Sciences
Advanced Research Projects Agency
The Pentagon, Room 3E153
Washington 25, D.C.
ATTN: Mr. Charles F. Yost (1)

Advanced Research Projects Agency
The Pentagon, Room 3E157
Washington 25, D.C.
ATTN: Dr. John H. Huth (1)

U. S. Atomic Energy Commission
Division of Reactor Development
Washington 25,D.C.
ATTN: Mr. G. Montgomery Anderson (1)

U. S. Atomic Energy Commission
Division of Reactor Development
Auxiliary Power Branch (SNAP)
Washington 25, D.C.
ATTN: Lt. Col. George H. Ogburn, Jr. (1)

Headquarters
National Aeronautics and Space
Administration
Office of Nuclear Flight Systems
Washington 25, D.C.
ATTN: Mr. David Novik (RNN) (1)

National Aeronautics and Space
Administration
1520 H. Street N.W.
Washington 25,D.C.
ATTN: Mr. Walter C.Scott (1)

Equipment and Supplies Div.,
Office of Ordnance
Office, DOD R and E
The Pentagon
Washington 25, D.C.
ATTN: Mr. G.B.Wareham (1)

PSD Dist. List C (ARPA Mandatory)

January 1962

DISTRIBUTION LIST
Technical Summary Report No. 2
Contract No.DA 36-039 SC-87449

Director Advanced Research Projects Agency Washington 25,D.C.	(6)
Chief Signal Officer Department of the Army Washington 25,D.C.	(8)

DISTRIBUTION LIST
Technical Summary Report No. 2
Contract No. DA 36-039 SC-87449

Commanding General
U. S. Army Advent Management Agency
Fort Monmouth, N. J.
ATTN: Mr. William Shorr (1)

Mr. Phil Youngblood
Army Bassistic Missile Agency
ATTN: ORDAB-DCEG
Redstone Arsenal, Alabama (1)

Dr. Ralph Zirkind
Bureau of Aeronautics
Department of the Navy
Washington 25, D.C. (1)

Major George W. Austin
Air Force Ballistic Missile Div.
Headquarters ARDC
ATTN: WDZW
Air Force Unit Post Office
Los Angeles 45, California (1)

U.S. Army Research Office
Chemical and Material Branch
Office of Chief of Research and Development
Department of the Army
Washington 25, D.C. (1)

Mr. Rudolph A. Bradbury
Air Force Cambridge Research Center
ATTN: CRRSC
L. G. Hanscom Field
Bedford, Mass. (1)

Mr. Joseph M. Hallissy, Jr.
USA Langley Research Center
Langley Air Force Base
Virginia (1)

General Electric Company
Monmouth District Office
43 W. Front Street
Red Bank, New Jersey (1)

Engelhardt Industries
Hanovia Liquid Gold Division
113 Astor Street
Newark 2, N. J.
ATTN: Mr. T.W. Cushing (1)

Mr. R. W. Curran
Boeing Airplane Company
Seattle, Washington (1)

International Rectifier Corp.
233 Kansas Street
El Segundo, California
ATTN: Dr. C.A. Escoffery (1)

Texas Instrument Inc.
Semi Conductor Components Div.
P. O. Box 312
Dallas, Texas
ATTN: Pat Brown (1)

Californa Institute of Technology
4800 Oak Grove Drive
Pasadena 3, California
ATTN: Mr. K. Ray
Jet Propulsion Lab. (1)

Radio Corporation of America
RCA Laboratories
Princeton, N. J.
ATTN: Mr. P. Rappaport (1)

Lockheed Aircraft Corporation
Missiles and Space Div.
3251 Hanover Road
Palo Alto, California
ATTN: Dr. W. Kapp (1)

Armour Research Foundation
10 West 35th Street
Chicago 16, Illinois (1)

Transitron Electronic Corp.
168-182 Albion Street
Wakefield, Mass. (1)

Hoffman Electronics Corp.
Semi Conductor Division
1001 Arden Drive
El Monte, California (1

Heliotek Corporation
12500 Gladstone Avenue
Sylmar, California
ATTN: Dr. M. Wolf (1

DISTRIBUTION LIST
Technical Summary Report No. 2
Contract No.DA 36-039 SC-87449

Bell Telephone Laboratories (1)
Murray Hill
New Jersey

Westinghouse Electric Corp.
3 Gateway Center
P.O. Box 2278
Pittsburgh 30, Pa. (1)